STATE OF CALIFORNIA • DEPARTMENT OF TRANSPORTATION

TECHNICAL REPORT DOCUMENTATION PAGE

TR0003 (REV 10/98)

1. REPORT NUMBER CA16-2342	2. GOVERNMENT ASSOCIATION NUMBER	3. RECIPIENT'S CATALOG NUMBER

4. TITLE AND SUBTITLE Effects of Superstructure Creep and Shrinkage on Column Design in Posttensioned Concrete Box-Girder Bridges	5. REPORT DATE February 2017
	6. PERFORMING ORGANIZATION CODE
7. AUTHOR Ebadollah Honarvar, Sri Sritharan, and Matt Rouse	8. PERFORMING ORGANIZATION REPORT NO.
9. PERFORMING ORGANIZATION NAME AND ADDRESS Department of Civil, Construction and Environmental Engineering Iowa State University	10. WORK UNIT NUMBER
	11. CONTRACT OR GRANT NUMBER 65A0463
12. SPONSORING AGENCY AND ADDRESS California Department of Transportation Division of Engineering Services 1801 30th Street, MS #9-2/5i Sacramento, CA 95816	13. TYPE OF REPORT AND PERIOD COVERED Final Report June, 2012 – January, 2015
	14. SPONSORING AGENCY CODE 913

15. SUPPLEMENTARY NOTES

Prepared in cooperation with the State of California Department of Transportation

16. ABSTRACT

During and after construction, cast-in-place posttensioned concrete box-girder bridges (CIP/PS Box) experience continuous movement primarily due to time-dependent shortening of the superstructure caused by creep and shrinkage. As a result, displacement-induced forces are developed in columns. These forces must be accurately estimated in order to ensure satisfactory performance of the bridge as well as to produce cost-effective design. When computer models are not used, California Department of Transportation (Caltrans) has adopted a simplified method (SM) to estimate the displacement-induced column forces, which has not been validated.

This report systematically investigates the displacement-induced column forces using eight representative CIP/PS Box bridges using a combination of an experimental program and finite element analyses. It was found that Caltrans SM has deficiencies due to the estimation of strain rate and accurately accounting for concrete relaxation. Recommendations are presented to improve the Caltrans SM, thereby increasing the accuracy of calculated column design forces with due consideration to strain rate, concrete relaxation, and effects of column flexural cracking.

17. KEY WORDS Creep, Relaxation, Shrinkage, Posttensioned concrete, box-girder, bridge, Finite element, Displacement-induced, column, forces	18. DISTRIBUTION STATEMENT No restriction. This document is available to the public through the National Technical Information Service, Springfield, Virginia 22161	
19. SECURITY CLASSIFICATION *(of this report)* Unclassified	20. NUMBER OF PAGES 159	21. COST OF REPORT CHARGED

Reproduction of completed page authorized.

E. Honarvar, S. Sritharan, M. Rouse

Effects of Superstructure Creep and Shrinkage on Column Design in Posttensioned Concrete Box-Girder Bridges

Submitted to the
California Department of Transportation
Caltrans Project Contract: 65A0463

FEBRUARY 2017

Final

REPORT

IOWA STATE UNIVERSITY
OF SCIENCE AND TECHNOLOGY

Department of Civil, Construction
and Environmental Engineering

Effects of Superstructure Creep and Shrinkage on Column Design in Posttensioned Concrete Box-Girder Bridges

by

Ebadollah Honarvar
Structural/Bridge Engineer, Jacobs Engineering

Sri Sritharan
Wilson Engineering Professor, Iowa State University

Matt Rouse
Senior Lecturer, Iowa State University

Caltrans Project Contract: 65A0463

A Final Report to the California Department of Transportation

Department of Civil, Construction and Environmental Engineering
Iowa State University
Ames, IA 50011

February 2017

DISCLAIMER

ACKNOWLEDGMENTS

The authors would like to thank the California Department of Transportation for sponsoring this research project and Dr. Charles Sikorsky for serving as the project manager. Thanks are also due to the following individuals for serving on the technical advisory committee of this project: Marc Friedheim, Ahmed Ibrahim, Richard Schendel, Gudmund Setberg, Rodney Simmons, Foued Zayati, and Toorak Zokaie. Their guidance and feedback during the course of the project are also greatly appreciated.

The help and guidance provided by Doug Wood, the manager of the structural engineering laboratories at Iowa State University, in performing the concrete relaxation tests on a tight schedule are much appreciated.

ABSTRACT

Creep and shrinkage of cast-in-place post-tensioned concrete box-girder bridges (CIP / PS Box) designed with longitudinal prestressing introduce significant lateral displacement demands to the supporting columns within each continuous multi-span frame. Consequently, the columns are subjected to lateral forces and flexural stresses as a function of time following the construction of the superstructure. These forces must be accurately estimated in order to ensure satisfactory performance of the bridge as well as to produce cost-effective design.

Although computer models are routinely used for estimating the column forces, California Department of Transportation (Caltrans) has adopted a simplified method (SM) to estimate displacement-induced column forces using the strain rates established for joints and bearing design. The Caltrans SM has never been validated, raising the following two concerns: 1) the shortening strain rate of the superstructure in CIP/ PS Box may not be appropriate for estimating the displacement-induced column forces because it was originally established for joints and bearing design; and (2) it may not accurately capture the beneficial effects of concrete relaxation on the displacement-induced forces. Using a combination of an experimental program and analytical models, this report investigates the displacement-induced column forces in CIP/ PS Box and presents recommendations to address the aforementioned concerns, thereby improving the calculation of column design forces.

After demonstrating the beneficial effects of concrete relaxation on displacement-induced forces through an experimental investigation, the corresponding effects were studied on eight CIP/ PS Box frames of various configurations and lengths. Using the finite-element models (FEM), the shortening strain rate of the superstructure and the variation of the column lateral displacement were calculated, including the effects of concrete relaxation in the columns. For the eight analyzed CIP/ PS Box frames, the shrinkage of the superstructure had a significantly larger contribution to the shortening strain rate of the superstructure, the column top lateral displacement and the corresponding base shear force compared to the corresponding effects due to dead load, prestress, and creep. The contribution of the dead load was the smallest compared to the corresponding effect due to prestress, creep, and shrinkage.

Using the FEM results for the strain rates, four simplified approaches were developed to more accurately calculate the displacement-induced column forces in CIP / PS Box frames, without conducing detailed computer modeling. Similar to the Caltrans SM, Approaches 1a and 1b use the FEM creep and shrinkage strains for each frame type (i.e., short-, medium-, and long-span), and average of the eight frames, respectively, to calculate forces. Whereas, columns forces are calculated based on Approaches 2a and 2b using the FEM total strains for each frame type, and average of the eight frames, respectively.

These approaches and the Caltrans SM were compared to the FEM results to determine the most appropriate simplified approach. When displacements were evaluated, Approach 1a resulted in the best agreement with the FEM results. A better correlation was found between the Caltrans SM and the FEM results when the total strains were used rather than the creep and shrinkage stains. For shear force calculation using simplified analysis, Approaches 2a and 2b resulted in the best agreement with the FEM results, while the Caltrans SM resulted in the poorest agreement with the FEM results. Although Approach 2b was found to be the most appropriate simplified approach, Approach 1b has an advantage of using creep and shrinkage strains, like the Caltrans SM and account for the prestress strains as part of the structural analysis. Therefore, Approach 1b is recommended by this study to calculate the displacement-induced column forces in CIP / PS Box frames.

TABLE OF CONETENTS

LIST OF FIGURES

LIST OF TABLES

CHAPTER 1: INTRODUCTION

1.1 Overview

In a prestressed concrete bridge, stresses and strains continuously change as a function of time due to characteristics of time-dependent behavior of materials. Although not studied herein, changes in bridge temperature due to varying environmental conditions will also cause thermal stresses and strains with time. Concrete undergoes creep and shrinkage behavior while steel experiences relaxation, producing time-dependent movements. In structurally indeterminate bridges, these movements are restrained, which, in turn, cause changes to reactions and internal forces as a function of time. When these bridges are built on site, the time dependent effects are expected to take place during and after construction. Hence, the time-dependent analysis used for estimating the corresponding stresses and deformations require information related to the time-dependent properties of concrete and prestressing steel. Steel relaxation is mainly dependent on the magnitude of the applied stress and can be determined fairly accurately. However, estimation of creep and shrinkage is more involved since concrete is a versatile composite material. Both creep and shrinkage are influenced by intrinsic and extrinsic factors. Intrinsic factors typically include proportion and the properties of mixtures, while size of concrete, age of concrete, curing conditions, ambient temperature, and relative humidity are considered as extrinsic factors.

Prediction of stresses and strains within a partially completed structure at a particular stage of construction may impact the subsequent stages, and consequently the long-term state of stresses and strains of a bridge. Quantities characterizing structural behavior such as deformations and stresses continue to change during and after the construction. The changes are due to varying time dependent properties such as creep, shrinkage, modulus of elasticity, and steel relaxation. Furthermore, since the structural configuration continuously changes with different loading and/or support locations, and each construction stage affects the subsequent stages, the design of certain structural components may be governed during construction. Therefore, the time dependent construction stage analysis is required to examine the changes in stresses and strains in each stage of the construction. If such analyses are ignored, the post-construction analyses of bridges may be meaningless because members have already developed significant stresses and strains. These developed strains and stresses may also be accounted for when assessing bridges based on health monitoring data or calculating their strength and displacement corresponding to yield and ultimate conditions.

Among different types of prestressed concrete bridge superstructures, the cast-in-place post-tensioned concrete box-girder (CIP / PS Box) bridge has become the choice of many jurisdictions for long spans structures. In addition, the inherently high torsional stiffness of the box-girder cross section helps to effectively resist the high torsional forces induced in the curved bridges. However, concerns have been expressed with respect to the long-term behavior and durability of CIP / PS Box because of the effects of concrete creep and shrinkage (Lark et al. 2004). Excessive long-term mid-span deflections of such bridges have been observed in the past (Vitek 1995 and Bazant et al. 2012).

The superstructure of CIP / PS Box experiences continuous movements due to shortening of the structure length, resulting from creep caused primarily by prestressing and shrinkage as well as a temperature. Unless provisions are made in design, these movements can, in the long run, cause significant internal stresses and strains, resulting in undesirable consequences to critical bridge members. Typically, deck expansion joints, bearing systems, and/or restraining devices have been used to minimize the internal forces resulting from thermal and shortening movements. Because addition of these elements increases the maintenance and repair costs, there is an increasing inclination to design bridges with less number of frames, minimizing the number of expansion joints. When bridges are designed with a minimum number of expansion joints, the continuous movements of the bridge can cause significant internal stresses in the integral column bents. Since the movement of CIP / PS Box due to thermal effects is adequately addressed in current design guidelines, this study only focuses on the shortening of the superstructure due to creep and shrinkage and the corresponding effects on column forces. Accurately estimating column forces are critical for the design of the columns and their performance under extreme loads such as those due to earthquakes. When they are underestimated, yielding of the columns may occur prematurely as they are subjected to external lateral loads. When forces are overestimated, columns will become unnecessarily large, which in turn can attract more forces and amplify the problem.

1.2 Problem Statement

During and after construction, time-dependent shortening of superstructures of CIP / PS Box bridges due to creep and shrinkage produces significant lateral movements in the cast-in-place superstructures. When they are monolithically connected to the concrete piers, they continue to shorten because of their high axial stiffness compared to the lateral stiffness of the columns. As a result, displacement-induced forces are produced in columns (see Figure 1.1), which are significant in magnitude, but are not systematically addressed in the current design guidelines. Two specific design issues associated with this problem are: (1) unrealistic estimate for the shortening strain rate of the superstructure; and (2) not accurately accounting for the beneficial effects of concrete relaxation in columns on the displacement-induced column forces. Due to these issues, the displacement-induced column forces are suspected to be overestimated. When these forces are combined with the effects of other loads such as live loads and seismic loads, the result, as previously noted, is a larger column cross section, inefficient design of columns and foundation, increase in the adverse effects of time-dependent issues, and thus increased construction costs.

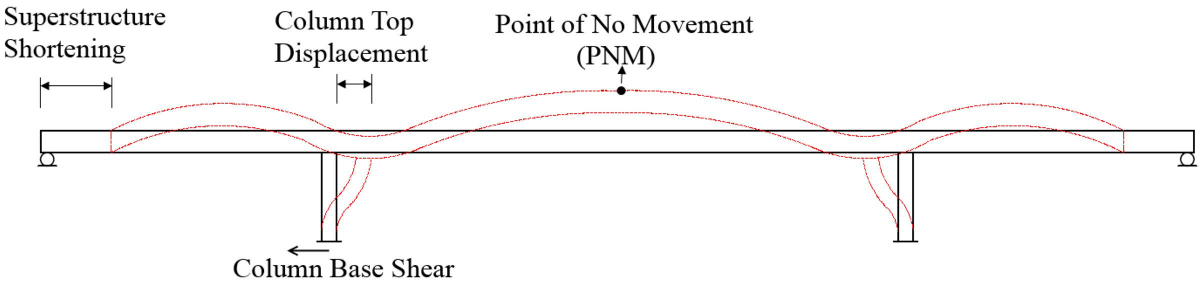

Figure 1.1: Continuous prestressed concrete bridge frame deformations due to axial force, creep and shrinkage

1.3 Design Practice

A state that uses a large number of CIP / PS Box bridges is California. Although computer models, appropriately capturing the members' stiffness, are routinely used for bridge design, a simplified hand calculation procedure that has been used by Caltrans to estimate the forces due to creep and shrinkage is as follows:

1. Assume shortening of the CIP / PS Box superstructure due to creep and shrinkage at a rate of 16 mm (0.052 ft) per 30.5 m (100 ft) of structure length. This assumption, as shown in Figure 1.2, is from a deck expansion joint design memorandum (Caltrans 1994-Attachment 4) and is based on approximating total long term shortening of 31 mm (0.1 ft) per 30.5 m (100 ft) and subtracting off 15 mm (0.048 ft) to account for the elastic shortening, creep, and shrinkage that takes place in the first 12 weeks. This memorandum may not be directly applicable for estimating column design shear forces induced by time dependent strains developed in the superstructure. However, a justification for the

approach described above is that use of a strain rate of 16 mm (0.052 ft) per 30.5 m (100 ft) for CIP / PS Box superstructures would adequately capture the expected forces in the columns.

2. Determine the location of point of no movement (PNM), where the longitudinal displacement of the CIP / PS Box superstructure frame due to the time-dependent effects can be assumed to be zero.
3. Multiply the strain rate by the distance of the column to the PNM to calculate the column top lateral displacement.
4. Calculate the column base shear force as the product of column displacement and stiffness based on the theory of elasticity with consideration to the column potentially experiencing flexural cracking (Caltrans 2015). The cracked column stiffness is typically approximated to 50% of gross stiffness.

The design guidelines described above, identified herein as the Caltrans Simplified Method (or Caltrans SM), have not been validated and the following concerns have been identified as part of the current research:

- The shortening strain rate of superstructures assumed for the column design force may not be appropriate. The deck joint and seal memorandum assumes a total shortening of 31 mm (0.1 ft) per 30.5 m (100 ft), which may be appropriate for deck joints (Caltrans 1994). However, the assumed shortening strain rate of 16 mm (0.63 in.) per 30.5 m (100 ft) for estimating the column forces due to CR and SH may not be accurate;
- The columns in a CIP / PS Box will undergo different degrees of lateral movements depending on the locations to PNM and thus assuming cracked section properties for all columns may not be appropriate; and

- The developed column forces will experience the beneficial effects of concrete relaxation due to the displacement constraints imposed by the superstructure, which should be adequately addressed. It is acknowledged that the simplified design approach is believed to make some accommodation for this in the process, but this aspect has not been validated.

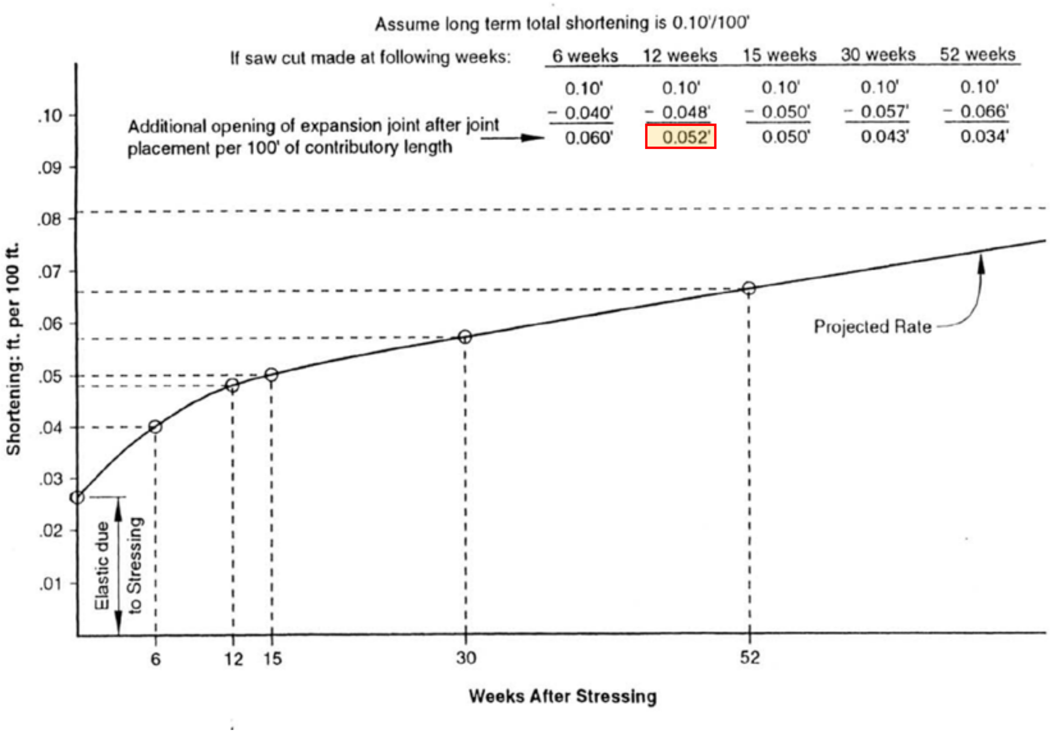

Figure 1.2: Shortening of prestressed concrete bridges due to prestressing, creep, and shrinkage as a function of time (Caltrans 1994- Attachment 4)

1.4 Scope of Research

The scope of research presented in this report is to improve the prediction of concrete time-dependent effects on CIP / PS Box, thereby estimating the displacement-induced forces more accurately in columns of CIP / PS Box. Giving consideration to the shortcomings of the Caltrans SM, the following tasks were used to accomplish the project scope:

1. Experimentally quantify the concrete relaxation with respect to its beneficial effects on displacement-induced column forces in CIP / PS Box bridges;

2. Examine the beneficial effects of concrete relaxation on the displacement-induced forces in the columns of a prototype CIP / PS Box using a detailed finite element model (FEM);
3. Select eight different CIP / PS Box bridges of various lengths and configurations for the study such that the analyses would include representative short-, medium-, and long-span California bridge frames, multiple and single column bents, pinned and fixed base columns, and varying amount of prestress;
4. Investigate the time-dependent effects on eight different CIP / PS Box frames using FEMs selected from the above task;
5. Systematically evaluate the range of expected shortening strain rate of the superstructure due to dead load, prestress, creep, and shrinkage imposed on California bridge columns and compare these ranges with the assumptions used in the current practice;
6. Assess the effects of time-dependent deformations on the behavior of columns in various California CIP / PS Box frame configurations; and
7. Develop rational design recommendations that may be used by engineers and consultants to account for these effects in routine bridge design.

1.5 Report Layout

Completed research presented in this report consists of seven chapters. Following the introductory chapter, an extensive literature review of time-dependent material properties, time-dependent analysis methods, and available prediction models for the time-dependent material properties are presented in Chapter 2. Chapter 3 describes the experimental program conducted at the Iowa State University structural laboratory to quantify concrete relaxation with respect to its beneficial effects on the displacement-induced column forces in CIP / PS Box frames. In Chapter 4, the details of the eight CIP / PS Box frames and the selected frames for the analytical investigation are presented, which shows the variation in span lengths, cross section of the superstructure, elevation views, and foundation type across the eight frames. The details of the FEM and the methodology used to examine the time-dependent effects are described for one of the eight box-girder frames in detail in Chapter 5. In this chapter, model assumptions, material models, beneficial effects of concrete relaxation, moment curvature analysis of columns, details of construction stages, and loading ages for creep and relaxation are discussed. In line with findings presented in Chapter 5, design recommendations are provided in Chapter 6 to incorporate the time-dependent effects in the design of frame columns by examining eight different CIP / PS Box frames. Finally, Chapter 7 provides a summary of research and the corresponding conclusions as well as recommendations for future work to validate the analytical findings of this study.

CHAPTER 2: LITERATURE REVIEW

2.1 Overview

Over the years, prestressed concrete has established itself as a preferred choice for bridge design because it satisfies engineering, economic, and aesthetic criteria. Prestressing in bridges is utilized to counteract high internal tensile forces and stresses due to dead and live loads by developing axial compression, which also minimizes the deflection as well of restressed members.

Prestressed concrete offers many advantages over conventional reinforced concrete. For example, prestressed concrete allows for the use of stronger materials, such as high-strength steel (with yield strengths of 270 ksi) and high-strength concrete (with compressive strengths in excess of 5 ksi). These materials cannot be used effectively with conventional reinforced concrete since their properties lead to cost effective design solutions. The higher strength concrete and steel allow for smaller and lighter sections, than those used for conventional reinforced concrete members with the same load carrying capacity. Cracking, deflections, and service load stresses can be controlled easily using these high-strength materials used in prestressed concrete. In general, except for chemical prestressing, the methods of applying prestress can be ramified into two major groups: pretensioning and posttensioning.

Concrete and steel strands are considered the main constituents of each prestressing method. High-strength steel with low relaxation characteristic is generally used to accommodate high elongations. High-strength concrete is primarily used to sustain the high compressive stresses and exhibit lower volume changes. In recent years, the Federal Highway Administration (FWHA) has stimulated the development and implementation of high performance concrete (HPC) as well as ultra-high performance concrete (UHPC). The use of HPC in bridge design offers a way to utilize higher compressive strength while ensuring long-term durability in these already popular bridges. Increased span lengths and fewer structural components resulting from use of UHPC lead to cost savings during construction, while the bridges' longer service life (e.g., increased bridge deck longevity) reduces their lower life-cycle cost (Honarvar et al. 2016).

2.2 Posttensioned Concrete Box-Girder Bridges

In posttensioning, the prestressing tendons are stressed and anchored at the ends of the concrete member after the concrete has been cast and attained sufficient strength to securely withstand the prestressing force. The tendons used in posttensioning can be either bonded or unbonded to the concrete. Posttensioning is more suitable in cast-in-place construction where bridge girders are too large to be transported, even though it can be used in precast prestressed operations. Posttensioning is widely used in CIP / PS Box bridges to resist high internal forces and stresses.

A box-girder bridge is comprised of the main girders in the shape of a hollow box with generally a rectangular or trapezoidal cross section, as shown in Figure 2.1. Due to cast-in-place construction of box-girder bridges, any desired alignment in plan including straight, skew and curved bridges of various shapes can be accommodated. A box-girder bridge is specifically suited to bridges with significant curvature because of high torsional resistance. Typically, box-girders can be categorized using three definitions as follows:

1. Based on geometry: monocellular, monocellular with ribs or struts, and multicellular
2. Based on material: concrete, steel, and composite
3. Based on reinforcement: reinforced concrete, pretensioned concrete, and posttensioned concrete

The main constituents of a CIP / PS Box are typically either prestressed concrete, structural steel, or a composite of steel and reinforcement concrete. CIP / PS Boxs have been widely used for medium to long-span crossings since the 1950s. Despite the widespread use of such bridge systems, concerns have been expressed about the effects of creep, shrinkage, and corrosion of prestressing steel on their long-term performance and durability (Lark et al. 2004). Additionally, some cast-in-place long-span bridges have been found to exhibit excessive long-term mid-span deflections (Vitek 1995 and Bazant et al. 2012).

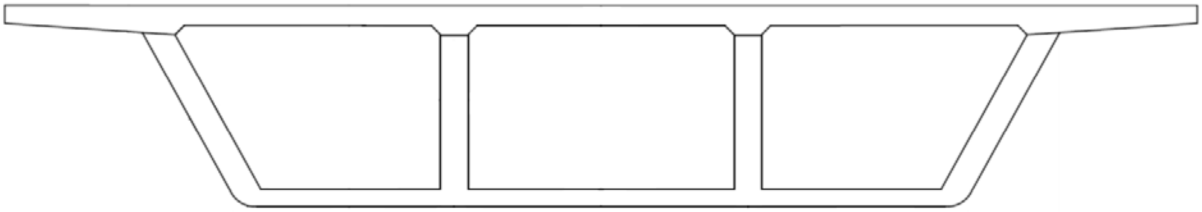

Figure 2.1: A typical cross sectional view of a CIP / PS Box used for bridge construction

2.3 Time-Dependent Material Properties

The behavior of CIP/ PS Box over time is dependent on the material behavior. Creep and shrinkage of concrete, and the relaxation of prestressing steel are the most significant parameters affecting the long-term stresses and deformations of CIP / PS Box. The long-term prestress losses in CIP / PS Box occur due to the creep and shrinkage of concrete and the relaxation of prestressing steel.

The time-dependent properties are best obtained from results of tests conducted on test samples made of materials used in the actual structure and subjected to conditions similar to those to which the structure will be subjected. Owing to the long period of time required to obtain such test results for each structure, reliable methods and equations for prediction of the aforementioned properties of concrete and prestressing steel are available in the literature and they are suitable for incorporation in computer programs for the required analysis. The most commonly used sources for prediction of these properties are AASHTO LRFD Bridge Design Specifications (2010), the CEB-FIP Mode1 Code (1990), and the ACI Committee 209 (1992).

2.3.1 Compressive Strength of Concrete

Compressive strength is the most common performance indicator of concrete, which is calculated from the failure load divided by the cross-sectional area of a concrete specimen. The compressive strength of concrete is affected by several factors, including the water-to-cementitious (w/c) ratio, mix proportion, and curing conditions. Typically, the compressive strength of concrete decreases when the w/c ratio increases. The compressive strength of concrete also depends on the strength of the aggregate itself and the relative ratio between the aggregate and cement paste. The higher the strength of the aggregate, the higher the compressive strength of concrete becomes. The cement type also plays an important role in the compressive strength of concrete. Because Portland Type III cement hydrates more rapidly than Type I, Type III cement would result in a higher early strength than Type I. In HPC, supplementary materials such as slag and fly ash are frequently added to increase the early strength of the concrete.

2.3.1.1 Prediction of Compressive Strength

The empirical Equation (2-1) recommended by ACI 209R may be used to calculate the compressive strength of concrete at different ages.

$$f_c'(t)=\frac{t}{\alpha+\beta t}f_c'(28) \quad \textbf{(2-1)}$$

where α and β are the constants and depend on the type of cement and the type of curing; $f_c'(28)$ is the 28-day compressive strength; and t is the age of concrete in days.

2.3.2 Modulus of Elasticity of Concrete

The modulus of elasticity is an important property of hardened concrete. Concrete is a composite material that includes aggregate and cement paste. The modulus of elasticity of concrete highly depends on the properties and proportions of the mixture materials. ASTM Standard C469 provides the method to measure the static modulus of elasticity of concrete in compression. The elastic modulus of concrete has a significant effect on the behavior of CIP / PS Box, including deflections and stresses. In Section 2.3.2.1, four prediction models to calculate the modulus of elasticity are presented.

2.3.2.1 Prediction of Modulus of Elasticity

Typically, the relation between the modulus of elasticity of concrete and the corresponding compressive strength is provided. This relation in not due to a direct relation between elastic moduli and compressive strength, but because the measurement of compressive strength is readily available. The following four models are commonly used for the prediction of the modulus of elasticity when the actual measurements are not available.

2.3.2.1.1 AASHTO LRFD (2010)

In the absence of measured data, the modulus of elasticity, E_c, for concretes with unit densities between 90 and 155 pcf and specified compressive strengths up to 15.0 ksi may be calculated using Equation (2-2).

$$E_c = 33\ K_1 w_c^{1.5} \sqrt{f_c'} \qquad \textbf{(2-2)}$$

where E_c is the elastic modulus of elasticity of concrete (psi); K_1 is the correction factor for a source of an aggregate to be taken as 1.0 unless determined by a physical test and approved by the authority of jurisdiction; w_c is the unit density for concrete (lb/ft3); and $f_c^{'}$ is the compressive strength of concrete (psi).

2.3.2.1.2 ACI 318-05 (1992)

The modulus of elasticity of concrete may be predicted using Equation (2-3) recommended by ACI 318-05.

$$E_c = 33\, w_c^{1.5}\sqrt{f_c^{'}} \qquad \textbf{(2-3)}$$

2.3.2.1.3 CEB-FIP (1990)

Values of the modulus of elasticity for normal weight concrete can be estimated from the specified characteristic strength by using Equation (2-4).

$$E_{ci} = E_{co}\left[\frac{f_{ck}+\Delta f}{f_{cmo}}\right]^{\frac{1}{3}} \qquad \textbf{(2-4)}$$

where E_{ci} is the modulus of elasticity (MPa) at a concrete age of 28 days; E_{co} is 2.15×10^4 MPa; f_{ck} is the characteristic strength (MPa) mentioned at Table 2.1.1 in CEB-FIP 1990; Δf is 8 MPa; and f_{cmo} is 10 MPa.

When the actual compressive strength of concrete at an age of 28 days f_{cm} is known, E_{ci} may be estimated using Equation (2-5).

$$E_{ci} = E_{co}\left[\frac{f_{cm}}{f_{cmo}}\right]^{\frac{1}{3}} \qquad \textbf{(2-5)}$$

When only an elastic analysis of a concrete structure is carried out, a reduced E_c can be calculated in order to account for an initial plastic strain using Equation (2-6).

$$E_c = 0.85\, E_{ci} \qquad \textbf{(2-6)}$$

2.3.2.1.4 Tadros (2003)

The modulus of elasticity of high performance concrete can be calculated using Equation (2-7).

$$E_c = 33{,}000\ K_1\ K_2 (0.140 + \frac{f'_c}{1000})^{1.5} \sqrt{f'_c} \quad (\ E_c \text{ and } f'_c \text{ are in ksi}) \qquad \textbf{(2-7)}$$

where K_1 is the correction factor for local material variability, and K_1 is 1.0 for the average of all data obtained by the author; K_2 is the correction factor based on the 90th percentile upper-bound and the 10th percentile lower-bound for all data, and for the average of all data K_2 is 0.777 (10th percentile) and K_2 is 1.224 (90th percentile).

2.3.3 Concrete Creep

Creep of any material in general is defined as the increase of strain with time under constant sustained stress. Concrete creep comprises of two components: basic creep and drying creep. Basic creep occurs under a condition of no moisture movement to or from the environment whereas drying creep which is the additional creep that occurs during drying of concrete. Both components affect prestress losses. The amount of creep observed in stressed concrete over time is a function of many variables. They include mixture proportions, level of applied stress, relative humidity, maturity of concrete when load is applied, and duration of load. Mixture proportions greatly affect concrete’s ability to resist creep, including type and amount of cement, aggregate properties, and water-to-cement ratio. Different types of cement experience different amounts of creep, and the inclusion of supplemental cementitious materials yields even more variability in creep of concrete. Creep effects are primarily a result of stress redistribution away from the paste and towards aggregate in the concrete. Stiffer aggregates resist more load and reduce creep. Also, aggregate with a rougher surface reduces creep because the load is better transferred along the paste-aggregate interface. Finally, the water-to-cementitious material ratio is significant as mixes with less free water lead to smaller volume changes due to creep.

As applied stress increases, greater creep can be expected. Creep is proportional to the stress level of the concrete up to a point of 40 to 60% of the concrete compressive strength. Relative humidity affects drying creep and hence the total creep. In regions with lower relative humidity, more creep can be expected. Concrete that is more mature when loaded will experience less total creep.

A typical stress-strain curve for concrete compressive behavior is shown in Figure 2.2. It is common practice to assume that the stress in concrete is linearly proportional to the strain in the service conditions. The strain occurring during the application of load, or immediately after the application of load, is referred to as the instantaneous strain and is defined by Equation (2-8).

$$\varepsilon_c(t_0) = \frac{\sigma_c(t_0)}{E_c(t_0)} \tag{2-8}$$

where $\sigma_c(t_0)$ is the concrete stress; $E_c(t_0)$ is the modulus of elasticity of concrete at age t_0; and t_0 is the time of application of the stress. The value of E_c, the secant modulus defined in Figure 2.2 depends on the magnitude of the stress, but this dependence is ignored in the practical applications. The value of E_c is typically proportional to the square root of concrete compressive strength, which is highly affected by the age of concrete at loading. Under sustained stress, the strain increases with time due to creep as shown in Figure 2.3, and the total stress-dependent strain (i.e., instantaneous plus creep strain) can be expressed using Equation (2-9) (Ghali et al. 2002).

$$\varepsilon_c(t) = \frac{\sigma_c(t_0)}{E_c(t_0)}[1 + \varphi(t, t_0)] = J(t, t_0)\sigma_c(t_0) \tag{2-9}$$

where $J(t, t_0)$ is the creep or compliance function and can be calculated using Equation (2-10); $\varphi(t, t_0)$ is a dimensionless coefficient and depends on the age at loading t_0; and t is age at which the total strain is calculated. The creep coefficient φ represents the ratio of creep strain to instantaneous strain. This value decreases with an increase of age at loading, t_0 and the decrease of the length of the period $(t - t_0)$ during which the stress is sustained.

$$J(t, t_0) = \frac{1+\varphi(t,t_0)}{E_c(t_0)} \qquad \textbf{(2-10)}$$

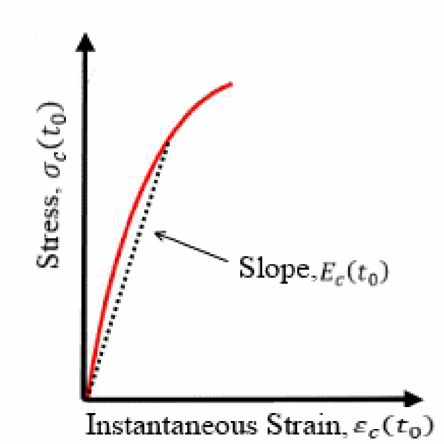

Figure 2.2: Concrete stress-strain curve

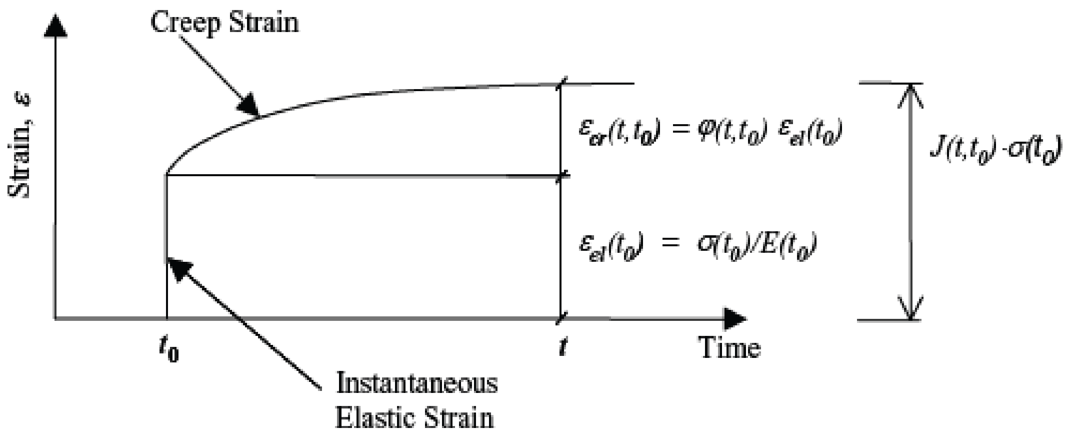

Figure 2.3: Concrete creep under the effect of sustained stress

2.3.3.1 Prediction of Concrete Creep

For the prediction of concrete creep without actual measurements of local material mixtures, the following five models are commonly used, including AASHTO LRFD Bridge Design Specifications (2010), ACI 209R (1990), Huo (2001), CEB-FIP (1990), and Bazant B3 Model (2000). CEB-FIP (1990) also provides a relation between the temperature and maturity of the concrete. Therefore, if concrete is steam-cured, the maturity of concrete after steam-curing could be calculated, and the adjusted age of concrete could be used in the creep and other concrete models of CEB-FIB.

2.3.3.1.1 AASHTO LRFD (2010)

Equations provided by AASHTO LRFD Bridge Design Specifications (2010) are applicable for a concrete strength up to 15.0 ksi. Equation (2-11) may be used to calculate the creep coefficient.

$$\Phi(t,t_i) = 1.9k_{vs}\ k_{hc}\ k_f\ k_{td}\ t_i^{-0.118} \qquad \textbf{(2-11)}$$

where t is the maturity of concrete (day), defined as the age of the concrete between the time of loading for the creep calculations, or the end of curing for shrinkage calculations, and the time being considered for the analysis of the creep or shrinkage effect. The age of the concrete is t_i (day) when the load is initially applied and k_{vs} is the factor for the effect of the volume-to-surface ratio and can be found using Equation (2-12).

$$k_{vs} = 1.45 - 0.13\left(\frac{V}{S}\right) \geq 1.0 \qquad \textbf{(2-12)}$$

or using the detailed Equation (2-13):

$$k_{vs} = \left[\frac{\frac{t}{26e^{0.0142(V/S)}+t}}{\frac{t}{45+t}}\right]\left[\frac{1.80+1.77e^{-0.0213(V/S)}}{2.587}\right] \qquad \textbf{(2-13)}$$

where v/s is the volume-to-surface ratio, and the maximum ratio is 6 inches.

k_{hc} is the humidity factor for the creep and can be found using Equation (2-14).

$$\mathrm{k_{hc}} = 1.56 - 0.008\mathrm{H} \qquad \textbf{(2-14)}$$

where H is the relative humidity of the ambient condition in percent.

k_f is the factor for the effect of the concrete strength and can be found using Equation (2-15).

$$\mathrm{k_f} = \frac{35}{7+\mathrm{f'_{ci}}} \qquad \textbf{(2-15)}$$

where f'_{ci} is the specified compressive strength of the concrete at the time of prestressing and at the time of the initial loading for nonprestressed members.

k_{td} is the time development factor and can be found using Equation (2-16).

$$\mathrm{k_{td}} = \frac{\mathrm{t}}{61-0.58\mathrm{f'_{ci}}+\mathrm{t}} \qquad \textbf{(2-16)}$$

2.3.3.1.2 ACI 209R (1992)

The expression for the creep coefficient at the standard condition is given in Equation (2-17). This equation is applicable for both 1-3 days of steam cured concrete and 7-day moist-cured concrete.

$$\mathrm{v_t} = \frac{\mathrm{t^{0.60}}}{10+\mathrm{t^{0.60}}}\mathrm{v_u} \qquad \textbf{(2-17)}$$

where t is the days after loading; ν_t is the creep coefficient after t days of loading; ν_u is the ultimate creep coefficient, and the average suggested value of ν_u is $2.35\times\gamma_c$; and γ_c is the correction factors for conditions other than the standard concrete composition, which is defined by Equation (2-18).

$\gamma_c = \gamma_{la}\,\gamma_\lambda\,\gamma_{vs}\,\gamma_s\,\gamma_\rho\,\gamma_\alpha$ **(2-18)**

where γ_{la} is the correction factor for the loading age, which is defined as:

$\gamma_{la} = 1.25t^{-0.118}$ for loading ages later than 7 days for moist cured concrete **(2-19)**

$\gamma_{la} = 1.13t^{-0.094}$ for loading ages later than 1 to 3 days for steam cured concrete **(2-20)**

γ_λ is the correction factor for the ambient relative humidity, which is defined by Equation (2-21).

$\gamma_\lambda = 1.27 - 0.0067\lambda$ for $\lambda > 40$ **(2-21)**

where λ is the relative humidity in percent.

γ_{vs} is the correction factor for the average thickness of a member or a volume-to-surface ratio. When the average thickness of a member is other than 6 in. or a volume-to-surface ratio is other than 1.5 in., two methods are offered: (1) average thickness method; and (2) volume-surface ratio method.

2.3.3.1.2.1 Average Thickness Method

For the average thickness of a member less than 6 in., the factors are given in Table 2.5.5.1 in ACI 209R (1992). For the average thickness of members greater than 6 in. and up to about 12 in. to 15 in., Equations (2-22) and (2-23) may be used.

$\gamma_{vs} = 1.14 - 0.023h$ during the first year after loading **(2-22)**

$\gamma_{vs} = 1.10 - 0.017h$ for ultimate values **(2-23)**

where h is the average thickness of the member in inches.

2.3.3.1.2.2 Volume to Surface Ratio Method

For members with a volume-to-surface area other than 1.5 in., Equation (2-24) can be used.

$$\gamma_{vs} = \frac{2}{3}\left[1 + 1.13e^{-0.54(\frac{v}{s})}\right] \quad \textbf{(2-24)}$$

where v/s is the volume to surface ratio in inches.

γ_s is the correction factor for slump, and can be determined using Equation (2-25).

$$\gamma_s = 0.82 + 0.067s \quad \textbf{(2-25)}$$

where s is the observed slump in inches.

γ_ρ is the correction factor for the fine aggregate percentage, which is defined by Equation (2-26).

$$\gamma_\rho = 0.88 + 0.0024\rho \quad \textbf{(2-26)}$$

where ρ is the ratio of the fine aggregate to total aggregate by weight expressed as a percentage.

γ_α is the correction factor for the air content, which is defined by Equation (2-27).

$$\gamma_\alpha = 0.46 + 0.09\alpha \geq 1.0 \quad \textbf{(2-27)}$$

where α is the air content in percent.

2.3.3.1.3 Huo (2001)

This model is the same as ACI 209 (1990), with an additional modification factors for the compressive strength, as expressed in Equation (2-28).

$$v_t = \frac{t^{0.60}}{K_C + t^{0.60}} v_u \quad \textbf{(2-28)}$$

where

$$K_C = 12 - 0.5f_c' \tag{2-29}$$

$\gamma_{st,c}$ is the correction factor, which is additionally introduced in Equation (2-18) to account for the compressive strength of concrete and can be found using Equation (2-30).

$$\gamma_{st,c} = 1.18 - 0.045f_c' \tag{2-30}$$

where f_c' is the 28-day compressive strength in ksi.

2.3.3.1.4 CEB-FIP (1990)

Equation (2-31) is recommended by CEB-FIP (1990) to calculate creep coefficient.

$$\varphi(t, t_0) = \varphi_0\beta_c(t - t_0) \tag{2-31}$$

where t is the age of concrete (days) at which creep coefficient is calculated; t_0 is the age of concrete at the time of loading (days); φ_0 is the notional creep coefficient and is calculated using Equation (2-32); and β_c is the coefficient to describe the development of the creep with time after the loading.

$$\varphi_0 = \varphi_{RH}\,\beta(f_{cm})\beta(t_0) \tag{2-32}$$

where φ_{RH} is the coefficient for the relative humidity and the dimension of member, and is calculated using Equation (2-33).

$$\varphi_{RH} = 1 + \frac{1 - RH/RH_0}{0.46 \cdot (h/h_0)^{1/3}} \tag{2-33}$$

where RH is the relative humidity of the ambient environment in percent (%), RH_0 is 100%; and h is the notational size of the member (mm), and is defined as $2A_c/u$, where A_c is the area of a cross section, and u is the perimeter of the member in contact with the atmosphere; and h_0 is 100 mm.

$$\beta(f_{cm}) = \frac{5.3}{(f_{cm}/f_{cmo})^{0.5}} \quad \textbf{(2-34)}$$

where f_{cm} is the mean compressive strength of the concrete at the age of 28 days (MPa); and f_{cmo} is 10 MPa.

$$\beta(t_0) = \frac{1}{0.1 + (t_0/t_1)^{0.2}} \quad \textbf{(2-35)}$$

where t_1 is taken as 1 day.

The expression for the development of the creep with time is given by Equation (2-36).

$$\beta_c(t - t_0) = [\frac{(t - t_0)/t_1}{\beta_H + (t - t_0)/t_1}]^{0.3} \quad \textbf{(2-36)}$$

where:

$$\beta_H = 150\left[1 + 1.2(\frac{RH}{RH_0})^{18}\right]\frac{h}{h_0} + 250 \leq 1500 \cdot \quad \textbf{(2-37)}$$

where t_1 is 1 day; RH_0 is 100%; and h_0 is 100 mm.

If concrete undergoes elevated or reduced temperature, the maturity of the concrete could be calculated using Equation (2-38).

$$t_T = \sum_{i=1}^{n} \Delta t_i \, e^{\left[13.65 - \frac{4000}{273 + T(\Delta t_i)/T_0}\right]} \quad \textbf{(2-38)}$$

where t_T is the maturity of the concrete, which can be used in the creep and shrinkage models; Δt_i is the number of days where a temperature T prevails; $T(\Delta t_i)$ is the temperature (°C) during the time of period Δt_i; and T_0 is 1 °C.

2.3.3.1.5 Bazant B3 (2000)

The compliance function for loaded specimens is expressed by Equation (2-39).

$$J(t,t') = q_1 + C_0(t,t') + C_d(t,t',t_0) \quad \textbf{(2-39)}$$

where q_1 is the instantaneous strain due to the unit stress and can be found using Equation (2-39).

$$q_1 = \frac{10^6}{E_{ci}} \text{ or } \frac{6\times10^6}{E_{c28}} \quad \textbf{(2-40)}$$

in which

$E_{ci} = 57000\sqrt{f'_{ci}}$ (f'_{ci} is the compressive strength at the age of loading, psi) **(2-41)**

$E_{c28} = 57000\sqrt{f'_{c28}}$ (f'_{c28} is the 28-day compressive strength, psi) **(2-42)**

$C_0(t, t')$ is the compliance function for the basic creep (in/in/psi) and can be found using Equation (2-43).

$$C_0(t,t') = q_2Q(t,t') + q_3\ln[1+(t-t')^n] + q_4\ln({}^{t}/_{t'}) \quad \textbf{(2-43)}$$

where t is the age of the concrete after casting (days); t' is age of the concrete at the loading (days); and t_0 is the age of the concrete at the beginning of the shrinkage (days).

$q_2 = 451.4\ c^{0.5}\ {f'_{c28}}^{0.9}$ (c is the cement content in pcf) **(2-44)**

$$Q(t,t') = Q_f(t')\left[1+\frac{Q_f(t')^{\Upsilon(t')}}{Z(t,t')}\right]^{{}^{1}/_{\Upsilon(t')}} \quad \textbf{(2-45)}$$

$$Q_f(t') = \left[0.056(t')^{{}^{2}/_{9}} + 1.21(t')^{{}^{4}/_{9}}\right]^{-1} \quad \textbf{(2-46)}$$

$$Z(t,t') = t'^{-m}\ln[1+(t-t')^n] \ (m = 0.5, n = 0.1) \quad \textbf{(2-47)}$$

$$\Upsilon(t') = 1.7(t')^{0.12} + 8 \quad \textbf{(2-48)}$$

$C_d(t, t', t_0)$ is the additional compliance function due to the simultaneous drying (in/in/psi) and can be found using Equation (2-49).

$$\mathrm{C_d(t, t', t_0) = q_5\left[e^{-8H(t)} - e^{-8H(t')}\right]^{1/2}} \quad \textbf{(2-49)}$$

$$\mathrm{q_5 = 7.57 \times 10^5 (f'_{c28})^{-1} |(\varepsilon_{sh\infty})^{-0.6}|} \quad \textbf{(2-50)}$$

$$\mathrm{\varepsilon_{sh\infty}} = \alpha_1 \alpha_2 [26 w^{2.1} (\mathrm{f'_{c28}})^{-0.28} + 270] \text{ (ω is the water content in pcf)} \quad \textbf{(2-51)}$$

with:

$$\alpha_1 = \begin{cases} \text{1.0 for type I cement} \\ \text{0.85 for type II cement} \\ \text{1.1 for type III cement} \end{cases} \quad \textbf{(2-52)}$$

and

$$\alpha_2 = \begin{cases} \text{0.75 for steam} - \text{curing} \\ \text{1.2 for sealed or normal curing in air with inital protection against drying} \\ \text{1.0 for curing in water or at 100\% relative humidity} \end{cases} \quad \textbf{(2-53)}$$

$$\mathrm{H(t) = 1 - (1 - h)S(t)} \quad \textbf{(2-54)}$$

where *h* is the relative humidity.

$$\mathrm{S(t) = tanh\left[\frac{t - t_0}{\tau_{sh}}\right]^{1/2}} \quad \textbf{(2-55)}$$

$$\mathrm{\tau_{sh} = k_t (k_s D)^2} \quad \textbf{(2-56)}$$

$$\mathrm{D = 2v/s} \quad \textbf{(2-57)}$$

$$\mathrm{k_t = 190.8 (t_0)^{-0.08} (f'_{c28})^{-0.25}} \quad \textbf{(2-58)}$$

$\mathrm{k_s} = 1$ for infinite slab

= 1.15 for infinite cylinder

= 1.25 for infinite square prism

= 1.30 for sphere

= 1.55 for cube

= 1.00 for undefined member

$$H(t') = 1 - (1 - h)S(t') \qquad \textbf{(2-59)}$$

$$S(t') = \tanh\left[\frac{t' - t_0}{\tau_{sh}}\right]^{1/2} \qquad \textbf{(2-60)}$$

The creep strain should be calculated using Equation (2-61).

$$\epsilon_{cr} = [C_0(t, t') + C_d(t, t', t_0)\,]\sigma \qquad \textbf{(2-61)}$$

where σ is the applied stress in psi.

The creep coefficient should be expressed by Equation (2-62).

$$\varphi(t, t') = \frac{\epsilon_{cr}}{q_1\sigma} \qquad \textbf{(2-62)}$$

The total strain may be expressed by Equation (2-63).

$$\epsilon_{total} = J(t, t')\sigma + \epsilon_{sh} \qquad \textbf{(2-63)}$$

where ε_{sh} is the shrinkage strain and can be estimated using the equations presented in Section 2.3.5.1.5.

2.3.4 Concrete Relaxation

Relaxation is the loss of stress under a state of constant strain for viscoelastic materials such as steel, concrete, and aluminum. Creep and relaxation are two alternative descriptions of the same phenomenon but different manifestation of the same fundamental viscoelastic properties. If a structural concrete member can freely deform under a permanent constant stress, its deformation increases due to creep. If free development of creep deformation is prevented, then the original stress is reduced over time, i.e., relaxation takes place.

When a concrete member is subjected to an imposed axial stress at time t_0, which varies with time, the stress-dependent strain as a function of time may be written as shown in Equation (2-64).

$$\varepsilon_c(t) = \frac{\sigma_c(t_0)}{E_c(t_0)}[1+\varphi(t,t_0)] + \int_0^{\tau} \frac{1+\varphi(t,\tau)}{E_c(\tau)} d\sigma_c(\tau) = \sigma_c(t_0) \times J(t,t_0) + \int_0^{\tau} J(t,\tau)\, d\sigma_c(\tau) \qquad \textbf{(2-64)}$$

where $E_c(t_0)$ is the modulus of elasticity of concrete at age t_0; τ is an indeterminate age between t_0 and t; $\sigma_c(t_0)$ is the initial stress applied at age t_0; $d\sigma_c(\tau)$ is an elemental stress applied at age τ; $E_c(\tau)$ is the modulus of elasticity of concrete at age τ; $\varphi(t,\tau)$ is the creep coefficient at time t for loading at age τ; and $J(t,t_0)$ and $J(t,\tau)$ are the creep functions at time t for loading at age t_0 and τ, respectively.

If the length of the member is subsequently maintained constant, the strain ε_c will not change, but the stress will gradually decrease because of creep. The value of stress at any time $t > t_0$ may be defined by Equation (2-65) (Ghali et al. 2002).

$$\sigma_c(t) = \varepsilon_c\, R(t,t_0) \qquad \textbf{(2-65)}$$

where $R(t,t_0)$ is the relaxation function and can be mathematically determined using the time-step method, provided the concrete creep behavior. $R(t,t_0)$ is defined as the stress at age t due to a unit strain introduced at age t_0 and sustained constant during the period $(t-t_0)$.

Using a unit step function for the history of stress-dependent strain, the history of stress is consequently represented by the relaxation function as expressed by Equation (2-65).

$$\sigma_c(t) = R(t, t_0) \quad \textbf{(2-66)}$$

Subsequently, combining Equations (2-66) and (2-64) yields Equation (2-67).

$$R(t, t_0) \times J(t, t_0) + \int_0^\tau J(t, \tau)\, d\sigma_c(\tau) = E_C(t_0) \times J(t, t_0) + \int_0^\tau J(t, \tau)\, d\sigma_c(\tau) = 1 \quad \textbf{(2-67)}$$

Subdividing time t by discrete times t_0, t_1,…t_i…t_k into sub intervals $\Delta t_i = t_i - t_{i-1}$ (with $\Delta t_1 = t_1 - t_0 = 0$ and as a result $\Delta_{\varepsilon c}(t_1) = 1$), Equation (2-67) may be expressed by Equation (2-68).

$$\sum_{i=1}^{k} \frac{1}{2} [J(t_k, t_i) + J(t_k, t_{i-1})] \Delta R(t_i) = 1 \quad \textbf{(2-68)}$$

For $t = t_{k-1}$ (k>1), Equation (2-68) can be rewritten as shown in Equation (2-69).

$$\sum_{i=1}^{k} \frac{1}{2} [J(t_{k-1}, t_i) + J(t_{k-1}, t_{i-1})] \Delta R(t_i) = 1 \quad \textbf{(2-69)}$$

By subtracting Equation (2-68) from Equation (2-67), the relaxation function may be calculated using Equations (2-70) and (2-71).

$$\Delta R(t_i) = -\frac{\sum_{i=1}^{k} [J(t_k, t_i) + J(t_k, t_{i-1}) - J(t_{k-1}, t_i) - J(t_{k-1}, t_{i-1})] \Delta R(t_i)}{J(t_k, t_k) + J(t_k, t_{k-1})} \qquad \text{when } k > 1 \quad \textbf{(2-70)}$$

$$\Delta R(t_i) = \frac{1}{J(t_1, t_1)} = \frac{1}{J(t_0, t_0)} = E_C(t_0) \qquad \text{when } k = 1 \quad \textbf{(2-71)}$$

However, Bazant (1979) showed that the exact solution presented in Equation (2-70) may be approximated by Equation (2-72) with 2% error between the exact and approximate solution.

$$R(t, t_0) = \frac{1 - \Delta_0}{J(t, t_0)} - \frac{0.115}{J(t, t-1)} \left[\frac{J(t_0 + \xi, t_0)}{J(t, t - \xi)} - 1\right] \quad \textbf{(2-72)}$$

where $\mathit{\Delta}_0$ is the coefficient for age-independent correction and can be neglected except for $(t - t_0) < 1\ day$, where $\Delta_0 \approx 0.008$; and the optimum value of ξ can be found using Equation (2-73).

$$\xi = \frac{1}{2}(t - t_0) \quad \textbf{(2-73)}$$

Additionally, if the stress remains constant over time the relaxation function can be calculated directly from Equation (2-64), which yields to Equation (2-74).

$$R(t, t_0) = \frac{1}{J(t,t_0)} \quad \textbf{(2-74)}$$

2.3.5 Concrete Shrinkage

Shrinkage of concrete is the decrease in its volume under zero stress due to loss of moisture. Shrinkage of concrete occurs at several stages during the life of a prestressed member and is caused by different mechanisms. However, not all types of shrinkage lead to loss of prestress. First, plastic shrinkage refers to a volume loss due to moisture evaporation in fresh concrete, generally at exposed surfaces (Mindess et al. 2002). This shrinkage occurs before prestressing force is applied and does not affect the long-term prestressing forces. Drying shrinkage is the strain due to loss of water in hardened concrete (Mindess et al. 2002). Since drying shrinkage occurs in hardened concrete, it affects the time-dependent behavior and loss of prestress. Drying shrinkage occurs almost entirely in the paste of the concrete matrix, with aggregate providing some restraint against volume changes. Since drying shrinkage involves moisture loss, it is largely affected by the ambient relative humidity. Drying shrinkage is also affected by the specimen’s shape and size if there is a large surface area to volume ratio that can cause more moisture to escape from concrete. Additionally, drying shrinkage is affected by the concrete porosity, which is a function of mixture proportions and curing conditions. Two special cases of drying shrinkage in hardened concrete are autogeneous and carbonation shrinkage. Since both occur after the concrete is hardened, they can contribute to the time-dependent behavior of concrete. Autogeneous shrinkage occurs as cement paste hydrates, because the volume of hydrated cement paste is less than the total solid volume of unhydrated cement and water. Carbonation shrinkage results from the carbonation of the calcium-silicate-hydrate molecules in concrete, which causes a decrease in volume (Mindess et al. 2002). Due to the complex and uncertain nature of shrinkage, most predictive models are empirical fits to experimental data. In most cases the models asymptotically approach an ultimate shrinkage value that was determined from the test data and can be further adjusted by a series of factors which account for differences between the test conditions and the in-situ conditions.

Stresses develop when the change in volume by shrinkage is restrained, which may be caused by the presence of reinforcing steel, by the supports, and/or by the difference in volume change of various parts of the structure. These stresses due to shrinkage are generally alleviated by the effect of concrete creep. Hence, in the stress analysis, the effects of these two simultaneous phenomena should be taken into account. At time t_0, when moist curing terminates, shrinkage starts to develop. The strain that develops due to free shrinkage between t_s and a later time t may be expressed by Equation (2-75) (Ghali et al. 2002).

$$\mathrm{\varepsilon_{cs}(t, t_s) = \varepsilon_{cs0}\beta_s(t - t_s)} \quad \textbf{(2-75)}$$

where ε_{cs0} is the total shrinkage that occurs after concrete hardening up to the infinity. The values of ε_{cs0} depends on the quality of concrete and the ambient air humidity. The function $\beta_s(t - t_s)$ depends on the size and shape of the element considered.

2.3.5.1 Prediction of Shrinkage of Concrete

For the prediction of the shrinkage of concrete, several models are typically used, including AASHTO LRFD Bridge Design Specifications (2010), ACI 209R (1990), Huo (2001), CEB-FIP (1990), and Bazant B3 Model (2000). They are considered to be appropriate in the absence of measured data.

2.3.5.1.1 AASHTO LRFD (2010)

The expression for the shrinkage strain is given by Equation (2-76), for which the ultimate shrinkage strain is taken as 0.00048 in./in.

$$\varepsilon_{sh} = k_{vs} k_{hs} k_f k_{td} 0.48 \times 10^{-3} \qquad \textbf{(2-76)}$$

where

$$k_{vs} = 1.45 - 0.13\left(\frac{v}{s}\right) \geq 1.0 \qquad \textbf{(2-77)}$$

or is obtained from a detailed expression given in Equation (2-78).

$$k_{vs} = \left[\frac{\frac{t}{26 \cdot e^{0.0142\left(\frac{v}{s}\right)} + t}}{\frac{t}{45+t}}\right]\left[\frac{1064 - 3.7\left(\frac{v}{s}\right)}{923}\right] \text{ (maximum v/s is 6 in.)} \qquad \textbf{(2-78)}$$

k_{hs} is the humidity factor and can be found using Equation (2-79).

$$k_{hs} = 2.00 - 0.014H \qquad \textbf{(2-79)}$$

2.3.5.1.2 ACI 209R (1992)

The expression for the shrinkage strain at the standard condition is given by Equations (2-80) and (2-81).

$$\varepsilon_{sh} = \frac{t}{35+t}(\varepsilon_{sh})_u \text{ shrinkage after 7 days for moist cured concrete} \qquad \textbf{(2-80)}$$

$$\varepsilon_{sh} = \frac{t}{55+t}(\varepsilon_{sh})_u \text{ shrinkage after 1-3 days for steam cured concrete} \qquad \textbf{(2-81)}$$

where t is days after the end of the initial wet curing; $(\varepsilon_{sh})_t$ is shrinkage strain after t days; and $(\varepsilon_{sh})_u$ is the ultimate shrinkage strain, and the suggested average value can be found using Equation (2-82).

$$(\varepsilon_{sh})_u = 780\gamma_{sh} \times 10^{-3} \frac{in.}{in.}$$ **(2-82)**

where γ_{sh} is the correction factors for conditions other than the standard concrete composition, which is defined by Equation (2-83).

$$\gamma_{sh} = \gamma_\lambda \gamma_{vs} \gamma_s \gamma_\rho \gamma_c \gamma_\alpha$$ **(2-83)**

where γ_λ is correction factor for the ambient relative humidity and can be determined using Equations (2-84) and (2-85).

$\gamma_\lambda = 1.40 - 0.0102\lambda$ for $40 \leq \lambda \leq 80$, where λ is the relative humidity in percent **(2-84)**

$\gamma_\lambda = 3.00 - 0.030\lambda$ for $80 < \lambda \leq 100$, where λ is the relative humidity in percent **(2-85)**

γ_{vs} is the correction factor for the average thickness of a member or volume-to-surface ratio. When the average thickness of a member is other than 6 in. or the volume-to-surface ratio is other than 1.5 in., two methods are proposed: (1) average thickness method; and (2) volume-surface ratio method.

2.3.5.1.2.1 Average Thickness Method

For the average thickness of members less than 6 in. (150 mm), the factors are given in Table 2.5.5.1 which is found in ACI 209R (1992). For the average thickness of members greater than 6 in. and up to 12 to 15 in., Equations (2-86) and (2-87) are given.

$\gamma_{vs} = 1.23 - 0.038h$ during the first year after loading **(2-86)**

$\gamma_{vs} = 1.17 - 0.029h$ for ultimate values **(2-87)**

where h is the average thickness of the member in inches.

2.3.5.1.2.2 Volume to Surface Ratio Method

For members with a volume-to-surface area other than 1.5 in., the following equations are given:

$$\gamma_{vs} = 1.2e^{-012(\frac{v}{s})} \qquad \textbf{(2-88)}$$

where v/s is the volume-surface ratio in inches.

γ_s is the correction factor for slump, and can be found using Equation (2-89).

$$\gamma_s = 0.89 + 0.041s \qquad \textbf{(2-89)}$$

where s is the observed slump in inches.

γ_ρ is the correction factor for the fine aggregate percentage, which is defined by Equations (2-90) and (2-91).

$$\gamma_p = 0.30 + 0.014\rho, \text{when } \rho \leq \ 50 \text{ percent} \qquad \textbf{(2-90)}$$

$$\gamma_p = 0.90 + 0.002\rho, \text{when } \rho > \ 50 \text{ percent} \qquad \textbf{(2-91)}$$

where ρ is the ratio of the fine aggregate to the total aggregate by weight expressed as a percentage.

γ_c is the correction factor for the cement content, which is defined by Equation (2-92).

$$\gamma_c = 0.75 + 0.00036c \qquad \textbf{(2-92)}$$

where c is the cement content in lb/yd^3.

γ_α is the correction factor for the air content, which is defined by Equation (2-93).

$$\gamma_\alpha = 0.95 + 0.008\alpha \qquad \textbf{(2-93)}$$

where α is the air content in percent.

2.3.5.1.3 Huo (2001)

This model is the same as ACI 209 (1990), with an additional modification factors for the compressive strength, as shown in Equation (2-94).

$$\varepsilon_{sh} = \frac{t}{K_s + t}(\varepsilon_{sh})_u \qquad \textbf{(2-94)}$$

where

$$K_s = 45 - 2.5f_c' \qquad \textbf{(2-95)}$$

$\gamma_{st,s}$ is the correction factor, which is additionally introduced in Equation (2-83) to account for the compressive strength of concrete and can be found using Equation (2-96).

$$\gamma_{st,s} = 1.20 - 0.05f_c' \qquad \textbf{(2-96)}$$

where f_c' is the 28-day compressive strength in ksi.

2.3.5.1.4 CEB-FIP (1990)

Equation (2-97) is given by CEB-FIP (1990) to calculate shrinkage strain.

$$\varepsilon_{cs}(t, t_s) = \varepsilon_{cs0}\beta_s(t - t_s) \qquad \textbf{(2-97)}$$

where ε_{cs0} is the notional shrinkage coefficient; β_s is the coefficient to describe the development of shrinkage with time; t is the age of concrete (days); and t_s is the age of concrete (days) at the beginning of the shrinkage.

The notional shrinkage coefficient is given by Equation (2-98).

$$\varepsilon_{cs0} = \varepsilon_s(f_{cm})\beta_{RH} \qquad \textbf{(2-98)}$$

and,

$$\varepsilon_s(f_{cm}) = \left[160 + 10\beta_{sc}(9 - \frac{f_{cm}}{f_{cm0}})\right] \times 10^{-6} \qquad \textbf{(2-99)}$$

where f_{cm} is the mean compressive strength of concrete at the age of 28 days (MPa); f_{cm0} is 10 MPa; β_{sc} is the coefficient which depends on the type of cement: β_{sc} is 4 for slowly hardening cements SL, β_{sc} is 5 for normal or rapid hardening cements N and R, and β_{sc} is 8 for the rapid hardening high strength cements RS.

$$\beta_{RH} = -1.55\beta_{sRH} \; for \; 40\% \leq RH \leq 99\% \qquad \textbf{(2-100)}$$

$$\beta_{RH} = +0.25 \text{ for } RH > 99\% \qquad \textbf{(2-101)}$$

where

$$\beta_{sRH} = 1 - (\frac{RH}{RH_0})^3 \qquad \textbf{(2-102)}$$

where RH is the relative humidity of the ambient atmosphere (%) and RH_0 is 100%.

The development of the shrinkage with time is given by Equation (2-103).

$$\beta_s(t - t_s) = \left[\frac{(t - t_s)/t_1}{350 \cdot (h/h_0)^2 + (t - t_s)/t_1}\right]^{0.5} \qquad \textbf{(2-103)}$$

where h is the notational size of member (mm), and is defined as $2A_c/u$, where A_c is the area of cross section, and u is the perimeter of the member in constant with the atmosphere. Also, h_0 is100 mm, and t_1 is one day.

2.3.5.1.5 Bazant B3 Model (2000)

In this model, the shrinkage strain is expressed using Equation (2-104).

$$\varepsilon_{sh}(t, t') = \varepsilon_{sh\infty} K_h S(t) \qquad \textbf{(2-104)}$$

where $\varepsilon_{sh\infty}$ could be calculated using Equation (2-51); $S(t)$ could be calculated by using Equation (2-55); and K_h could be calculated using Equation (2-105).

$$\mathrm{K_h} = \begin{cases} 1 - \mathrm{h}^3 \text{ for } \mathrm{h} < 0.98 \\ -0.2 \text{ for } \mathrm{h} = 1 \\ \text{use linear interpolation for } 0.98 < \mathrm{h} < 1 \end{cases} \qquad \textbf{(2-105)}$$

2.3.6 Relaxation of Prestressing Steel

Steel relaxation is a loss of stress in the prestressing steel when held at a constant strain (i.e., intrinsic relaxation). The strands typically used in practice today are called low-relaxation strands. They undergo a strain tempering process during production that heats them to about 660°F and then cools while under tension. This process reduces relaxation losses to approximately 25% of that for stress-relieved strand. Equation (2-106) is widely used to calculate the intrinsic relaxation of prestressing steel at any time τ (Ghali et al. 2002).

$$\frac{\Delta\sigma_{\mathrm{pr}}}{\sigma_{\mathrm{p0}}} = \frac{\log(\tau - t_0)}{10}\left[\frac{\sigma_{\mathrm{p0}}}{f_{\mathrm{py}}} - 0.5\right] \qquad \textbf{(2-106)}$$

where f_{py} is the yield strength, defined as the stress at a strain rate of 0.01. The ratio of f_{py} to the characteristic tensile stress, f_{ptk} varies between 0.8 and 0.9, with lower value for prestressing bars and the higher value for low-relaxation strands; σ_{p0} in the initial stress; and $(\tau - t_{0)}$ is the period of time in hours for which the tendon is stretched.

2.3.6.1 Reduced Relaxation

In case of a prestressed concrete member, the prestressing strand is not held at constant strain because the actions of elastic shortening, shrinkage and creep of the concrete continuously reduce the tension strain in the steel. Therefore, the relaxation is expected to be smaller than the intrinsic value. The intrinsic relaxation of the steel resulting from maintaining constant strain must be considered in developing a procedure to estimate prestress loss. Thus, Equation (2-107) can be used to calculate the reduced relaxation value in prestressed concrete members (Ghali et al. 2002).

$$\Delta\overline{\sigma}_{\mathrm{pr}} = \chi_{\mathrm{r}}\Delta\sigma_{\mathrm{pr}} \qquad \textbf{(2-107)}$$

where $\Delta\sigma_{pr}$ is the intrinsic relaxation that would occur in a constant length relaxation test and can be calculated using Equation (2-105); and χ_r is a dimensionless coefficient smaller than unity.

2.4 Prestress Losses

The prestressing force in tendons of a CIP/ PS Box continuously decreases with time, and asymptotically levels off after a long time. The losses in prestressing force comprised of two major time components: (1) short-term losses, which occur immediately after the transfer of prestressing force; (2) long-term losses, which occur due to time-dependent material properties. Total loss of pretressing force in a CIP/ PS Box is the summation of short-term losses and long-term losses, which is typically attributed to the cumulative contribution of the following sources (Naaman 2004):

- Elastic shortening: Elastic shortening occurs when there is a reduction in strain in the prestressing strands at the transfer of prestress due to the concrete member shortening.
- Friction: The friction between the posttensioned tendons and the concrete during the tensioning process results in losses in the presressing force.
- Seating: Seating is the movement of prestressing steel when it is allowed to rest in the anchorage, which leads to a loss of stress in the tendon.
- Relaxation of prestressing steel: Relaxation occurs due to the loss in tension in a prestressing strand with respect to time when it is held at a constant length or strain.
- Concrete creep: The compressive stress caused by the concrete creep induces a shortening strain in the concrete which leads to loss of prestressing force in tendons.

- Concrete shrinkage: The free water is gradually lost from the concrete as a result of concrete shrinkage, which creates a shortening in the concrete producing losses in the presressing force.

For a CIP/ PS Box, the total prestress losses, ΔP_T, can be defined by Equation (2-108).

$$\Delta P_T = \Delta P_{ST} + \Delta P_{LT} \qquad \textbf{(2-108)}$$

where ΔP_{ST} is the total short-term losses and ΔP_{LT} is the total long-term losses.

The calculation of the short-term losses is a more straightforward task than the calculation of long-term losses due to complexity of time-dependent material behavior, and the interaction among the different long-term losses.

2.4.1 Prediction of Short-Term Losses

Assuming tendons are posttensioned simultaneously which eliminates the elastic shortening losses, short-term losses primarily occurs due to seating and friction between the prestress tendons and sheathing. Thus, the short-term losses can be calculated using Equation (2-109).

$$\Delta P_{ST} = \Delta P_F + \Delta P_S \qquad \textbf{(2-109)}$$

where ΔP_F is the prestress loss due to friction, and ΔP_S is the prestress loss due to seating, which can be estimated using the equations presented in Sections 2.4.1.1 and 2.4.1.2, respectively.

2.4.1.1 Prestress Loss Due to Friction

In a posttensioned concrete member, friction loss is due to a combination of linear and curvature effects. The linear effect, also known as the wobble effect, pertains to the fact that a theoretically linear duct, is never exactly linear after placing it in the concrete beam. The curvature effect reflects the friction losses due to the intended curvature of tendons. Hence, Equation (2-110) can be used to estimate the tendon force after the occurrence of friction losses.

$$P_x = P_0 e^{-(\mu\alpha + kx)} \quad \textbf{(2-110)}$$

where P_x is the tendon force at a distance x away from the end with the angular change, α, representing curvature effect; μ is the coefficient of angular friction; and k is the wobble coefficient, per unit length.

2.4.1.2 Prestress Loss Due to Seating

In a wedge-type anchorage system, upon transfer of pretressing force to the anchorage, the wedges get seated into the anchor head, thus causing the tendon to slacken slightly. This movement causes prestress losses which is known as the seating losses. This loss is sometimes referred as the anchorage slip losses, which can be computed using Equation (2-111).

$$\Delta P = 2P_0 \eta l_{set} \quad \textbf{(2-111)}$$

where P_0 is the prestress force at the jacking end; η denotes the effect of reverse friction; and l_{set} is the setting length which can be computed using Equation (2-112).

$$l_{set} = \sqrt{\frac{\Delta_s A_p E_p}{P_0 \eta}} \quad \textbf{(2-112)}$$

where A_p is the tendon area; $E_p$is the modulus of elasticity of the steel tendon; and Δ_s is the amount of seating or the anchorage slip.

2.4.2 Prediction of Long-Term Losses

To accurately estimate the long-term prestress losses, sufficient knowledge of time-dependent material properties in addition to the interaction between creep, shrinkage of concrete and the relaxation of steel is required. However, in the absence of such information, several prediction methods have been developed to estimate the long-term prestress losses. These prediction methods are typically classified based on their analytical approach in the calculation of losses, as listed below:

1. Lump-sum methods
2. Refined methods
3. Time-step methods

In the lump-sum methods, the prestress losses are determined using the results from various parametric study conducted on prestressed beams under average conditions. The current AASHTO LRFD (2010) approximate method was developed according to the lump-sum method. To increase the accuracy of prediction of losses, the refined method was developed. In this method, the contribution of each component including creep, shrinkage, and steel relaxation are determined separately. Subsequently, the individual losses are summed up to obtain the total loss (AASHTO LRFD 2010), which is discussed in Section 2.4.2.1.

By using a step-by-step numerical analysis implemented in computer programs, the time-step method offers higher prediction accuracy compared to the previous two methods. In particular, this method is greatly appreciated in the estimation of prestress losses for multi-stage bridge constructions. Typically, the time-step method is developed by dividing time into intervals to account for the continuous interaction between the creep and shrinkage of concrete and relaxation of strands over time. The duration of each time interval can be continuously increased as concrete ages. The stress in the strands at the end of each time interval is determined by subtracting the calculated prestress losses during the interval from the initial condition at the beginning of that time interval. The strand stress and the deformation at the beginning of each time interval correspond to those at the end of the preceding interval. Using this method, the prestress level can be approximated at any critical time during the life of the prestressed member. More information about this method can be found in the studies carried out by Tadros et al (1977), Abdel-Karim (1993), the PCI-BDM (1997), and Hinkle (2006).

2.4.2.1 AASHTO LRFD Refined Method (2010)

Total long-term losses, ΔP_{LT} can be calculated using Equation (2-113) based on the AASHTO LRFD (2010) refined estimates of the time-dependent losses method.

$$\Delta P_{LT} = \Delta P_{SH} + \Delta P_{CR} + \Delta P_{R} \quad \textbf{(2-113)}$$

where ΔP_R is the prestress loss due to the relaxation of prestressing strands between the time of transfer and the deck placement; ΔP_{CR} is the prestress loss due to creep of the girder between the transfer and deck placement; and ΔP_{SH} is the prestress loss due to the shrinkage of the girder between the transfer and deck placement.

2.4.2.1.1 Prestress Loss Due to Shrinkage

Based on AASHTO LRFD (2010), the prestress loss due to the shrinkage between the transfer and deck placement can be determined using Equation (2-114).

$$\Delta P_{SH} = E_p \varepsilon_{bid} K_{id} \quad \textbf{(2-114)}$$

where ε_{bid} is the specified shrinkage strain (10^{-6} in/in).

2.4.2.1.2 Prestress Loss Due to Creep

Based on AASHTO LRFD (2010), the prestress loss due to creep between the transfer and deck placement can be determined using Equation (2-115).

$$\Delta P_{CR} = \Delta f_{pES} \Phi_{bid} K_{id} \quad \textbf{(2-115)}$$

where

$$\mathrm{K_{id}} = \frac{1}{1+\frac{\mathrm{E_p}}{\mathrm{E_{ci}}}\frac{\mathrm{A_{ps}}}{\mathrm{A}}(1+\frac{\mathrm{Ae_{pg}^2}}{\mathrm{I}})[1+0.7\Phi_{\mathrm{bif}}]} \quad \textbf{(2-116)}$$

In Equation (2-115), Φ_{bid} is the specified creep coefficient of concrete; Φ_{bif} is the ultimate creep coefficient of concrete; A_{ps} is the total area of prestressing strands (in.^{2}); A is the area of cross section (in.^{2}); I is the moment of inertia of cross section (in.^{4}); and e_{pg} is the eccentricity of strand with respect to the centroid of the girder (in.).

2.4.2.1.3 Prestress Loss Due to Relaxation

Based on AASHTO LRFD (2010), ΔP_R between the transfer and deck placement can be determined using Equation (2-117).

$$\Delta \mathrm{P_R} = \frac{\mathrm{f_{pt}}}{\mathrm{K_L}}(\frac{\mathrm{f_{pt}}}{\mathrm{f_{py}}} - 0.55) \quad \textbf{(2-117)}$$

where f_{pt} is the stress in prestressing strands immediately after transfer; K_L is a factor accounting for the type of steel, which is taken as 30 for low relaxation strands and is 7 for other prestressing steel; and f_{py} is the yield strength of prestressing steel.

Also, ΔP_R may be assumed equal to 1.2 ksi for low relaxation strands according to AASHTO LRFD (2010). Moreover, according to the study by Tadros (2003), the relaxation loss after the transfer is between 1.8 to 3.0 ksi, and comprises relatively a small part of the total prestressing losses.

2.5 Analysis of Prestressed Concrete Bridges

Time dependent estimation of stresses and deformations in prestressed concrete bridges can be approached with a different level of sophistication depending on the method of analysis. The critical mechanical properties needed for the analysis are typically concrete creep and shrinkage, steel relaxation, and concrete and steel moduli of elasticity. The accuracy of these mechanical properties directly affects the accuracy of strain and stress analyses, regardless of the method used. A number of numerical techniques and computer programs are available in the literature for the time-dependent analysis of prestressed concrete structures. One of the most accurate technique used to calculate long-term prestress losses, and subsequently stresses and deformations is the time-step method.

2.5.1 Time-Step Method

The time-step method can be developed by dividing time into a number of equal or unequal time intervals to account for the continuous interaction between creep and shrinkage of concrete and relaxation of strands with time. This allows for the computation of modulus of elasticity, creep, shrinkage, and relaxation at each considered time interval. Typically, initial curvature due to the initial prestressing force and beam self-weight is calculated, including the effects of instantaneous losses. Increase or decrease in section curvature along the member length due to long-term prestress losses is calculated at each time interval, which allows stresses and deformations to be determined. The stress in strands at the end of each time interval can be determined by subtracting the calculated prestress losses during the interval from the initial condition at the beginning of that time interval. The strands stress and deformation at the beginning of each time interval correspond to those at the end of the preceding interval. Using this method, the prestress level can be approximated at any critical time during the life of the prestressed member. Although several time-step methods have been recommended by Nilson (1987), Collins and Mitchell (1997), and Hinkle (2006), each is dependent on the accurate calculation of time-dependent material properties.

The total strain of a prestressed concrete member at age, t, is typically comprised of: elastic strain, creep strain, free shrinkage strain, and thermal strain, which can be expressed by Equation (2-118) (Ghali et al. 2002).

$$\varepsilon_c(t) = \frac{\sigma_c(t_0)}{E_c(t_0)}[1 + \varphi(t, t_0)] + \int_0^{\Delta\sigma_0(t)} \frac{1+\varphi(t,\tau)}{E_c(\tau)} d\sigma_c(\tau) + \varepsilon_{sh}(t, t_0) + \varepsilon_{th} \tag{2-118}$$

where t_0 and t is the age of concrete when the initial stress is applied and when the strain is calculated, respectively; τ is an indeterminate age between t_0 and t; $\sigma_c(t_0)$ is an initial stress applied at age t_0; $d\sigma_c(\tau)$ is an elemental stress applied at age τ; $E_c(\tau)$ is the modulus of elasticity of concrete at age τ; $\varphi(t, \tau)$ is the creep coefficient at time t for loading at age τ; $\varepsilon_{sh}(t, t_0)$ is the free shrinkage occurring between the ages t_0 and t, and ε_{th} is the thermal strain which can be calculated using Equation (2-119).

$$\varepsilon_{th} = \alpha_t \Delta T \tag{2-119}$$

where α_t is the coefficient of thermal expansion; and ΔT is the temperature difference. It should be noted that the second term in Equation. (2-117) pertains to the effects of creep when the magnitude of the applied stress changes with time.

Not only does the creep in posttensioned bridges translate into the increase in deformations, but it also affects the prestressing in the tendons, thereby affecting the structural behavior. In order to accurately account for the time dependent variables, a time history of stresses in a member and creep coefficients for numerous loading ages are required. Calculating the creep in such a manner demands a considerable amount of calculations and data space. Creep is a non-mechanical deformation, and as such only deformations can occur without accompanying stresses unless constraints are imposed.

One of the general methods used in practice to account for creep in concrete structures uses a predetermined creep coefficient for each element at each stage to determine the accumulated element stresses. Another commonly used method relies on specific functions for creep and these functions are integrated in determining stresses as a function of time. The first method requires creep coefficients for each element for every stage. The second method calculates the creep by integrating the stress time history using the creep coefficients specified in the built-in standards within the program.

If the creep coefficients for individual elements are calculated, the results may vary substantially depending on the coefficient values. For accurate results, the creep coefficients must be obtained from adequate data with suitable stress time history and loading times. If the creep coefficients at various stages are known from experience and experiments, directly using these values can be effective. The creep load group is defined and activated with creep coefficients assigned to elements. The creep loadings are calculated by applying the creep coefficients and the element stresses accumulated to the present. The user directly enters the creep coefficients and explicitly understands the magnitudes of forces in this method, which is also easy to use. However, it entails the burden of calculating the creep coefficients.

The principle of superposition was first introduced by McHenry (1943). It implies that the total strain induced by a number of stress increments applied at different ages is equal to the sum of the strains due to each stress increment considered separately. Using the principle of superposition, total creep strain at any time t is obtained as the sum of independent creep strains produced by stress changes at different ages with different duration of time up to t. Thus, creep strain at time t can be calculated using Equation (2-120).

$$\varepsilon_c(t) = \int_0^t C(t_0, t - t_0) \frac{\partial\sigma(t_0)}{\sigma(t_0)} dt_0 \quad \textbf{(2-120)}$$

where, $\varepsilon_c(t)$ is the creep strain at any time t; t_0 is the time of load application; and $C(t_0, t - t_0)$ is the specific creep which may be calculated using Equation (2-121).

$$C(t_0, t - t_0) = \frac{\varphi(t, t_0)}{E_c(t_0)} \quad \textbf{(2-121)}$$

In order to discretize Equation (2-120), a total of n intervals are assumed. Furthermore, it is assumed that the stress is invariant in each n time interval (see Figure 2.4). Denoting time interval as $\Delta t_n = t_n - t_{n-1}$ and stress increment as $\Delta\sigma_n = \sigma_n - \sigma_{n-1}$, the total creep strain can be defined by Equation (2-122).

$$\varepsilon_{c,n} = \sum_{j=1}^{n-1} \Delta\sigma_j C(t_j, t_{n-j}) \quad \textbf{(2-122)}$$

with each creep strain increment from t_n to t_{n-1} being defined by Equation (2-123).

$$\Delta\varepsilon_{c,n} = \varepsilon_{c,n} - \varepsilon_{c,n-1} = \sum_{j=1}^{n-1} \Delta\sigma_j C\big(t_j, t_{n-j}\big) - \sum_{j=1}^{n-2} \Delta\sigma_j C(t_j, t_{n-j}) \quad \textbf{(2-123)}$$

2.5.2 Finite-Element Analysis

The finite-element method (FEM), sometimes referred to as finite-element analysis (FEA), is a computational technique used to obtain fairly accurate solutions of boundary value problems in engineering. The FEA is also widely used to analyze prestressed concrete bridges for deformations and stresses. In the FEM, the actual continuum or body of matter is represented as an assemblage of subdivision called finite elements. These elements are considered to be interconnected at specific joints called nodes or nodal points. The nodes usually lie on the element boundaries where adjacent elements are considered to be connected. Since the actual variation of the field variable (e.g., displacement, stress, temperature, pressure, velocity, or acceleration) inside the continuum is not known, the variation of the field variable inside a finite element can be presumably estimated by a simple function. These approximating functions, also known as interpolation functions, are defined in terms of the values of the field variables at the nodes. When field equations, like equilibrium or compatibility equations, for the whole continuum are written, the new unknowns will be the nodal values of the field variable. By solving the field equations, which are generally in the form of matrix equations, the nodal values of the field variable will be known. Once these are known, the approximating functions determine the field variable throughout the assemblage of elements.

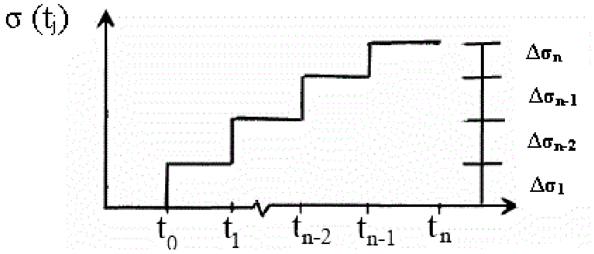

(a) Stress history

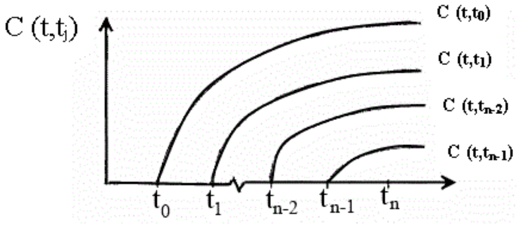

(b) Specific creep

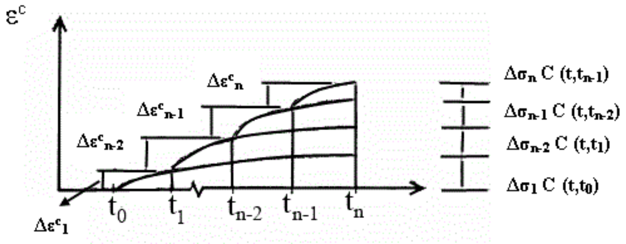

(c) Total strain

Figure 2.4: Creep deformation summed over increasing stress history

CHAPTER 3: CHARACTERIZATION OF CONCRETE RELAXATION

3.1 Introduction

As described in Section 1.2, time-dependent displacement-induced forces are developed during and after construction especially in columns supporting CIP / PS Box. These forces are primarily induced due to shortening of the superstructure and their magnitudes are highly influenced by the time-dependent behavior of the superstructure (e.g., shortening and prestress losses) as well as the effects of concrete relaxation in the columns. Although these forces are suspected to be reduced over time due to concrete relaxation, they are not systematically accounted for in routine design of columns supporting a CIP / PS Box, resulting in overestimation of lateral forces.

Concrete is a structural material with time-dependent behavior, such as shrinkage as well as creep and its associated stress relaxation, which significantly affect the structural behavior of CIP / PS Box. Creep and shrinkage are generally viewed unfavorably when they cause prestress losses and increase in deflections, which may impair serviceability of a bridge structure. However, creep and its associated stress relaxation can be beneficial if it contributes toward redistribution and/or reduction of stresses. Since creep and relaxation of concrete are different manifestations of the same viscoelastic material property, they have been used interchangeably in the literature. However, in this report, the relaxation term is referred to the loss of stress under a state of a constant strain and the creep term is used to identify the increase in strain under a constant sustained stress.

The effects of concrete relaxation may be beneficial at two stages: (1) at early ages during hardening of concrete; and (2) long-term after maturity of concrete. The main beneficial effect of concrete relaxation at early ages is that it reduces the restraint stresses induced by thermal dilation and autogenous shrinkage, thereby reducing the risk of cracking during hardening. In many cases, a reduction in restraint stress of as much as 30-40% due to stress relaxation has been reported during hardening of concrete (Bosnjak 2001, Atrushi 2003, Schutter 2004). After the concrete matures, the test data on a set of continuous reinforced concrete beams (Ghali et al. 1969) and continuous prestressed concrete beams (Digler et al. 1970) subjected to a fixed displacement (representing a settlement) verified the beneficial effects of relaxation by reducing the reaction forces with time. Moreover, Choudhury et al. (1988) showed that when designing reinforced concrete bridge columns subjected to imposed deformation, economical solutions can be achieved by including the beneficial effects of column creep resulting from axial loads. However, the beneficial role of concrete relaxation in reducing the deformation-induced forces in the columns of CIP/ PS Box caused by time-dependent shortening of the superstructure was not examined.

Upon review of the current literature, it was discovered that limited data exist on the effects of concrete relaxation, which may be due to the difficulties associated with maintaining a state of constant strain during a relaxation test. Hence, information available on creep is typically used in lieu of relaxation data for most of the theoretical studies involving relaxation. Though not useful for long-term studies, a few investigations have examined the characterization of concrete relaxation only at early ages. The relaxation of early age concrete under axial tension was studied by Rostásy (1993) and Gutsch (2001). They noted that relaxation increased as the loading age decreased, and relaxation and creep were accelerated at a temperature higher than 68 °F under loading. Moreover, they validated the assumption of using linear viscoelasticity behavior to model the concrete creep and relaxation.

Morimoto and Koyanagi (1994) conducted a comparative study on concrete stress relaxation in both tension and compression. The test results found that the main difference between tensile and compressive relaxation was that the tensile relaxation was much smaller and terminated in a shorter period compared to the compressive relaxation. Contrary to the findings by Gutsch (2001), Morimoto and Koyanagi (1994) concluded that the effect of temperature under loading on relaxation was marginal for the temperature lower than 140 °F. In addition, Atrushi (2003) investigated tensile and compressive creep and relaxation of early age concrete using a combination of testing and analytical molding. Atrushi (2003) found that the effect of stress relaxation, which was defined as the relative difference between the calculated elastic stresses and the measured self-induced stresses, was relatively large and significant in the development of self-induced stresses. Under isothermal temperature of 68 °F, the relaxation increased to about 40% of the fictive elastic stresses after three days and varied slightly after three days.

3.2 Experimental Investigation

Given the limited experimental data available on concrete relaxation, an experimental investigation was conducted in this study to characterize the relaxation phenomenon with respect to its beneficial effects on displacement-induced column forces. Unlike the previous studies, which focused on early age concrete relaxation, the proposed experimental program targeted the occurrence of relaxation after the concrete had sufficiently matured (i.e., after the age of 28 days).

3.2.1 Specimens

Three different specimens were used to characterize the relaxation of the normal strength concrete over short durations (i.e., less than five days). The descriptions of these specimens are presented in Table 3.1. Two column specimens were used to quantify the relaxation under uniaxial compression at different loading ages, while a reinforced concrete (RC) beam was used to quantify the relaxation under flexure. Both columns were unreinforced with two different cross section sizes, allowing the size effect to be observed.

Table 3.1: Descriptions of the specimens used for the relaxation tests

Specimen number	Type	Diameter	Height/Length	Loading age (day)
1	Circular concrete column	203.2 mm (8 in.)	1.22 m (4 ft)	48, 76, 78, 84
2	Circular concrete column	304.8 mm (12 in.)	1.22 m (4 ft)	67
3	Circular RC beam	203.2 mm (8 in.)	1.22 m (4 ft)	130, 150

3.2.2 Instrumentation

To ensure that the specimens were subjected to a state of constant strain, strain gauges were used to monitor the changes in concrete/steel strains during as concrete relaxation. For the column specimens, four surface mounted concrete gauges were attached in the four quadrants of the column’s outer surface at mid-height, as illustrated in Figure 3.1. To ensure smooth, flat surfaces at the column ends to uniformly apply the axial load, they were capped with a thin layer of Hydro-Stone ® (i.e., 3.175 mm [0.125 in.] to 6.35 mm [0.25 in.]). For the RC beam, two concrete strain gauges were attached to the top and bottom surfaces (i.e., on the extreme compressive and tensile regions). In addition, the longitudinal and transverse steel reinforcement of the beam were instrumented with strain gauges to monitor the changes in the steel strain with time. A total of six strain gauges were attached to the steel spirals at Sections 1 and 2 to monitor changes in the transverse reinforcement, as illustrated in Figure 3.2. Two of the six strain gauges were placed on the tension side while the remaining gauges were placed on the compression side. Instrumentation to monitor the longitudinal strains was similar to that of the spirals, where two of the six strain gauges were attached to the longitudinal bars on the tension side and the remaining gauges were attached to the longitudinal bars on the compression side at Sections 1 and 2, as illustrated in Figure 3.2.

Each of the 12 steel strain gauges was labelled, as shown in the example below:

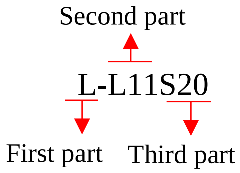

The first part describes whether the gauge was attached to the longitudinal reinforcement (L) or the transverse reinforcement (T). The second and the third parts identify the location of the gauge with respect to the position of the longitudinal and transverse reinforcement. The second part indicates the location of the nearest longitudinal bar to the gauge, while the third part determines the location of the nearest spiral to the gauge. The longitudinal bar numbers as well as the spiral numbers are indicated in Figure 3.2.

In addition, to quantify thermal and shrinkage strains, stress-independent strains were monitored for an unloaded specimen located adjacent to the test specimen while the specimen was loaded.

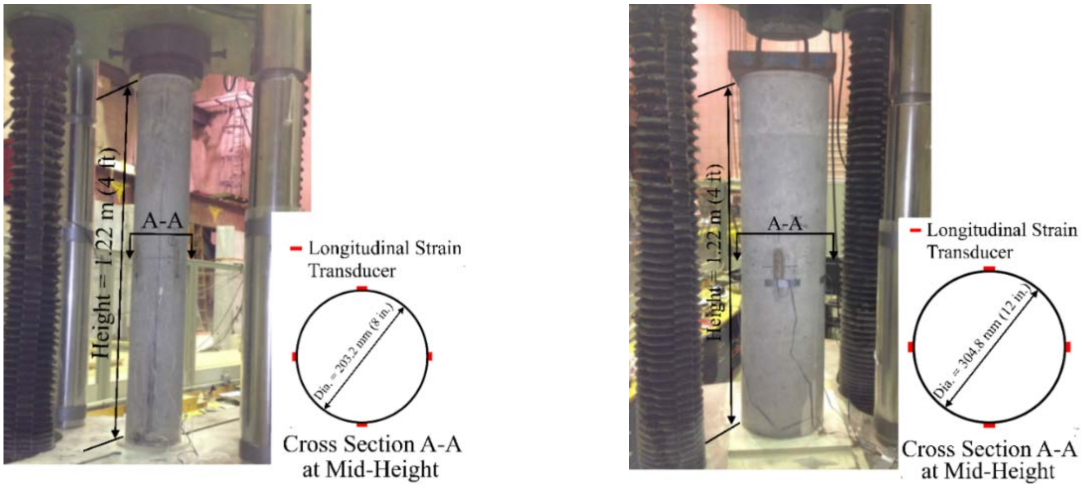

(a) 203.2 mm (8 in.) diameter specimen (b) 304.8 mm (12 in.) diameter specimen

Figure 3.1: Concrete column specimens used for relaxatoin tests under uniaxial compression strains

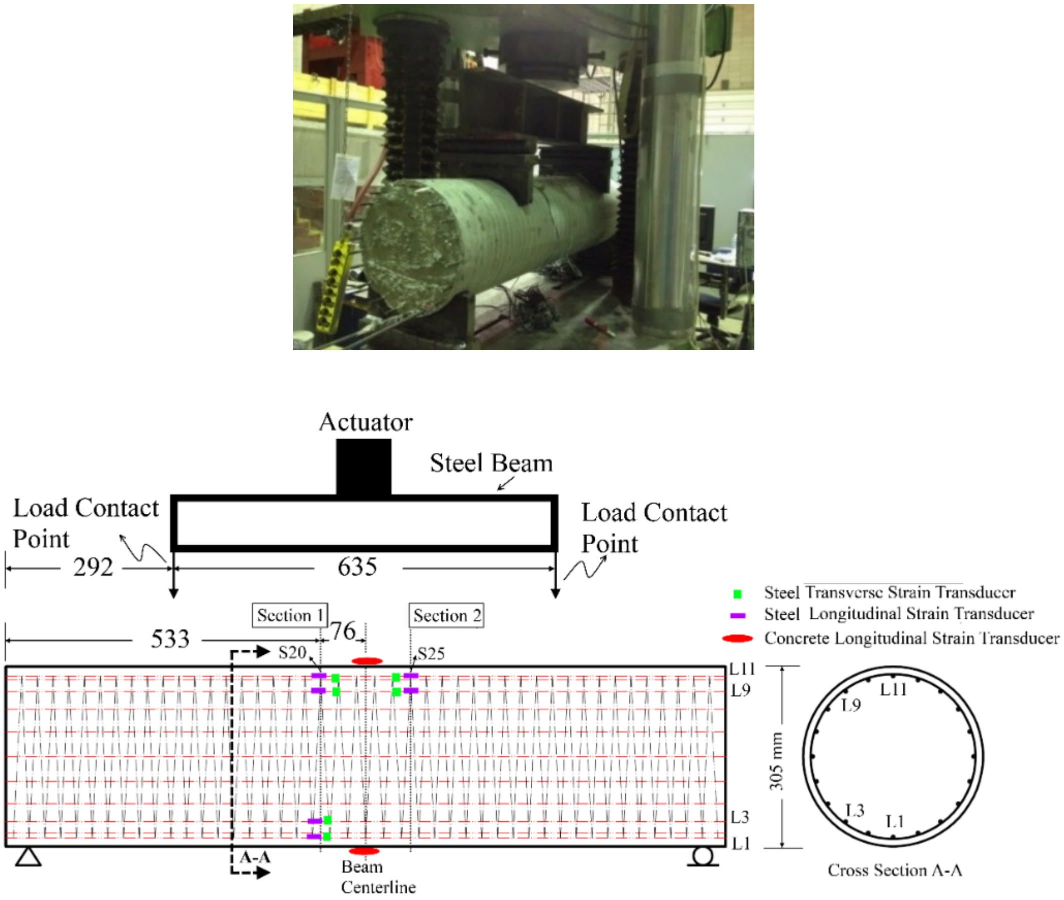

Figure 3.2: The RC beam specimen under four-point bending and the location of gauges

3.2.3 Testing Apparatus and Methodology

The SATEC uni-axial testing machine was used to perform the relaxation tests. The test unit included the hydraulic actuator and a data acquisition system. The SATEC machine was able to accommodate both the displacement and force control modes using the software provided with its data acquisition system. This software allows a test protocol to be defined by choosing the loading mode (displacement or force control mode), magnitude of the applied force or displacement, load rate, number of increments to apply the load, and test duration.

Initially, the specimens were loaded under a force control mode, in which the actuator displaced until the desired load was reached and the corresponding actuator displacement was recorded, as shown in Figure 3.3. Then, a displacement control mode was used to reach the previously recorded actuator displacement and made sure the expected load was on the specimen and the corresponding displacement was maintained for the duration of the test, as shown in Figure 3.4.

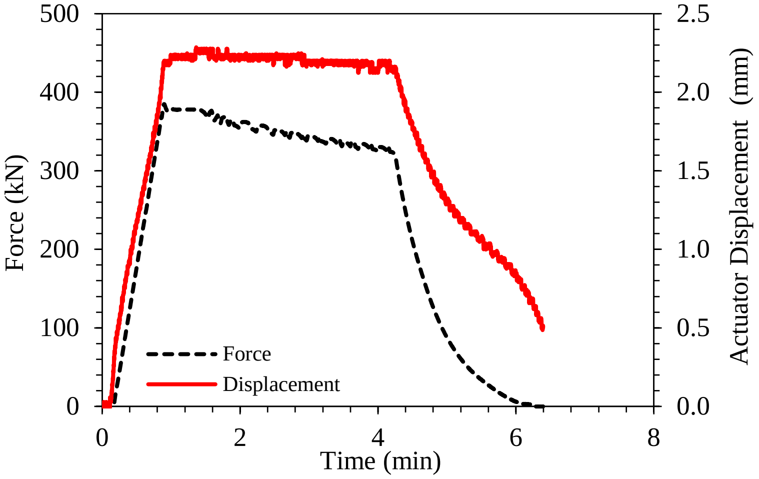

Figure 3.3: Loading under force-control mode

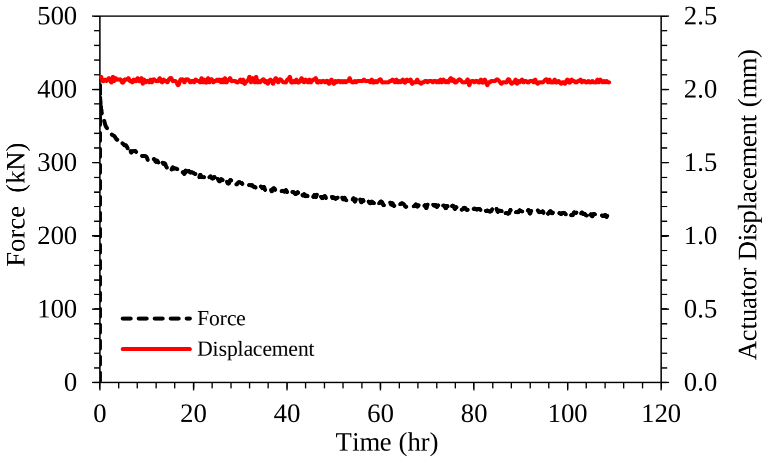

Figure 3.4: Loading under displacement-control mode

3.2.4 Loading

The three specimens were subjected to different states of constant strain, which included: (1) instantaneous axial compression; (2) incremental axial compression; and (3) instantaneous flexure. Using the three specimens and the three loading protocols, a total of seven tests at different concrete ages were performed. The details of these tests are summarized in Table 3.2.

Tests 1 through 3 were performed using the first loading protocol, in which an elastic strain was applied and maintained over the entire duration of the test. Tests 4 and 5 were performed using the second loading protocol, in which the uni-axial compression was incrementally applied to the column specimen through a number of time-steps over the duration of the test. At the beginning of each time step, the specimen was subjected to an elastic strain which was held constant until the beginning of the next time-step when the strain was increased. This procedure was repeated for all the time steps. The cumulative strain at the end of the time-steps was less than the elastic strain threshold. Test 4 consisted of 12 ten-hour time-steps, while six 15-hour time-steps were used for Test 5.

Table 3.2: Details of the seven relaxation tests

Test	Specimen used	Specimen age at loading (days)	Test duration (hours)	Loading type	Initial applied strain (με)
1	1	48	109	Instantaneous axial compression	422
2	2	67	112	Instantaneous axial compression	452
3	1	76	73	Instantaneous axial compression	435
4	1	78	116	Incremental axial compression	43*
5	1	84	90	Incremental axial compression	87*
6	3	130	119	Instantaneous flexure- precracking	198
7	3	150	120	Instantaneous flexure- postcracking	682

*The mean measured (targeted) strain for all of the time steps

Tests 6 and 7 were performed on RCCB subjected to the third loading protocol- four-point bending laoding. For Test 6, the specimen was loaded under constant flexural strain prior to the unit experiencing any flexural cracks. For Test 7, the load was applied to cause flexural cracks on the tension side, and then a constant flexural strain was applied and maintained. Soon after the completion of Test 7 (i.e., within half an hour) and the beam was unloaded, it was monotonically loaded under displacement control until failure. This was carried out to evaluate any impact of the relaxation test on the flexural behavior of the beam.

3.3 Observed Behavior

Variations in concrete strains and stresses with time recorded for Tests 1 through 5 are shown in Figure 3.5 through 3.11, sequentially. Variations in concrete strains and stresses and steel strains for Tests 6 and 7 are shown in Figure 3.10Figure 3.11, respectively. In general, the concrete strains and steel strains remained constant while the stress decreased with time for all of the tests. The variations in strain and stress and corresponding relaxation were quantified, as given in Table 3.3. For all of the tests, the combined shrinkage and thermal (stress-independent) strains were found to be less than 10 με, as shown in Figure 3.12, and were consequently considered negligible. The applied (stress-dependent) strain varied slightly with the time, but they were within ±22 $\mu\varepsilon$ for all the tests, except for Test 7, in which strain variations of ±57 $\mu\varepsilon$ were observed.

For the identical specimen sizes with similar initial axial compressive stresses, Test 1 resulted in 49% stress relaxation, while Test 3, which was loaded 28 days after completing Test 1, exhibited 39% reduction in stress. As expected from creep behavior, this observation confirms that the stress relaxation reduces as the age of loading is increased. The size effect on relaxation can be observed by comparing the results from Test 2 to Test 3, which had two different cross section sizes, but used the same concrete mix as well as similar applied stresses and loading ages. The results indicated that after 72.5 hours, the axial stress for the larger specimen used in Test 2 experienced 32% relaxation, while the corresponding reduction was 41% for the smaller specimen used in Test 3. For Tests 4 and 5, the concrete stress after 90 hours was reduced by 14.5% and 20.5%, respectively, as the concrete strain remained constant. Since the loading age and specimen size were similar for these two tests, the larger reduction in stress for Test 5 relative to Test 4 is attributable to the higher stress applied over a fewer time steps for Test 5 than Test 4.

For Test 6, the reduction in the load and the concrete stress at the end of the test was 20.4%. After cracking, the compressive stress was reduced by 14.6% at the end of Test 7. In both cases the concrete compressive strain did not change with time. The concrete strain gauges placed on the tension side remained zero due to cracking.

As shown in Figure 3.10, the longitudinal strains were below the yield strain of the steel reinforcement and the variation of strain in longitudinal reinforcement was insignificant for Test 6. For the transverse reinforcement, most of the strain gauges recorded zero strain which was expected since the beam was under pure flexure at the mid-span and no significant concrete compressive stress were developed due to flexure. However, two of the strain gauges showed strain as high as 100 microstrain (με), which could be attributed to the local micro cracks in the vicinity of these gauges.

For Test 7, the tensile longitudinal strains indicate yielding of the steel and slight strain variation with time, as shown in Figure 3.11. Similar to Test 6, the recorded transverse strains were generally insignificant, except for one strain gage which showed a strain as high as 200 με.

Table 3.3: Results of the seven relaxation tests

Test	Mean variation in applied strain (με)	Thermal and shrinkage strains (με)	Stress (MPa)		Stress relaxation (%)
			Initial	Final	
1	±6	< 10	13.7	7.0	49
2	±11	< 10	13.9	9.0	35
3	±22	< 10	14.3	8.7	39
4	±5	< 10	15.2	11.9	22
5	±4	< 10	15.0	11.9	21
6	±10	< 10	4.6	3.7	21
7	±57	< 10	17.2	14.5	16

Note: 1 MPa = 0.145 ksi

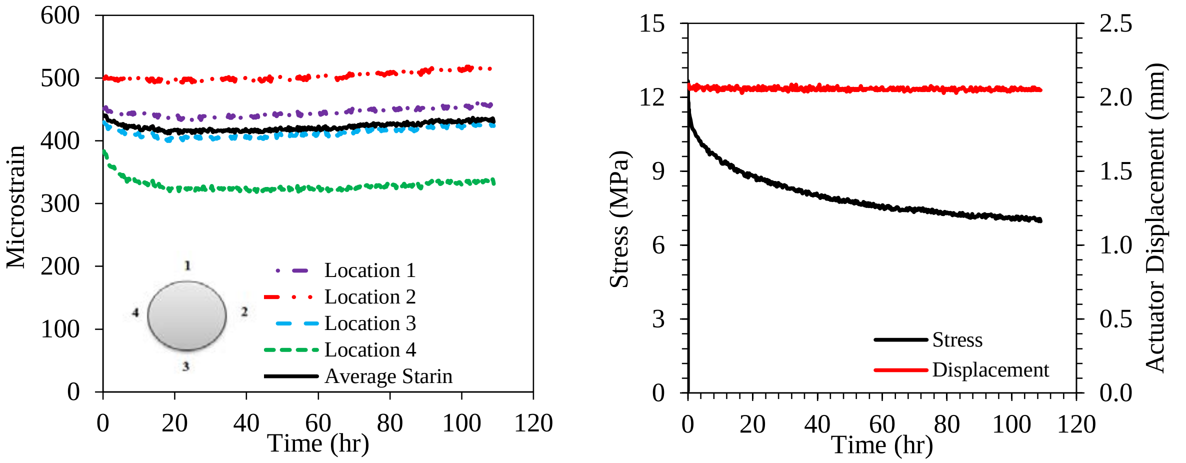

(a) Concrete strain variation with time (b) Stress and displacement variation with time

Figure 3.5: Measured strains, stresses and displacement from Test 1

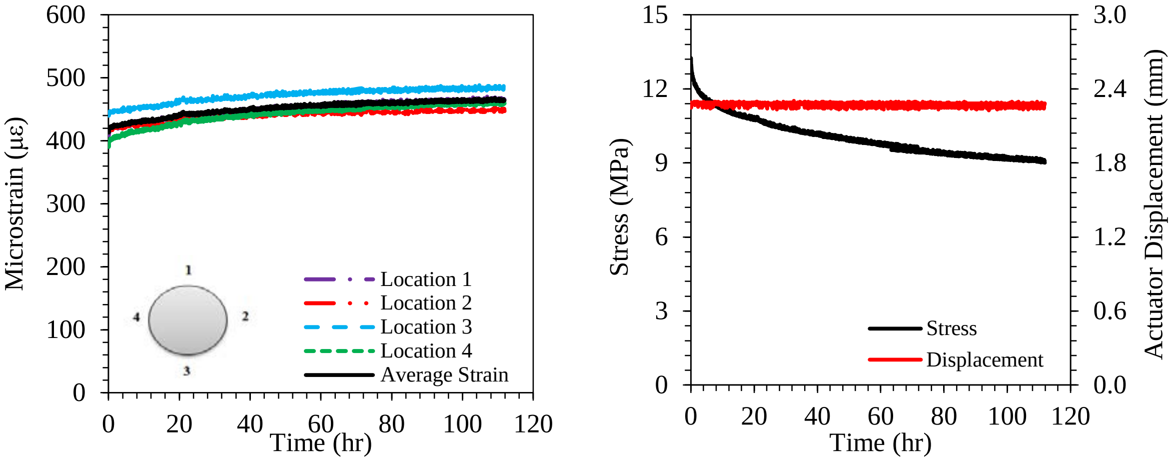

(a) Concrete strain variation with time (b) Stress and displacement variation with time

Figure 3.6: Measured strains, stresses and displacement from Test 2

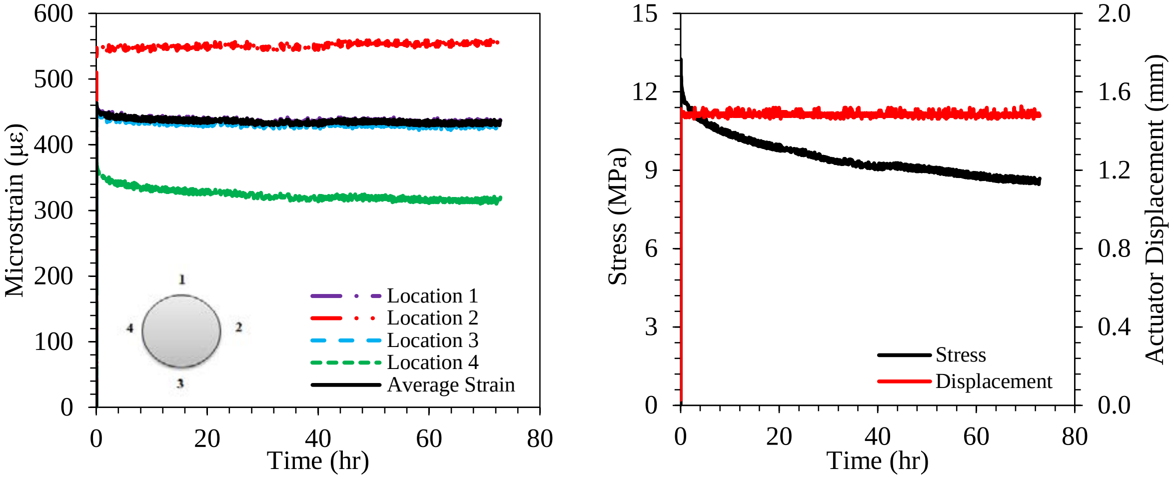

(a) Concrete strain variation with time (b) Stress and displacement variation vs. time

Figure 3.7: Measured strains, stresses and displacement from Test 3

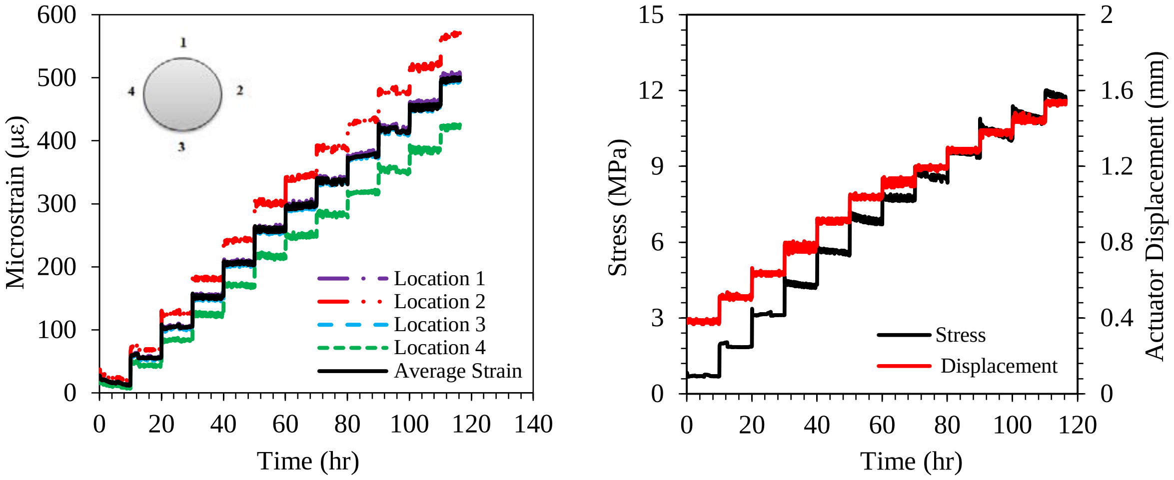

(a) Concrete strain variation with time (b) Stress and displacement variation vs. time

Figure 3.8: Measured strains, stresses and displacement from Test 4

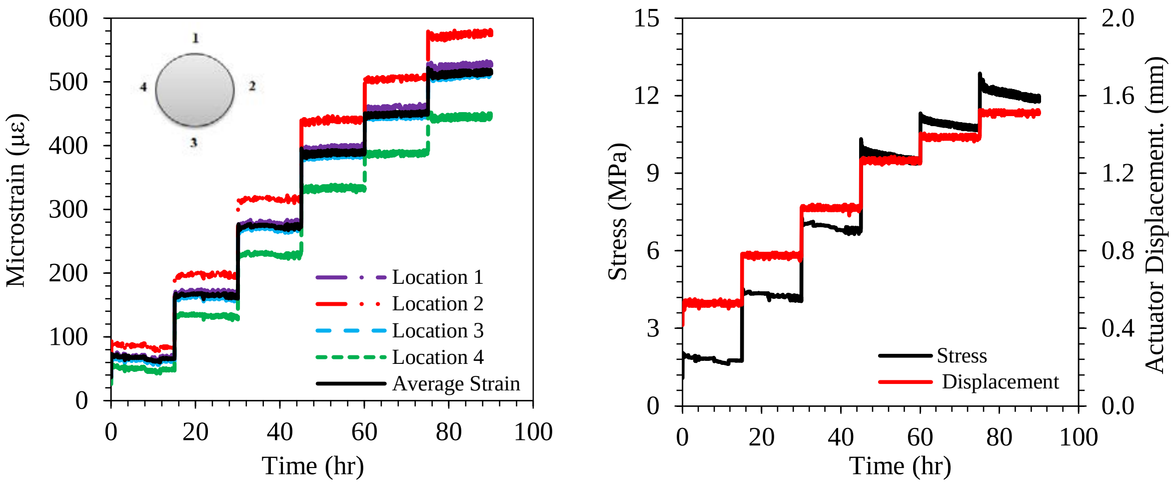

(a) Concrete strain variation with time (b) Stress and displacement variation vs. time

Figure 3.9: Measured strains, stresses and displacement from Test 5

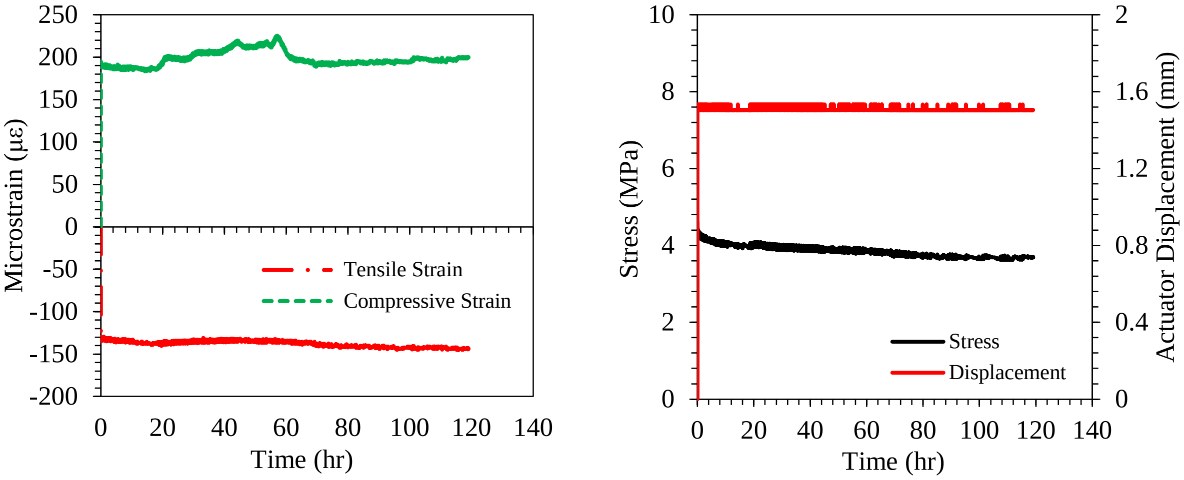

(a) Concrete strain variation with time

(b) Stress and displacement variation vs. time

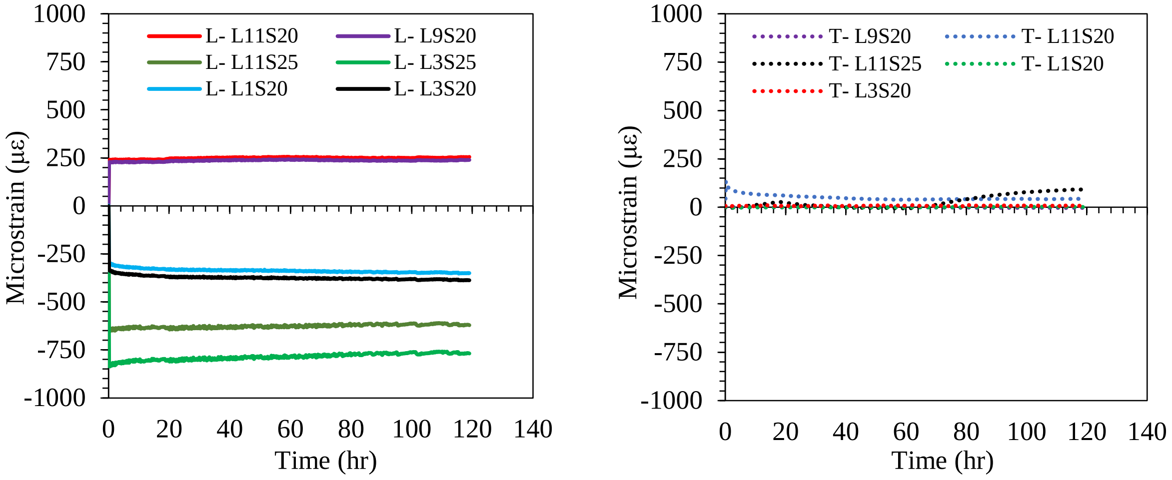

(c) Steel longitudinal strain variation with time

(d) Steel transverse strain variation with time

Figure 3.10: Measured strains, stresses and displacement from Test 6

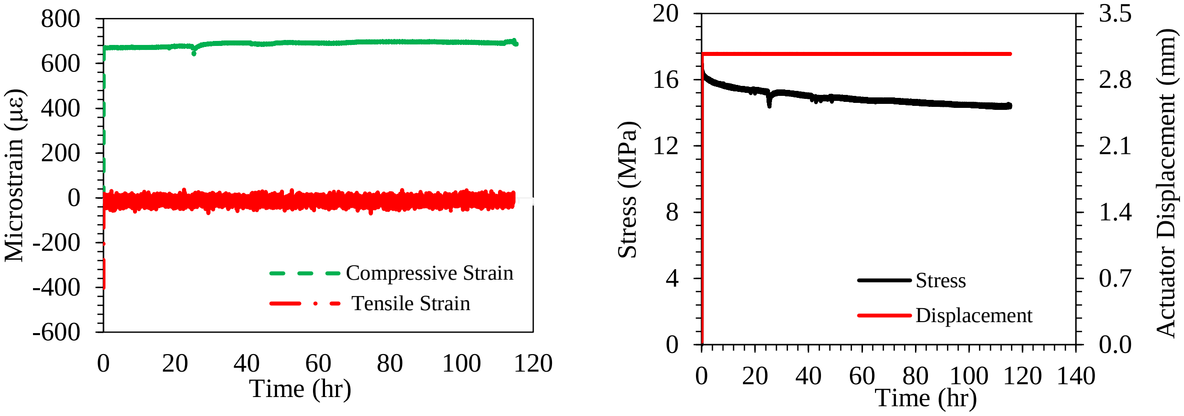

(a) Concrete strain variation with time

(b) Stress and displacement variation with time

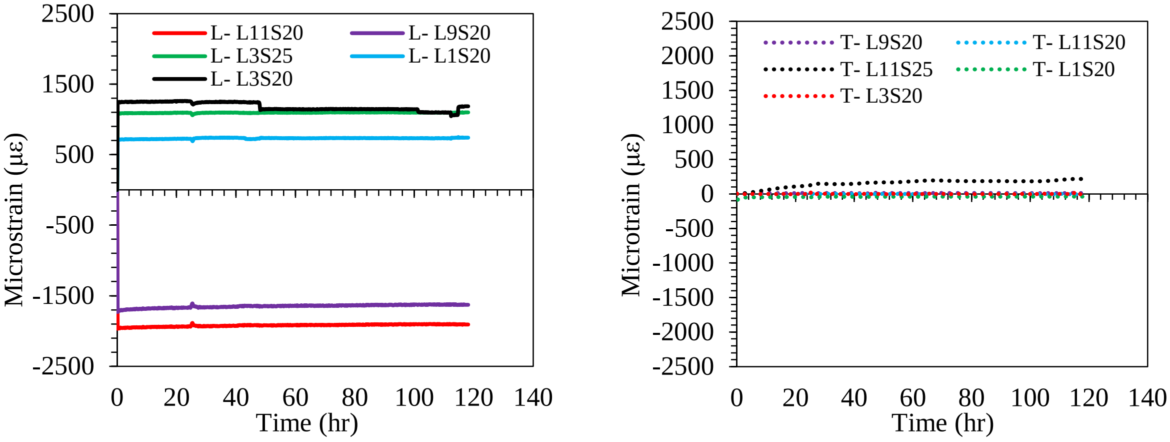

(c) Steel longitudinal strain variation with time

(d) Steel transverse strain variation with time

Figure 3.11: Measured strains, stresses and displacement from Test 7

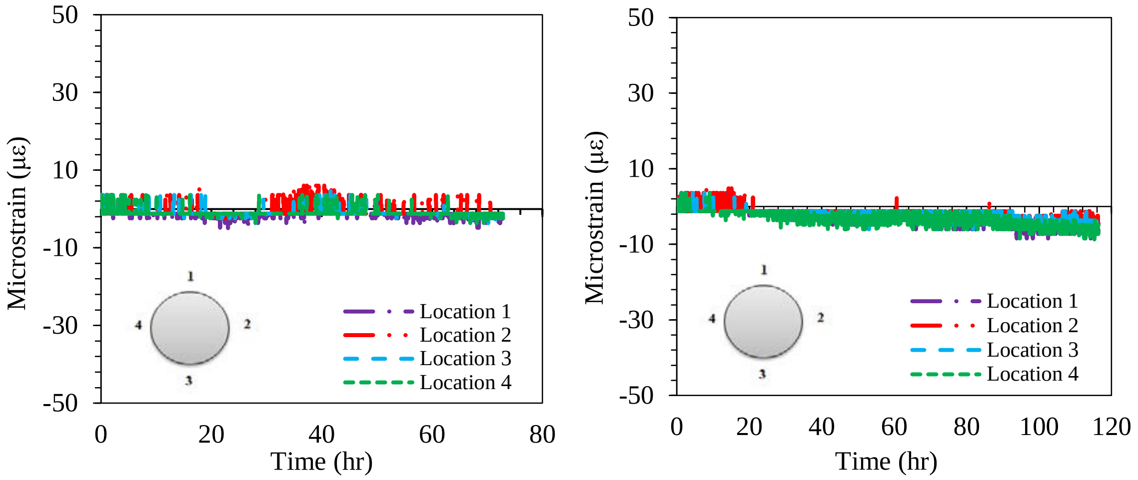

Test 3

Test 4

Figure 3.12: Thermal and shrinkage strains

The measured applied force and the corresponding tensile strain in the longitudinal steel after completion of the relaxation test and prior to the failure are shown in Figure 3.13. As the relaxation test was terminated, the strain in the steel returned to zero. This implies that the residual strain in steel was insignificant prior to the beginning of the test to failure.

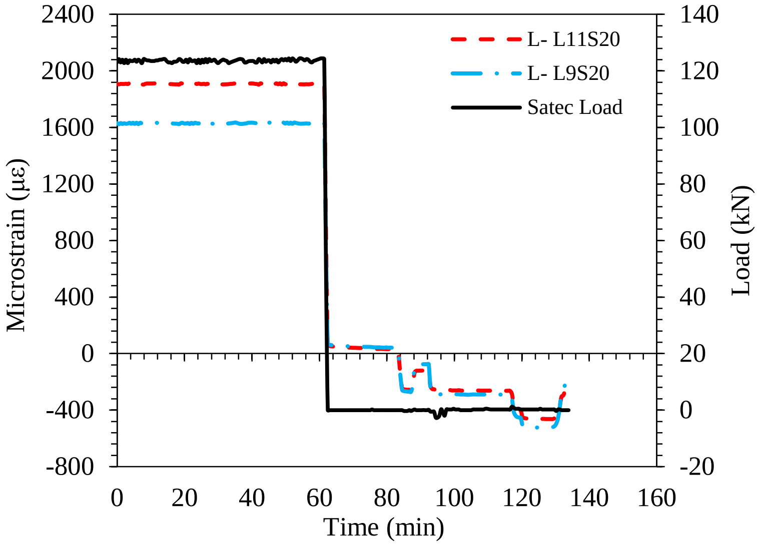

Figure 3.13: Variations of steel longitudinal tensile strain and load with the time at the end of Test 7 and prior to failing of the beam

3.3.1 Summary of Relaxation Tests

Figure 3.14 shows the variation of concrete strain and stress with time for the seven conducted relaxation tests. For all of the tests, concrete strain remained constant with time while concrete stress reduced as a function of time due to concrete relaxation. The maximum reduction in concrete stress occurred in Test 1 due to smaller age of loading than those used for the other tests.

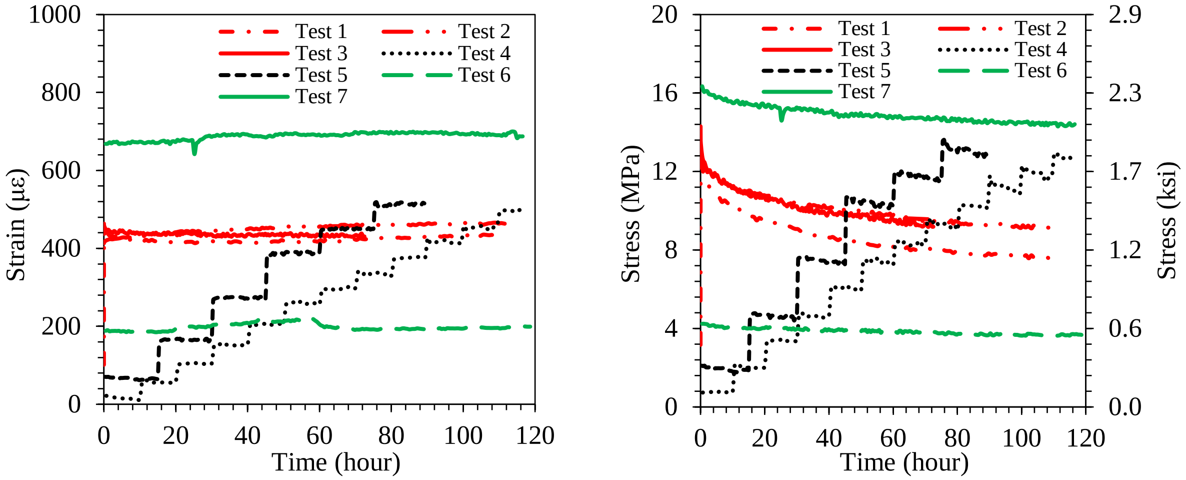

Figure 3.14: Concrete strain and stress variations with time

3.4 Relaxation Functions

The relaxation function was established to determine the reduction in the stress due to a unit constant strain based on the test results reported above and the analytical creep models summarized in Chapter 2. For the analytical models, a combination of the time step method based on FEA and a simplified analysis using Equations (2-69) and (2-71) were employed to estimate the relaxation function corresponding to each test. Accordingly, a creep coefficient was estimated for each case as a function of time using the AASHTO LRFD Bridge Design Specification 2010 prediction model. Except the loading age, the other parameters used in the AASHTO models, including the concrete compressive strength and humidity were calibrated for the first test such that the best agreement was found between the estimated and measured relaxation functions.

Using the midas Civil software (2013), a FEM of the tests were developed with due consideration to specimen geometry, creep, and loading protocol. A constant strain was applied to the FEM such that the corresponding initial stress was the same as the measured initial stress for the test. This was achieved by adjusting the concrete modulus of elasticity. The same calibrated values for concrete compressive strength and humidity were used to estimate creep in the analytical models developed for the remaining tests.

Figure 3.15 and Figure 3.16 show the comparison between the calculated relaxation functions based on the test results and the different analytical models for the concrete columns and RC beam, respectively. In general, a good agreement is found between the test results and the FEM results for the different tests. The simplified analysis and the Bazant's method (1979) resulted in identical approximation of the relaxation functions for the different tests due to the short duration of the tests (i.e., less than 5 days). The relaxation functions estimated by the simplified analysis and Bazant's method (1979) did not correlate well with the test results for the first 48 hours of Tests 1 through 5. After 48 hours, it is observed that the simplified analysis and Bazant's method (1979) resulted in the overestimation of the relaxation functions for Tests 1 and 2, while underestimated the relaxation functions for Tests 4 and 5.

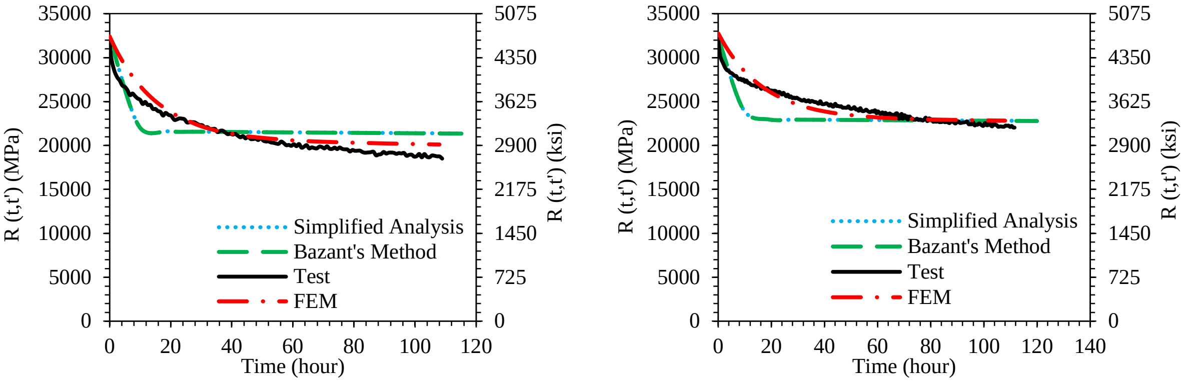

(a) Test 1

(b) Test 2

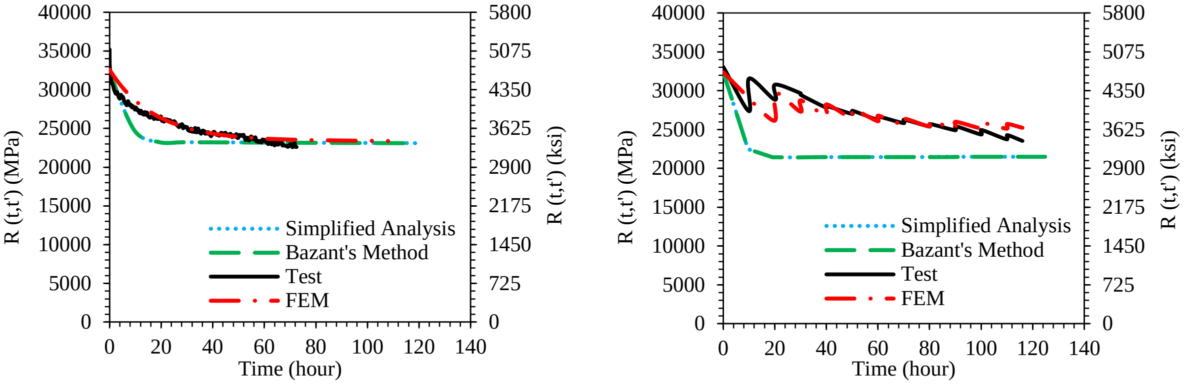

(c) Test 3

(d) Test 4

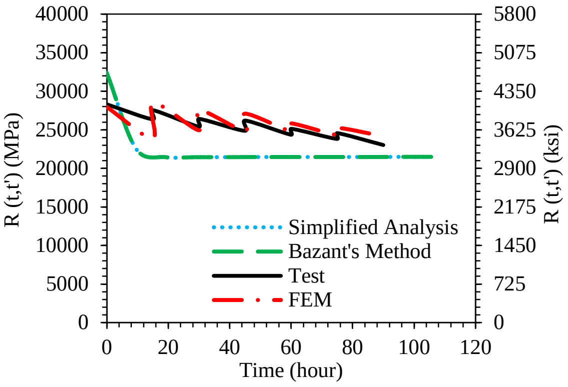

(e) Test 5

Figure 3.15: Relaxation functions established for the column specimens

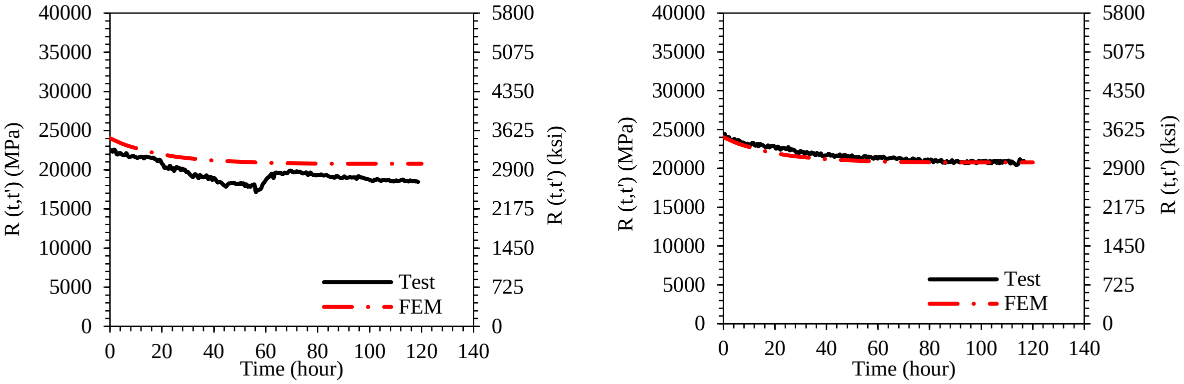

(a) Test 6

(b) Test 7

Figure 3.16: Relaxation functions obtained for the RC beam

3.5 Summary and Conclusions

Given the lack of available information in the literature, an experimental study was undertaken to characterize the concrete relaxation because it provided beneficial effects to displacement-induced forces columns supporting CIP / PS Box. Three different specimens were used to characterize the relaxation of normal strength concrete over short durations after the concrete had sufficiently matured. The three specimens were subjected to a state of constant strain using three different load protocols: (1) instantaneous axial compression; (2) incremental axial compression; and (3) instantaneous flexure. Loading protocols 1 and 2 were performed using concrete columns of two different cross section sizes, while the third load protocol was performed on a RC beam. Using the three specimens and the three loading protocol, a total of seven tests at was performed at different ages of loading, which led to the following findings:

- In all tests, the beneficial effects of concrete relaxation on the displacement-induced forces/stresses were observed by reducing concrete forces/stresses with time under the state of a constant strain. The most significant portion of the reduction of the stress occurred within the first 48 hours of the tests.
- Similar to creep, the relaxation was appreciably affected by the age of loading and the

magnitude of the initial applied load. Hence, Test 1 with the smallest loading age resulted in the largest relaxation (i.e., 49% reduction in stress after 109 hours) among the seven tests.

- By incrementally applying the constant displacement in Tests 4 and 5, a more realistic loading expected on columns supporting the CIP / PS Box was simulated, for which the beneficial effects of relaxation were still significant in reducing the stresses.
- Conducting the relaxation tests on the RC beam indicated that the relaxation was not affected by the cracking of the specimen except that the magnitude of stresses and strains in concrete and steel increased due to cracking.
- The relaxation function calculated by the FEM led to a better agreement with the test results compared to the approximate method proposed by Bazant (1979) and the simplified analysis. By applying these functions with the FEM of CIP / PS Box, column forces can be accurately calculated with due consideration to the effects of concrete relaxation.

CHAPTER 4: DETAILS OF SELECTED CIP/ PS BOX FRAMES

4.1 Introduction

To conduct detailed analyses on CIP / PS Box frames to quantify the time dependent effects of concrete and prestressing steel, several California CIP / PS Box frames were chosen with input from Caltrans engineers. Key variables that were used in selecting different frames encompassed pier type (e.g., multiple vs. single column bents), foundation type, lengths, and connection details. Accordingly, eight CIP / PS Box frames were chosen for detailed analyses. Based on the total frame length, they were categorized as short-, medium-, and long-span frames, as outlined in Table 4.1. For these CIP / PS Box frames, the number of spans varies between three and eight, and they were characterized as short, medium and long span bridge frames. When the longest span length from all bridges are compared, the largest value is 91.4 m (300 ft) in the S405-E22 CIP / PS Box and the smallest value is 50 m (164 ft) in Frame 8 of the Floodway Viaduct CIP / PS Box. The Trabuco Creek CIP / PS Box has the longest bridge frame with a total length of 426.7 m (1400 ft), while the WB SR60 HOV Connector CIP / PS Box has the shortest bridge frame with a total length of 131 m (430 ft).

Each CIP / PS Box frame was identified with a label comprised of a numeral which increases as the total length of the bridge increases (see Table 4.2). The column of each bent within the selected CIP / PS Box frame was then assigned a twofold label, for which the first part refers to the bridge name and the second part corresponded to the bent number in accordance with the details presented in Section 4.2. For instance, B4-C4 designates the column at Bent 4 in Frame 6 of the Floodway Viaduct CIP / PS Box. A summary of this nomenclature, as used in the remainder of this report, is presented in Table 4.2.

Table 4.1: Classification and details of the selected CIP / PS Box frames

Type	Range of frame length (m)	Bridge name	Range of maximum span length (m)		Number of spans	Longest span (m)	Frame length (m)
Short	Less than 152.4 (500 ft)	Floodway Viaduct- Frame 8	Short	Less than 53.3 (175 ft)	4	50.0	145.4
		WB SR60 HOV Connector	Medium	53.3-68.6 (175-225 ft)	3	62.0	131.0
		Not Applicable	Long	Over 68.6 (over 225 ft)		0.0	0.0
Medium	152.4-304.8 (500–1000 ft)	Estrella River	Short	Less than 53.3 (175 ft)	6	53.3	293.4
		Floodway Viaduct- Frame 6	Medium	53.3-68.6 (175-225 ft)	5	66.0	258.8
		S405-E22 Connector	Long	Over 68.6 (over 225 ft)	3	91.4	231.3
Long	Over 304.8 (over 1000 ft)	N805-N5 Truck Connector	Short	Less than 53.3 (175 ft)	8	47.5	358.0
		Trabuco Creek	Medium	53.3-68.6 (175-225 ft)	8	56.4	426.7
		Santiago Creek	Long	Over 68.6 (over 225 ft)	6	70.1	387.3

Table 4.2: Nomenclatures used for the CIP / PS Box frames and their columns

Type	Bridge	Frame label	Frame length (m)	Column label	
Short	WB SR60 HOV Connector	B1	145.4	B1-Ci; where	i=2:3
	Floodway Viaduct-Frame 8	B2	131.0	B2-Ci; where	i=31:33
Medium	S405-E22 Connector	B3	293.4	B3-Ci; where	i=2:3
	Floodway Viaduct -Frame 6	B4	258.8	B4-Ci; where	i=23:26
	Estrella River	B5	231.3	B5-Ci; where	i=2:6
Long	N805-N5 Truck Connector	B6	358.0	B6-Ci; where	i=2:8
	Santiago Creek	B7	387.3	B7-Ci; where	i=2:6
	Trabuco Creek	B8	426.7	B8-Ci; where	i=2:8

4.2 Elevation Views and Box-Girder Cross Sections

For short-, medium-, and long-span CIP / PS Box frames, Figure 4.1 through Figure 4.3 illustrate the elevation views and Figure 4.4 through Figure 4.6 present the typical box-girder cross sections, sequentially. In Figure 4.1 through Figure 4.3, the total length of the frames in addition to the individual span length is presented. Except for B2 and B4, which have a curvature in the horizontal plane, the remaining frames are straight. Additionally, the box-girders' height remains constant along the frame for all of the frames, except B3, in which the height varies in a parabolic shape along the frame, as shown in Figure 4.2a. Moreover, B3 is the only skewed frame, whereas other frames have zero degrees of skew.

As shown in Figure 4.4 through Figure 4.6, the box-girder cross section of the selected CIP / PS Box contained either four or five girders (i.e., three or four cells) as well as the soffit and the deck. The width and the height of the box-girder vary among different CIP / PS Box. The largest box-girder's height belongs to B3 which is 3048 mm (120 in.), while B6 has the smallest height of 1900 mm (74.8 in.). The widest box-girder belongs to B7 where the deck width is 18136 mm (714) in., while B1 has the least wide box-girder with the deck width of 9105 mm (358.5 in.). Moreover, the typical girder's thickness varies from 300 mm (11.8 in.) to 356 mm (14 in.), and the typical soffit's thickness ranges from 150 mm (5.9 in.) to 230 mm (9.1 in.). The typical deck thickness varies between 190 mm (7.5 in.) and 258 mm (10.1 in.). Additionally, the stem and the soffit of box-girders were flared over a short length (i.e., less than 3048 mm [120 in.]) at the bents and the abutments to account for the stress concentrations.

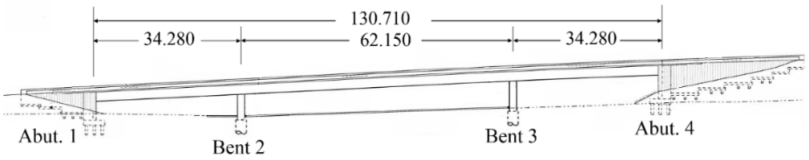

(a) B1

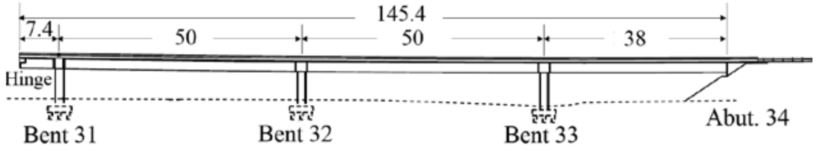

(b) B2

Figure 4.1: Elevation views of the short-span CIP / PS Box frames (all dimensions are in meter; 1 m = 3.28 ft)

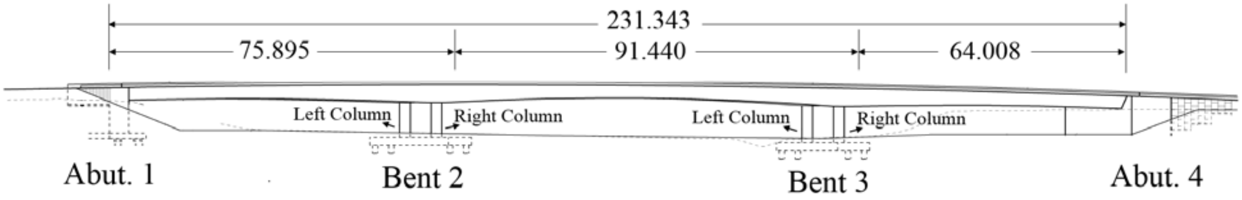

(a) B3

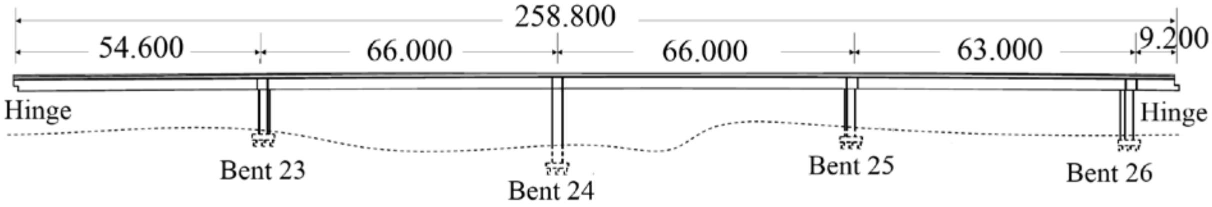

(b) B4

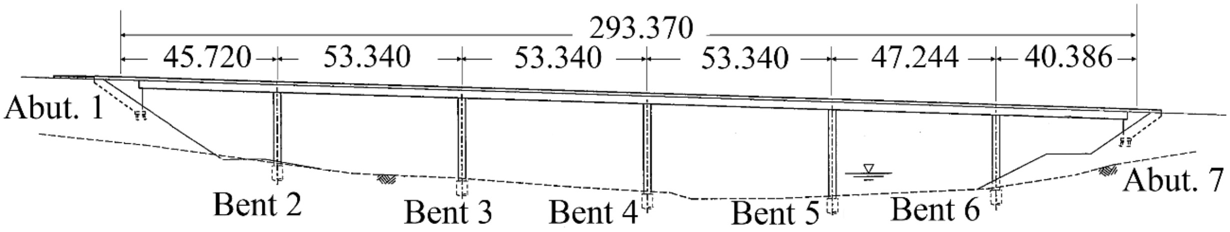

(c) B5

Figure 4.2: Elevation views of the medium-span CIP / PS Box frames (all dimensions are in meter; 1 m = 3.28 ft)

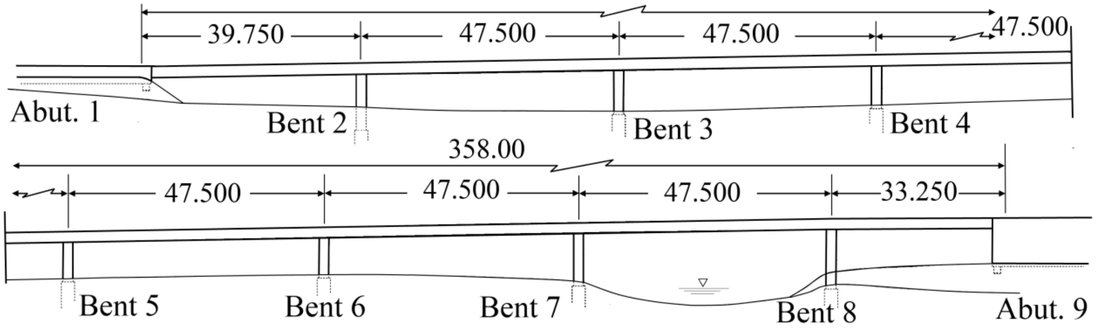

(a)B6

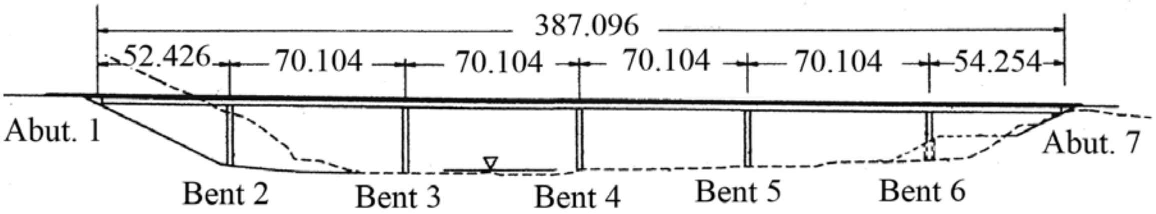

(b) B7

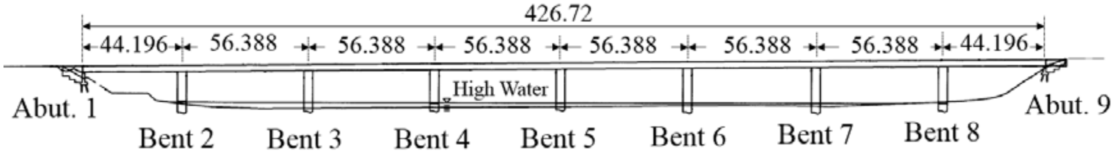

(c) B8

Figure 4.3: Elevation views of the long-span CIP / PS Box frames (all dimensions are in meter; 1 m = 3.28 ft)

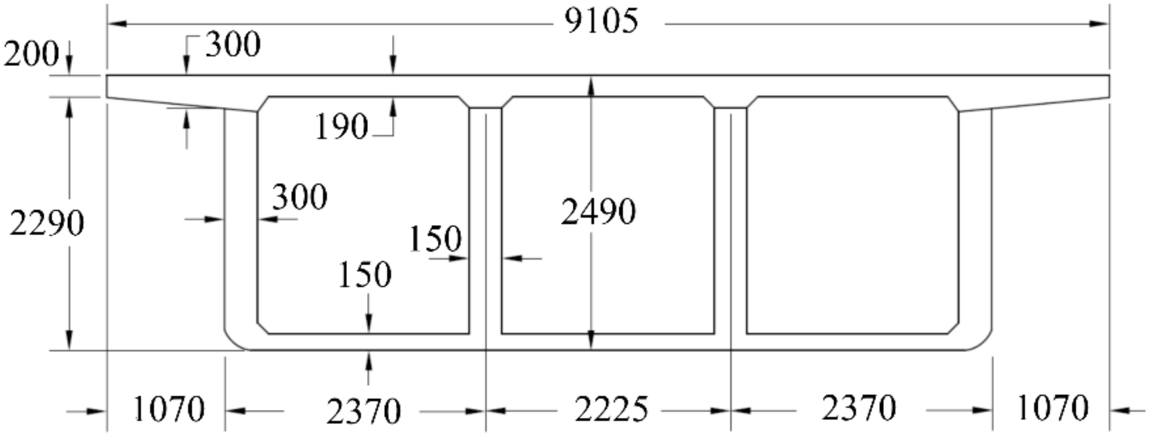

(a) B1

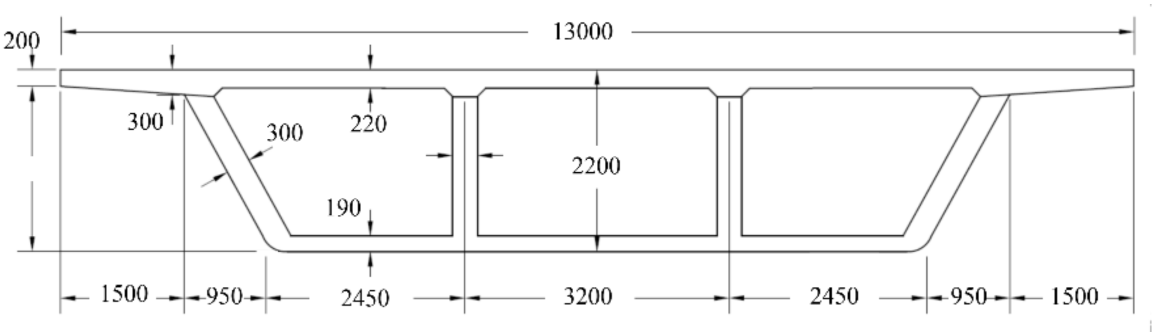

(b) B2

Figure 4.4: Typical mid-span cross sectional views of the short-span CIP / PS Box frames (all dimensions are in mm; 1 mm = 0.039 in.)

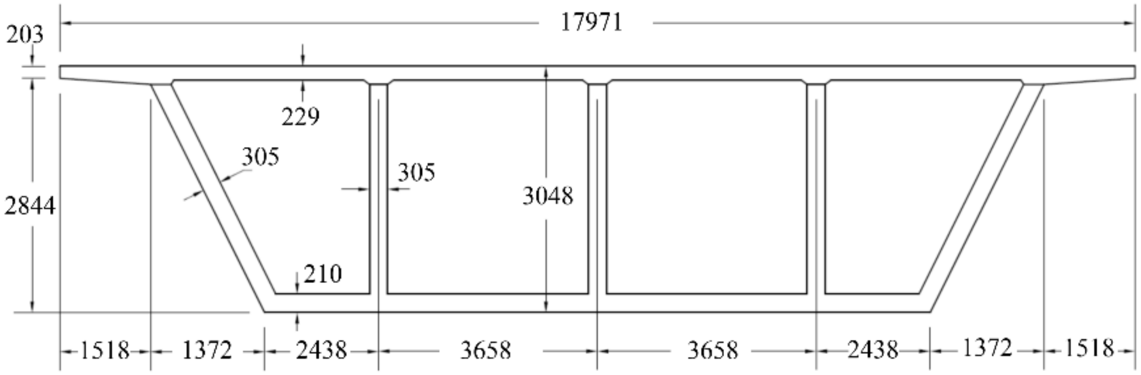

(a) B3

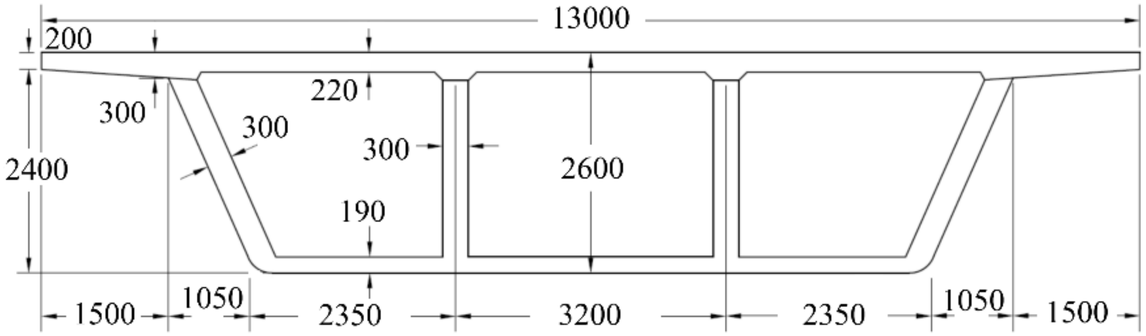

(b) B4

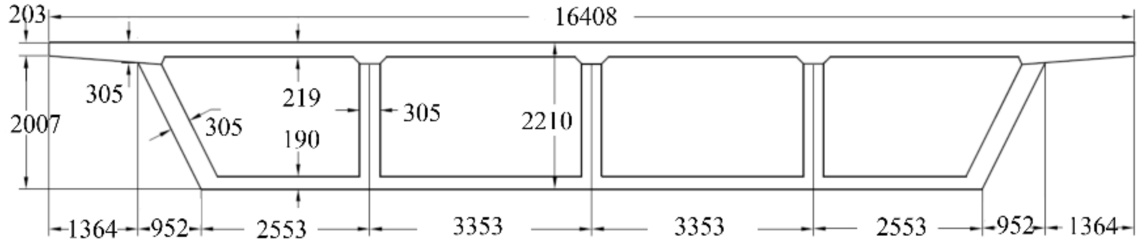

(c) B5

Figure 4.5: Typical mid-span cross sectional views of the medium-span CIP / PS Box frames (all dimensions are in mm; 1 mm = 0.039 in.)

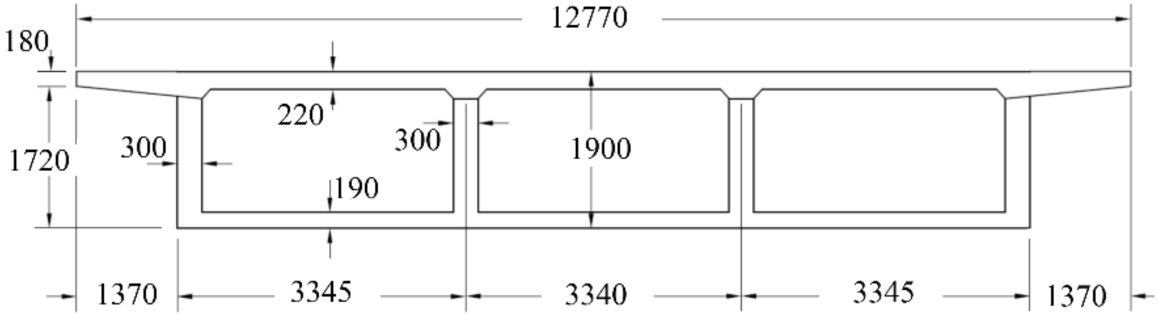

(a) B6

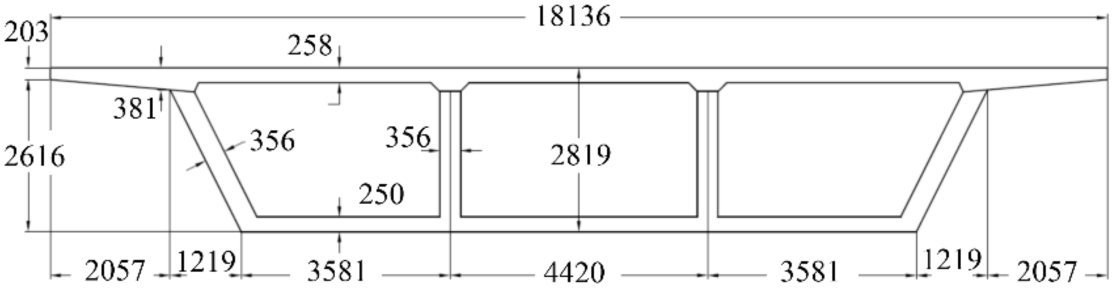

(b) B7

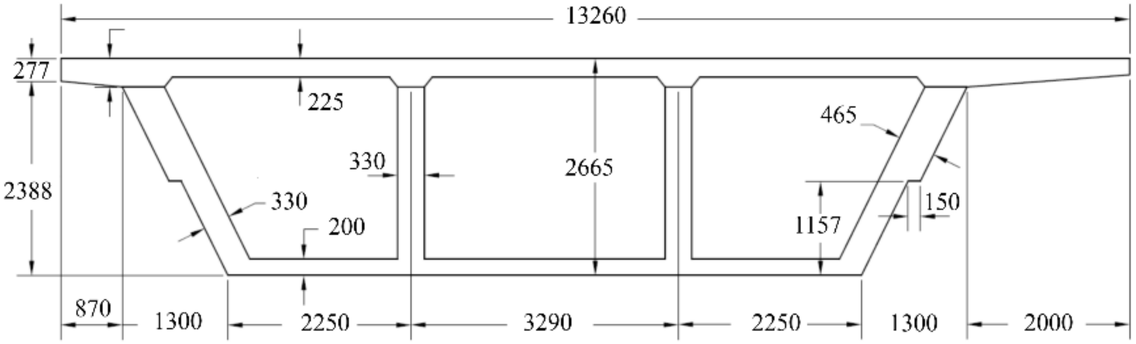

(c) B8

Figure 4.6: Typical mid-span cross sectional views of the long-span CIP / PS Box frames (all dimensions are in mm; 1 mm = 0.039 in.)

4.3 Bent Details

The details of each bent, including the connection of columns to the box-girder and the foundation, type of foundation, and column cross section are demonstrated in Figure 4.7 through Figure 4.9 for the short-, medium-, and long-span frames, sequentially. It is worth noting that the configuration of all the bents in Frames 6 and 8 of B4 are similar, except for Bent 24 which differs from the rest of the bents.

The columns are rigidly connected to the box-girder for all the frames, except for B3, where a hinge connection is used between the column top and the box-girder. The foundation type is either pipe piles or cast-in-place drilled hole (CIDH) shafts, where the former was mostly used for short- and medium-span frame and the latter was mostly used in the long-span frames. For the frames with the CIDH shafts, the column is integrated with the drilled shafts through the extension of column longitudinal reinforcement into the shaft, replicating a fixed connection at the bottom of the column. However, when the pipe pile foundation is used, the column is either connected to the foundation using a hinge (i.e., B2 and B4) or the column is rigidly connected to the foundation (i.e., B3). The bents are either a single- or a two-column bent. In B2, B4, and B5, the column cross section varies along the height for aesthetics purposes, whereas a uniform cross section was used for the columns in other CIP / PS Box frames. Furthermore, the height (H), the gross stiffness (k_g), and the effective flexural stiffness (k_{eff}) of the columns of the eight CIP / PS Box investigated in this study are presented in Table 4.3.

Table 4.3: The height and flexural stiffness of the columns in the eight CIP / PS Box frames

Frame	Column	H (m)	K_g (MN/m)	K_{eff} (MN/m)
B1	B1-C2	6.00	546.82	278.88
	B1-C3	7.00	344.35	175.62
B2	B2-C31	7.18	111.18	43.36
	B2-C32	6.81	132.68	132.68
	B2-C33	7.48	97.28	35.99
B3	B3-C2-L	8.17	239.56	124.57
	B3-C2-R	8.29	229.14	119.15
B4	B4-C23	9.43	66.32	41.78
	B4-C24	15.93	26.31	26.31
	B4-C25	10.08	53.40	29.37
	B4-C26	10.58	45.65	26.48
B5	B5-C2	23.02	8.05	8.05
	B5-C3	24.05	7.02	7.02
	B5-C4	26.06	5.47	5.47
	B5-C5	24.60	6.54	6.54
	B5-C6	22.91	8.17	8.17
B6	B6-C2	11.70	134.07	76.56
	B6-C3	11.10	157.01	79.29
	B6-C4	9.70	235.28	103.76
	B6-C5	10.20	202.35	202.35
	B6-C6	9.10	284.96	125.67
	B6-C7	11.60	137.57	69.47
	B6-C8	12.20	118.26	67.52
B7	B7-C2	24.25	32.49	15.27
	B7-C3	27.11	23.26	10.93
	B7-C4	25.44	28.14	28.14
	B7-C5	23.45	35.93	16.89
	B7-C6	23.39	36.21	17.02
B8	B8-C2	15.70	486.33	170.22
	B8-C3	17.28	365.07	127.78
	B8-C4	17.31	363.18	127.11
	B8-C5	17.57	346.99	346.99
	B8-C6	16.77	399.06	139.67
	B8-C7	17.00	383.42	134.20
	B8-C8	18.80	283.47	99.21

Note: 1 kN= 0.225 kip; 1 m = 3.28 ft

For the short- and medium-span CIP / PS Box frames, a circular column cross section with single or bundle hoops as the transverse reinforcement is typically used, except for B5, in which the column cross section is octagonal with additional stirrups to protect the column flare. An oval column cross section with the interlocking stirrups is used for the long-span frames, as shown in Figure 4.9. In B6, the details of cross section reinforcement vary among the different bents. The ratio of longitudinal steel reinforcement to the column cross sectional area of the exterior bents (i.e., Bents 2, 3, 7, and 8) is greater than the interior bents (i.e., Bents 4, 5, and 6). The cross sectional area of columns of long-span frames is greater than that of short- and medium-span frames.

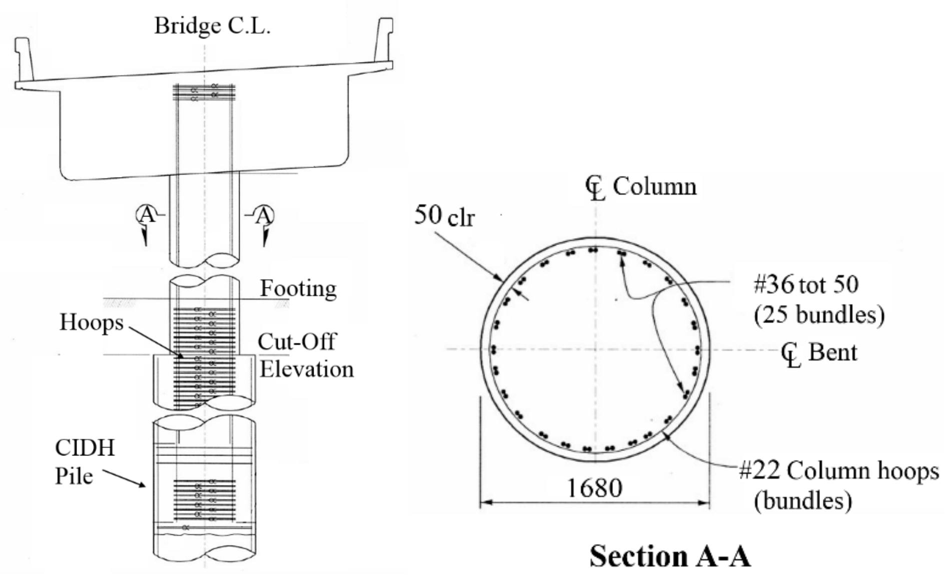

(a) B1

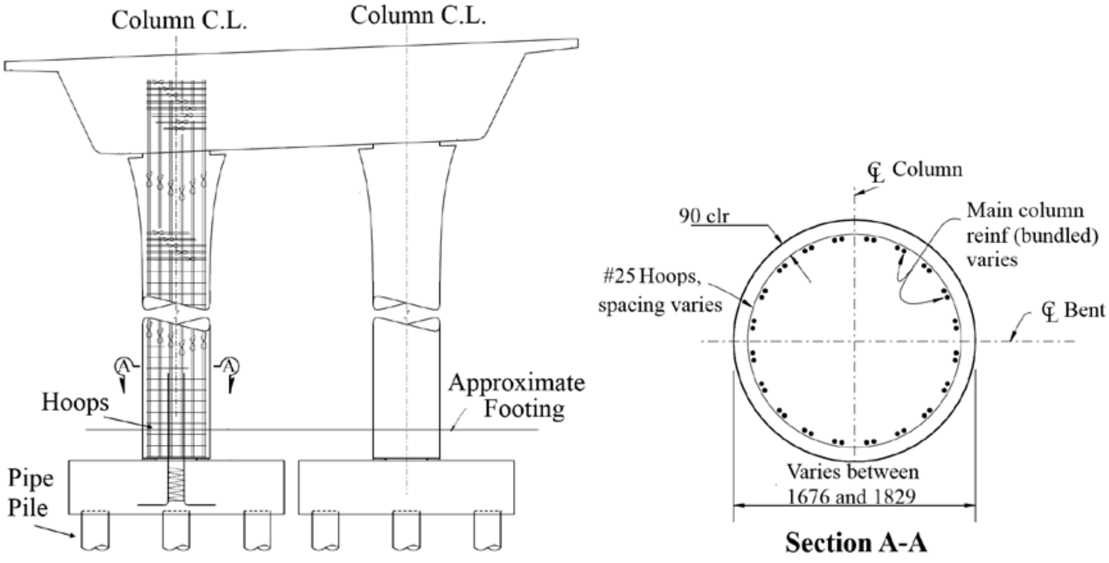

(b) B2

Figure 4.7: Bent details for the short-span CIP / PS Box frames (all dimensions are in mm; 1 mm = 0.039 in.)

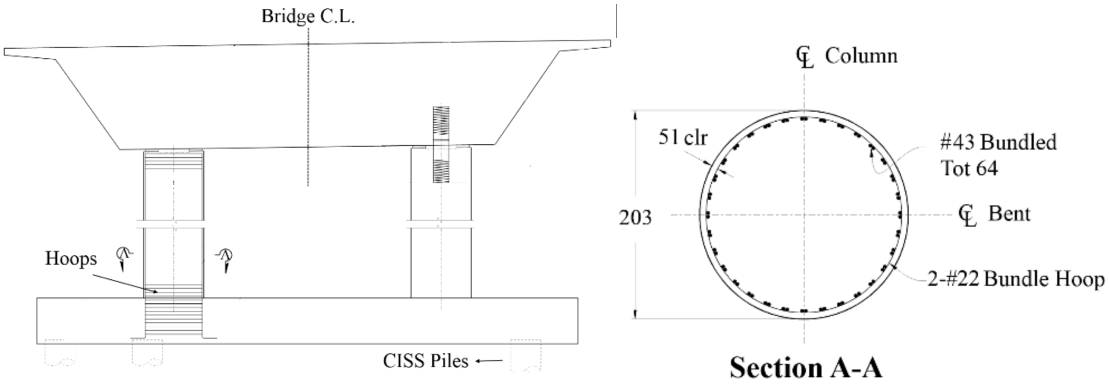

(a) B3

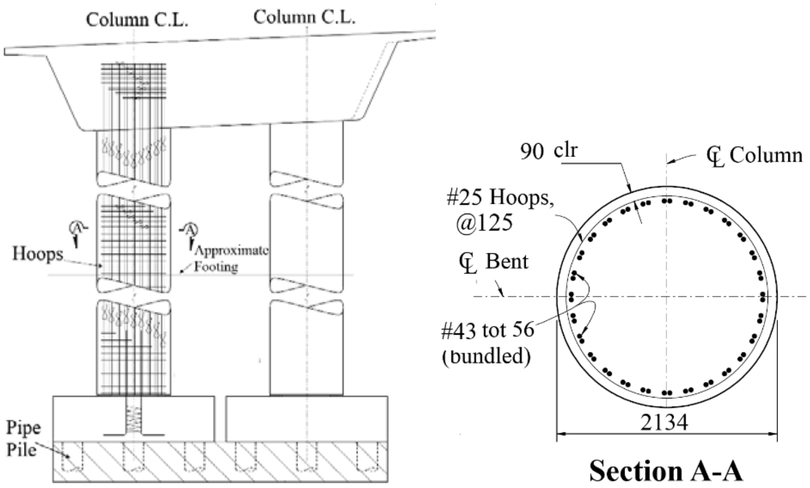

(b) B4

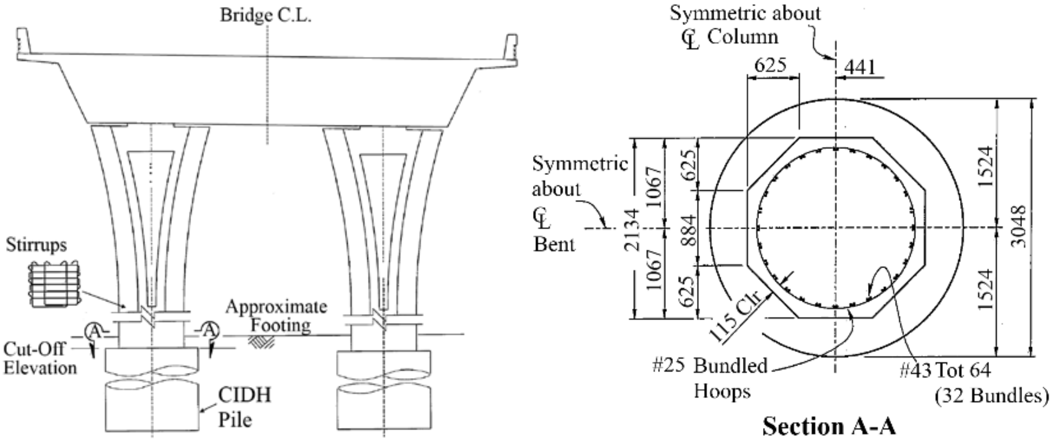

(c) B5

Figure 4.8: Bent details for the medium-span CIP / PS Box frames (all dimensions are in mm; 1 mm = 0.039 in.)

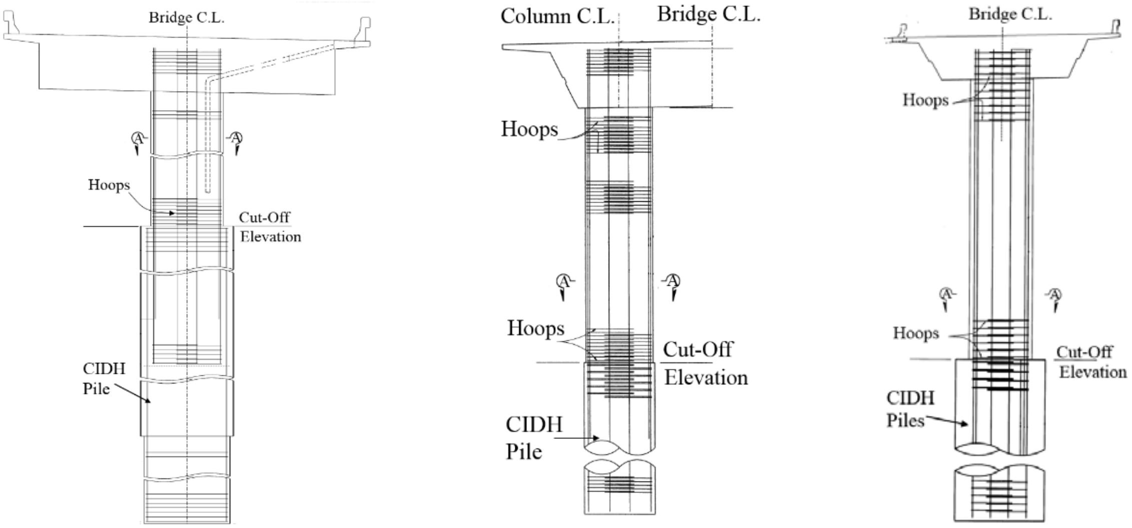

(a) B6 Elevation view (b) B7 Elevation view (c) B8 Elevation view

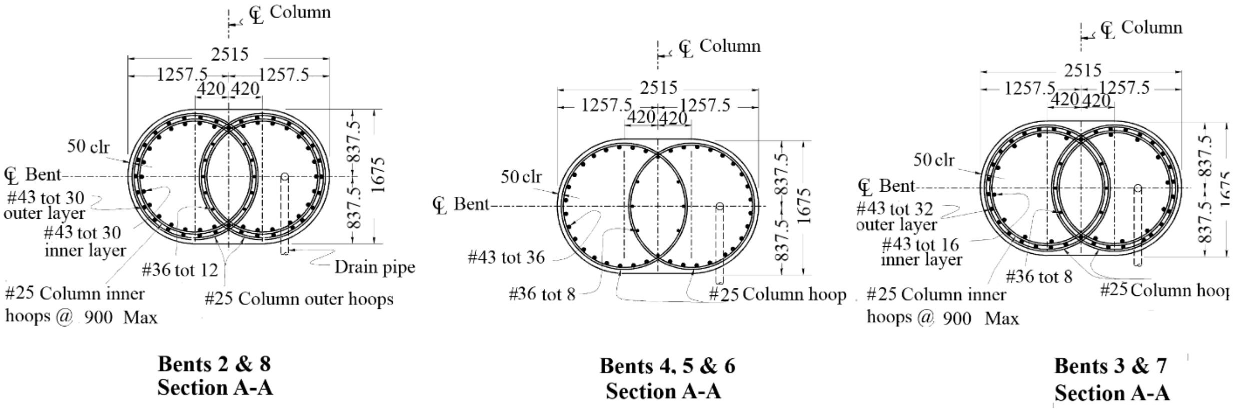

(d) B6 Column cross sections

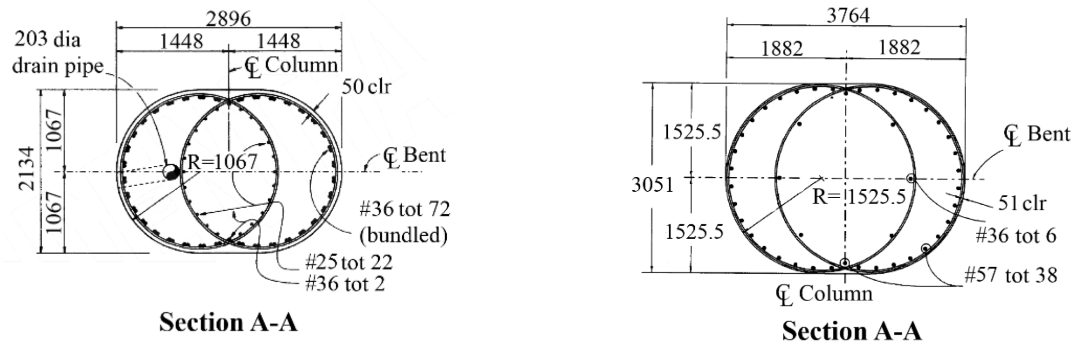

(e) B7 Column cross section (f) B8 Column cross section

Figure 4.9: Bent details of the long-span CIP / PS Box frames (all dimensions are in mm; 1 mm = 0.039 in.)

4.4 Prestressing Details

Using the prestressing details provided in the bridge drawings, the prestressing force along with the parameters required to estimate the instantaneous prestress losses are presented in Table 4.4. However, the details in regard to the application of prestressing force, including the size and location of the tendons, amount of prestressing force per girder, and the duct size were not included in the plans. Hence, these details were left to contractors to decide upon with the engineer's approval per the AASHTO LRFD 2010 recommendations.

Table 4.4: Details used for prestressing of the box-girders

Frame	Jacking force (kN)	Initial concrete axial stress (MPa)	Anchorage set (mm)	Friction coefficient, μ	Wobble coefficient, κ (1/mm)
B1	36700	6.7	10	0.15	6.60E-07
B2	32199	4.8	10	0.2	6.56E-07
B3	131928	11.4	10	0.2	6.56E-07
B4	49199	6.8	10	0.2	6.56E-07
B5	52042	5.9	10	N/A	N/A
B6	41059	6.2	10	N/A	N/A
B7	17298	6.8	0	0.2	0.00E+00
B8	63099	7.4	10	0.25	1.48E-06

Note: N/A = Not applicable; kN = 0.225 kip; 1 MPa = 0.145 ksi; 1 mm = 0.039 in.

Due to the different box-girder cross section sizes, a large variation in jacking forces is observed among the eight frames in order to satisfy the concrete stress limits upon the application of the prestressing force. The amount of anchorage set is almost the same for all the frames, except for B8 which has a noticeably smaller value for the anchorage set. For the friction coefficient, the lowest and the highest values used are 0.15 and 0.25, respectively, while the specified value of the friction coefficient is 0.2 for several frames. Except for B7 which has an appreciably higher wobble coefficient, the wobble coefficient is almost the same for the other frames. In addition, the friction and wobble coefficients were not specified for B5 and B6, and the wobble coefficient was specified to be zero for B8.

4.5 Material Properties

Low relaxation strands with an ultimate strength of 1862 MPa (270 ksi) were used specified as the prestressing steel for all of the frames. Mild steel with a yield strength of 414 MPa (60 ksi) was used for the reinforced concrete. For concrete, the compressive strength specified for the prestressed box-girder, including the deck, was slightly higher than that specified for the substructure (i.e., columns and foundations). However, the concrete used for prestressed box-girders and substructure was classified as normal strength concrete with similar mix designs. Using the details provided in the bridge drawings, Table 4.5 summarizes the material properties used for the eight frames. In general, the 28-day compressive strength of the box-girder is greater than that used in the substructure for the eight frames. It should be noted that the value of initial compressive strength of reinforced concrete was not specified in the plans, while this value was particularized for the prestressed box-girders.

Table 4.5: Details of material properties used in the CIP / PS Boxs

Bridge	Prestressing steel			Box-girder/Deck		Reinforced concrete	
	f_{pu} (MPa)	f_{py} (MPa)	f_{pj} (MPa)	f'_{ci} (MPa)	f'_c (MPa)	f_y (MPa)	f'_c (MPa)
B1	1862	1675	1396	25	31	420	25
B2	1862	1675	1396	28	35	420	25
B3	1862	1675	1396	28	38	420	25
B4	1862	1675	1396	28	35	420	25
B5	1862	1675	1396	24	28	420	25
B6	1862	1675	1396	25	28	420	25
B7	1862	1675	1396	24	31	420	22
B8	1862	1675	1396	26	31	420	28

Note: f_{pu}: ultimate strength of prestressing strands; f_{py}: yield strength of prestressing strands; f_{pj}: jacking stress of prestressing strands; f'_{ci}: release compressive strength; f'_c: 28-day compressive strength; and f_y: yield strength of mild streel reinforcement; 1 MPa = 0.145 ksi

CHAPTER 5: DETAILS OF ANALYTICAL MODELS

5.1 Introduction

Time-dependent effects on the behavior of a prestressed bridge differ from one structural system to another. In a statically indeterminate structure, creep and shrinkage result in redistribution of strains and stresses within individual sections meaning a decrease in the compression in concrete and in the tension in steel. The compression stresses induced in concrete by prestressing lead to a reduction of the prestressing force under the influence of concrete creep. Additionally, the initial prestressing force is reduced by shortening due to shrinkage in combination with the relaxation of the prestressing steel. By virtue of concrete creep and shrinkage, the reduction of internal stresses caused by prestressing, naturally is dependent on the prestressing force. In statically indeterminate structures, additional changes in stresses and in the reactions (i.e. secondary effects) will develop, producing continuous variation of internal forces along the bridge with time. In these structures, creep and shrinkage experienced by one member therefore induce forces and stresses in other members, facilitating redistribution of forces and stresses.

Given the interrelated and interdependent nature of time-dependent material properties, one needs a sophisticated analysis to accurately predict the time-dependent stresses and strains, especially in statically indeterminate prestressed bridges. Therefore, in this study, the time-dependent analysis of prestressed concrete bridges was carried out using the midas Civil software. This commercial software enables systematic analyses of FEMs with due considerations to creep and shrinkage effects using the time-step method, as detailed in Section 2.5, thereby producing time-dependent stresses and deformations in members of prestressed concrete bridges. Each selected bridge, identified in Chapter 4, was simulated in midas Civil following the details provided in the bridge plans and the selected assumptions and approximations. Using bridge frame B4, this chapter demonstrates the methodology including the assumptions and approximations employed in this study to investigate time-dependent effects on CIP / PS Box frames. The methodology was repeated for the analysis of the other seven CIP / PS Box frames and the analysis results are presented in Chapter 6.

5.2 Analytical Model

The FEM of B4 was first developed in midas Civil software (2013), accounting for the construction stages and an appropriate timeline. Beam elements were employed to model the box-girder and columns. The significant parameters affecting time-dependent behavior of prestressed concrete bridges, as outlined in Section 2.3, such as concrete creep (and relaxation) and shrinkage, changes in prestressing force, support conditions, and construction sequence were taken into account in the analytical models.

5.2.1 Model Assumptions

The following assumptions were used in the FEM of B4 and all other frames to so that the analysis results can be compared and appropriate recommendations can be formulated:

- The bridge was modeled with zero curvature in the horizontal plane.
- The box-girder remained elastic and uncracked when the time-dependent deformations were imposed;
- The restraining effects of box-girder nonprestressed reinforcement on shrinkage were disregarded;
- The loads acting on the bridge frame were dead load and prestressing force;
- Linear elastic behavior was used for columns, although the stiffness was modified to account

for the effects of flexural cracking; and

- Perfect bond between the prestressing steel and concrete.

5.2.2 Construction Stages

Figure 5.1 demonstrates the typical construction stages of a frame of a CIP / PS BOX in California, which involves the following stages: (1) construction of the foundation (e.g., cast-in-place drilled hole [CIDH] shafts); (2) construction of piers; (3) construction of soffit and stem of the box-girder on shoring; (4) construction of the deck; (5) application of prestressing force, (6) removal of shoring; and (7) construction of barriers followed by the service conditions. These seven construction stages were simulated in the FEM according to the average timeline shown in Figure 5.1 to reflect the most common practice used for the construction of CIP / PS Box in the state of California. The tendon profiles along the length of the box-girder modeled in the FEA are shown in Figure 5.2. The construction stages for B4 modeled in the midas Civil software (2013) are illustrated in Figure 5.3.

It can be inferred from the construction stages that the columns were approximately 180 days old when they were subjected to the lateral deformation imposed by the box-girder. Additionally, as soon as the concrete shrinkage begins in an indeterminate bridge frame (i.e., the box-girder prior to casting of the deck), tensile creep deformation in the box-girder is produced which indeed alleviates the shrinkage deformation. Assuming an age of seven days at the beginning of shrinkage resulted in a loading age of seven days for the initiation of creep in the box-girder. Consequently, the loading ages of seven and 180 days were used in the estimation of the creep coefficients for the box-girder and the columns, respectively.

The CIP / PS Box generally consisted of multiple frames, with multiple spans, which were isolated from each other with an expansion joint, in order to lessen the continuous longitudinal movement of CIP / PS Box. In the aforementioned construction stages of CIP / PS Box, the concrete for step 3 can be either poured concurrently for all spans within a short time, or one span at a time. The former generally induces more shortening in the box-girders, and subsequently more column forces than the latter. Adhering to the recommendation from the TAC, it was assumed that the concrete for the entire bridge frame length was poured at the same time. The same assumption was made for casting of the concrete columns. Therefore, the substantial portion of the duration of each construction stage shown by the diagram in Figure 5.1 was allocated to the preparation of the falsework. This was replicated in the analytical models by adjusting the loading age of elements upon activation.

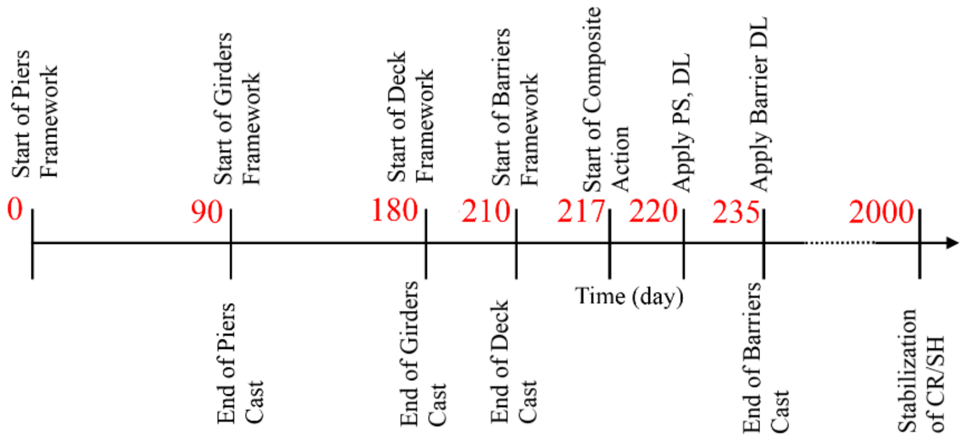

Figure 5.1: Timeline used for construction of B4

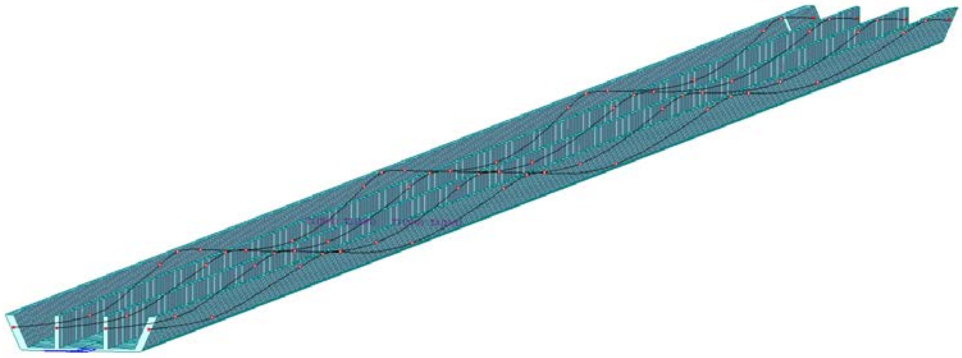

Figure 5.2: Tendons along the length of the box-girder as modeled in the FEM

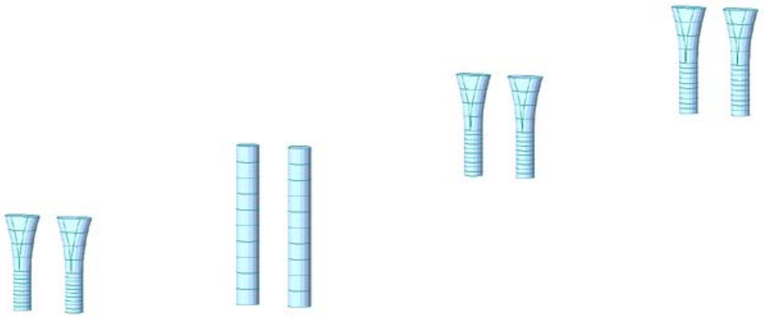

(a) Constructed piers

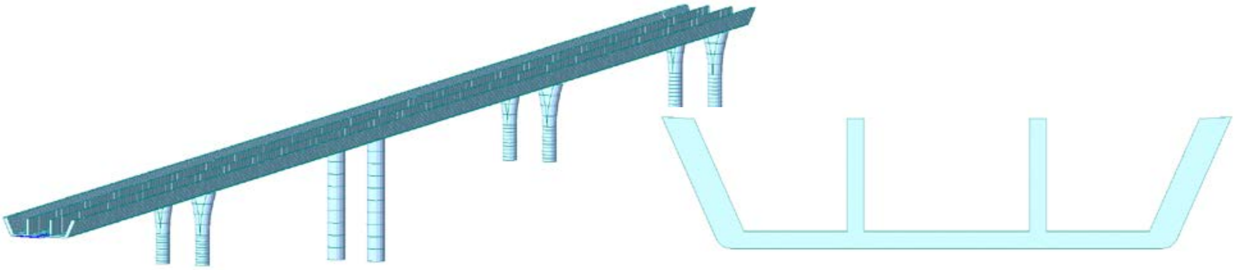

(b) Constructed box-girder

(c) Constructed deck

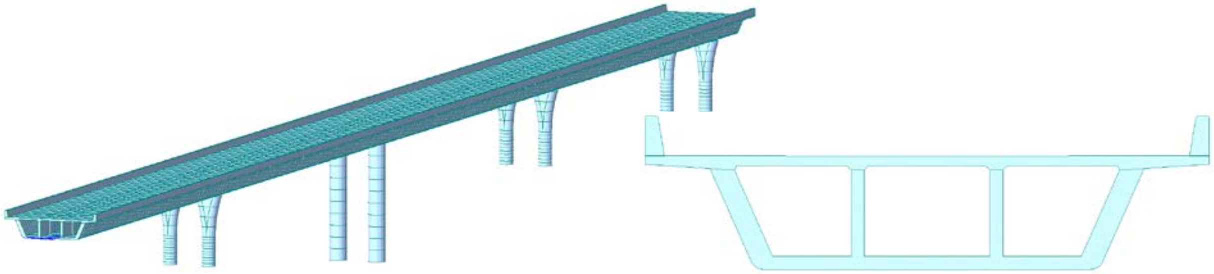

(d) Constructed barriers

Figure 5.3: Construction stages of B4 as used in the FEM

5.2.3 Material Properties

The material properties for the FEM of B4 were estimated using the prediction models presented in Table 5.1. The variation of compressive strength with time was disregarded for columns, since the columns were at least three months old by the time the box-girder was cast and the time-dependent deformations were imposed on them. The column modulus of elasticity was calculated using the AASHTO LRFD Bridge Design Specifications (2010) model based on the 28-day compressive strength; any further gain in the modulus of elasticity was neglected. For the box-girder, the variation of concrete compressive strength with time was estimated using ACI (2011).

Due to the difference in both the concrete compressive strengths and volume to surface ratios between the box-girders and columns, two separate creep and shrinkage models were employed for the box-girders and columns. The compressive strengths provided in Section 4.5, the assumption of 60% for the relative humidity, and the age of 7 days for the beginning of shrinkage were used to estimate the creep and shrinkage deformations based on the AASHTO LRFD Bridge Design Specifications (2010). In addition, the loading ages of seven and 180 days were assumed for the box-girders and the columns, respectively, to calculate the creep coefficient as previously noted.

Table 5.1: Prediction models used in the FEM to account for the time-dependent properties

Material property	**Model**	
	Box-girder	**Column**
Variation in concrete compressive strength with time	ACI	Not modelled
Modulus of elasticity	AASHTO	AASHTO
Concrete creep/relaxation	AASHTO	AASHTO
Concrete shrinkage	AASHTO	AASHTO
Relaxation of posttensioned tendons	AASHTO	Not Applicable

5.2.4 Boundary Conditions

The box-girder frames were allowed to move freely in the longitudinal direction during prestressing as well as due to concrete creep and shrinkage by providing roller supports at the expansion joints in the FEM. The connection of the box-girders to the columns was modeled according to the CIP / PS Box plans (see Section 4.3). For some CIP / PS Box, the box-girders were integrally connected to the columns, which accommodated moment transfer between the box-girders and the columns. In contrast, moment transfer was not allowed in other CIP / PS Box by providing hinges at the connection of the box-girders to the columns because their columns used pinned connections to the superstructure. Additionally, the barriers were rigidly connected to the bridge deck to impose compatible deformation between the deck and the barriers.

The boundary condition for the columns is one of the significant factors determining the force induced in the columns due to the restraint provided by the superstructure shortening. Hence, the column end conditions were modeled by following the connection details of the columns to the foundations outlined in Section 4.3. Typically for long span CIP / PS Box, CIDH shafts were used for the foundations with fixed connections to the columns. Therefore, these columns were modeled with fixed conditions at the base and the CIDH shafts were not modelled. In other CIP / PS Box, pile foundations were used with pinned connection to the columns and they were modelled as hinges.

5.2.5 Loading

Two load cases including dead load and prestressing force were imposed on CIP / PS Box models. Following the construction timeline, the prestressing force was applied 40 days after completing casting of the deck. Following the application of the prestressing force, the falsework is removed, which was simulated in the FEMs by activating the dead load of the CIP / PS Box.

The total prestressing force was equally distributed to all stems and was applied to each stem by placing a tendon in the plane through the middle of the girder thickness. The size of each tendon was chosen such that the geometry constraints were satisfied and the stress in each tendon was below the yield strength of the tendons as specified in the drawings. Based on the diameter of the tendons, the appropriate duct size was included in the FEM. In addition, the tendons were modeled as bonded tendons with perfect bonding to the surrounding concrete. Thus, the box-girder section properties used in the analyses reflected the transformed section properties.

5.2.6 Column Effective Stiffness

Moment-curvature analyses of columns were performed using the XSection software (ref) to determine when they would experience flexural cracking due to the displacement-induced forces. The required axial force for the moment-curvature analysis was estimated using the FEM of the CIP / PS Box when the bridge was subjected only to the dead load. The moment-curvature analysis results of the four bents of B4 are presented in Figure 5.4.

The time-dependent analysis was initially completed assuming columns remained uncracked (i.e., using the gross section properties) and then the resulting column moments were compared to the column cracking moments calculated using the XSection software. When a column was identified to be cracked, the effective stiffness calculated by the moment-curvature analysis was used to replace the corresponding gross stiffness value to account for cracking and the FEM analysis was repeated. This step was accomplished in the analyses by decreasing the column gross moment of inertia in the FEM using a reduction factor. The reduction factor represented the ratio between the effective to gross stiffness. Subsequently, the column moments were reevaluated and compared to the cracking moment to ensure use of appropriate column stiffness values.

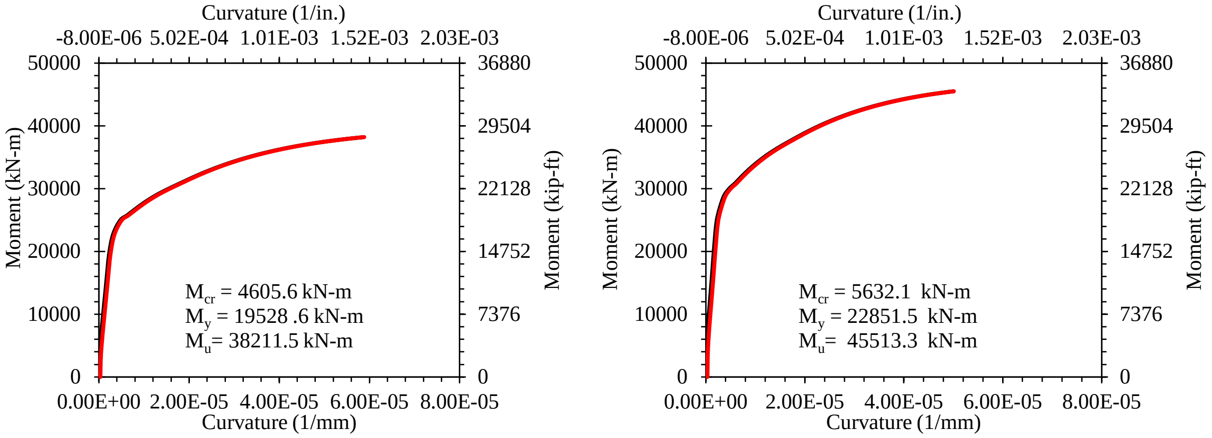

(a) B4-C23

(b) B4-C24

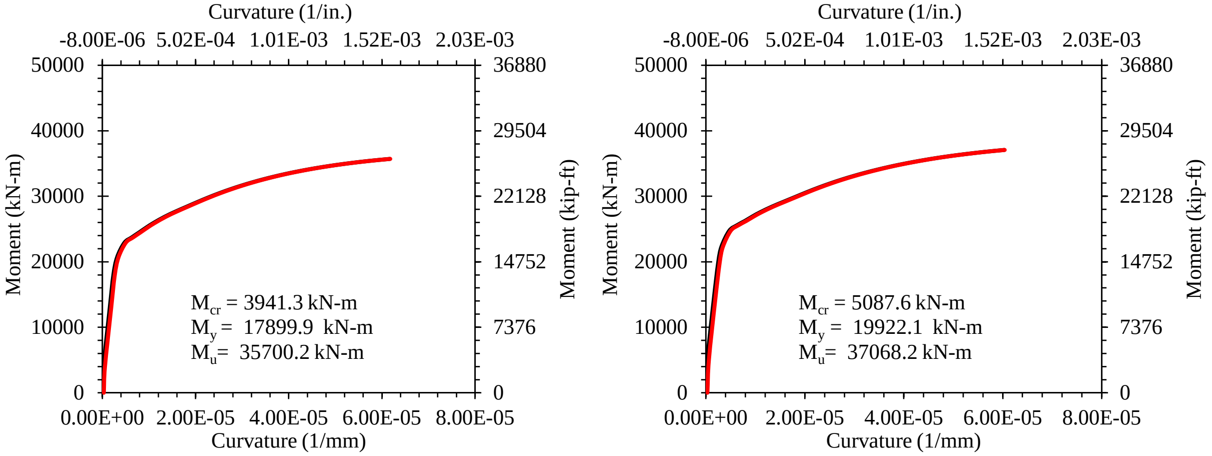

(c) B4-C25

(d) B4-C26

Figure 5.4: Moment curvature analysis of columns in B4

5.3 Analysis Results

The FEM results for the time-dependent effects on the box-girder and the columns of B4 are demonstrated in this section. The effects of concrete relaxation are integrated in the FEM results; however, the responses of the bridge with and without concrete column relaxation are shown for comparison purposes. For the superstructure (i.e., the box-girder), the shortening strain rate was evaluated by using the displacements at the ends of frames. For the columns, the variation of lateral top displacements and corresponding base shear forces with time were determined as a function of time. Figure 5.5 shows the deformed shape of B4 predicted by the FEM due to prestressing, creep, and shrinkage after 2000 days from completion of pier construction.

The application of prestressing force and time-dependent effects on a continuous CIP / PS Box produced reactions at the column bases and internal forces in each structural member that are collectively called secondary forces. The terminology given in Table 5.2 is used to present the FEA results with respect to the secondary effects. The primary effects of time-dependent deformation due to creep and shrinkage are used to calculated deformations. The calculation of total reaction, deformation, and forces/stresses due to dead load, prestress, creep, and shrinkage in an indeterminate CIP / PS Box frame are presented in Table 5.2.

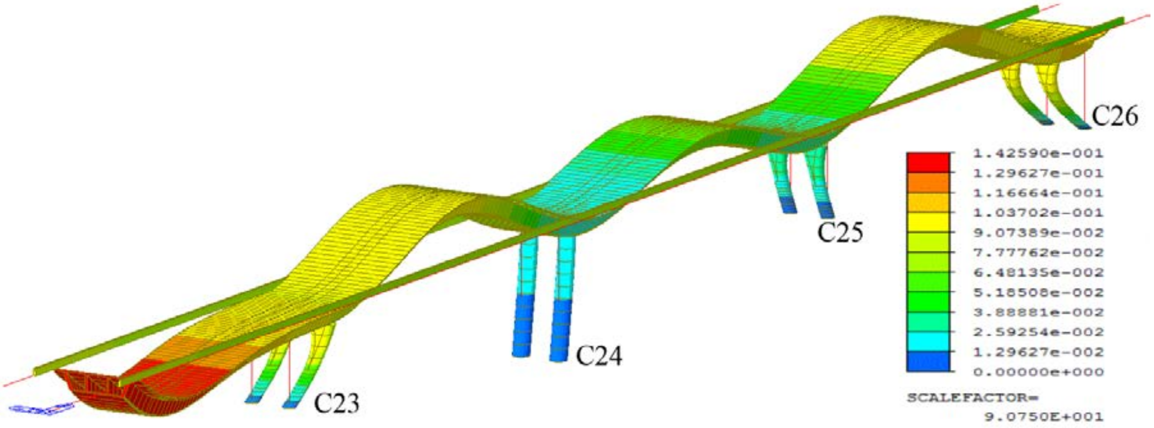

Figure 5.5: Deformed shape of B4 (in meters) predicted by the FEA due to presterssing, creep, and shrinkage after 2000 days from completion of pier construction

Table 5.2: Terminology used in the FEMs for the primary and secondary effects in continuous CIP / PS Box frames

Load case	Results	Description
1. Dead load		Results due to all dead load excluding the effects of creep, shrinkage, and tendon prestress
2. Tendon primary	Reaction Deformation Force/stress	 Deformation caused by tendon prestress Member forces/stresses caused by tendon prestress
3. Tendon secondary	Reaction Force/stress	Reactions caused by tendon prestress in an indeterminate structure Member forces/stresses caused by tendon prestress in an indeterminate structure
4. Creep primary	Reaction Deformation Force/stress	 Deformation due to imaginary forces required to cause creep strain Imaginary forces/stresses required to cause creep strain
5. Creep secondary	Reaction Force/stress	Reactions caused by creep in an indeterminate structure Member forces/stresses caused by creep in an indeterminate structure
6. Shrinkage primary	Reaction Deformation Force/stress	 Deformation due to imaginary forces required to cause shrinkage strain Imaginary forces/stresses required to cause shrinkage strain
7. Shrinkage secondary	Reaction Force/stress	Reactions caused by shrinkage in an indeterminate structure Member forces/stresses caused by shrinkage in an indeterminate structure
Total	Reaction Deformation Force/stress	1+3+5+7 1+2+4+6 1+2+3+5+7

5.3.1 Shortening Strain Rate of the Superstructure

The shortening strain rate of the superstructure was calculated as the difference between the displacements at the two ends of the bridge frame divided by its length. Figure 5.6 shows the shortening strain rate of the box-girder due to dead load, prestress, creep, and shrinkage components in addition to the summation of these components. It is observed that the total shortening strain rate is predominantly affected by the shrinkage. After 2000 days, the total shortening strain rate is comprised of 68.8%, 16.6%, 20.1%, and -5.6% due to shrinkage, creep, prestress, and dead load, respectively. For B4, the dead load acted in the opposite direction to the creep, shrinkage, and prestress strains. Since the superstructure is significantly stiffer than the columns, the column creep (or relaxation) did not affect the shortening of the superstructure, as shown in Figure 5.6.

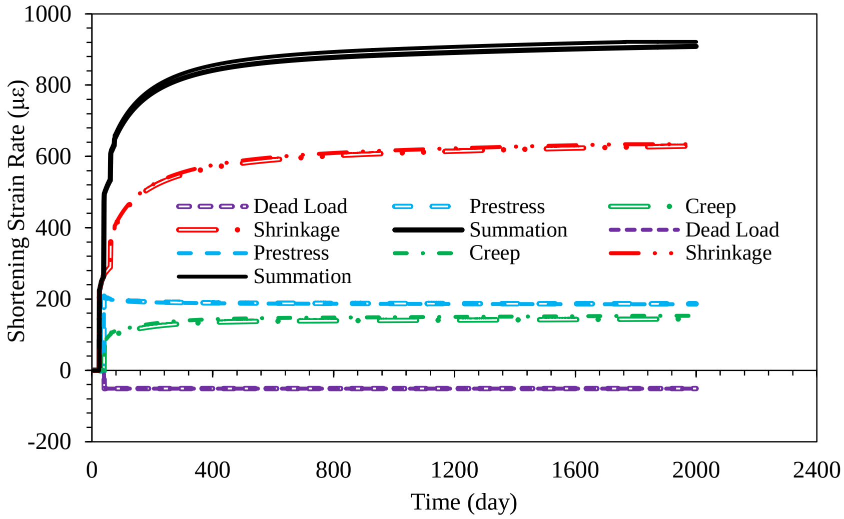

Figure 5.6: Shortening strain rate of the superstructure calculated using the FEM with concrete relaxation in the columns (single line) and without concrete relaxation (double line)

5.3.2 Column Top Lateral Displacement

Figure 5.7 shows the analysis results obtained for the column top lateral displacement due to dead load, prestress, creep, and shrinkage components as well as the summation of these components. As expected from the previous section, the shrinkage of the superstructure had the largest contribution to the column displacement compared to the other components. After 2000 days, the total displacement of B4-C26 comprised of 59.3%, 22.2%, 14.5%, and 4% due to shrinkage, creep, prestress, and dead load, respectively. Typically, the further away the column is from the point of no movement (PNM), the larger the lateral displacement due to the superstructure shortening that is imposed on the column. Accordingly, the displacement of the two exterior columns (i.e., B4-C23 and B4-C26) was significantly greater than that of the two interior columns (i.e., B4-C24 and B4-C25). The largest top of column displacement was 103 mm (4.1 in.) and belonged to B4-C26, while B4-C24 had the smallest displacement of 23 mm (0.9 in.), which was not even sufficient to cause flexural cracking in the column.

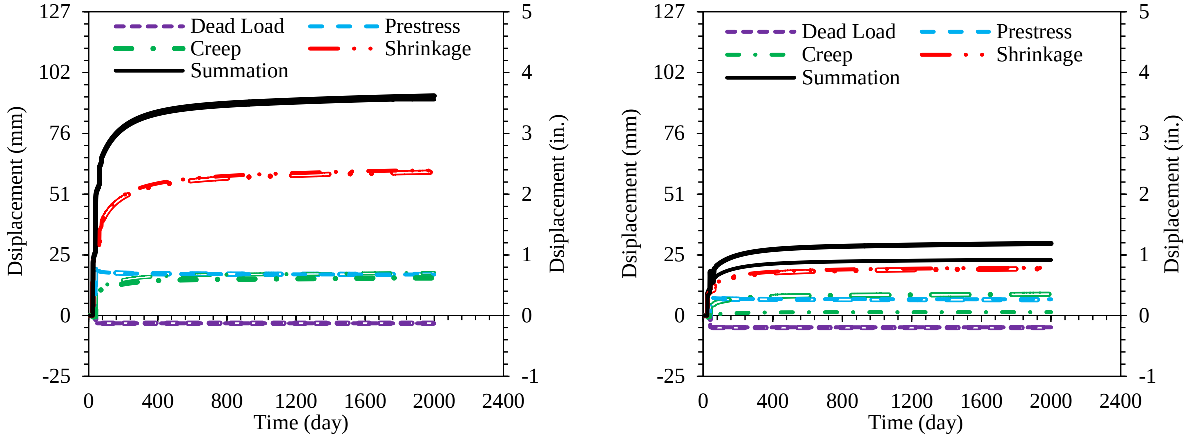

(a) B4-C23

(b) B4-C24

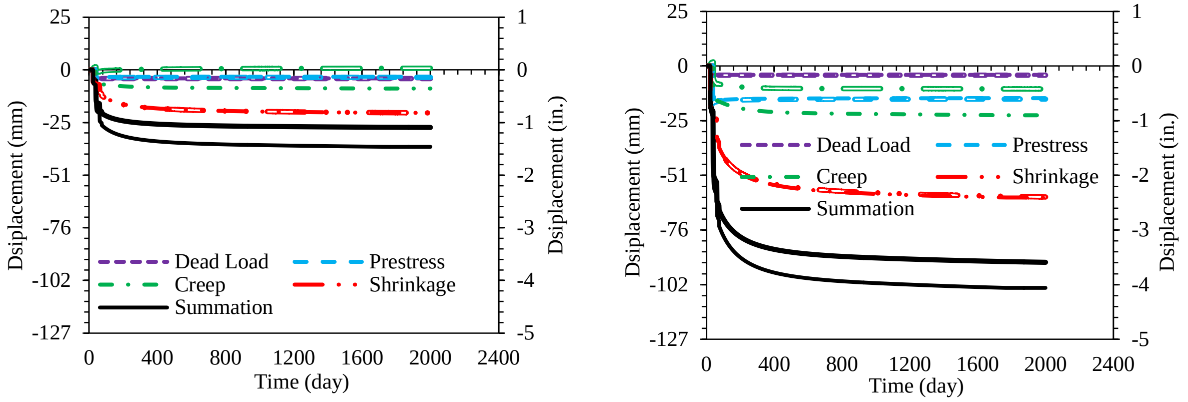

(c) B4-C25

(d) B4-C26

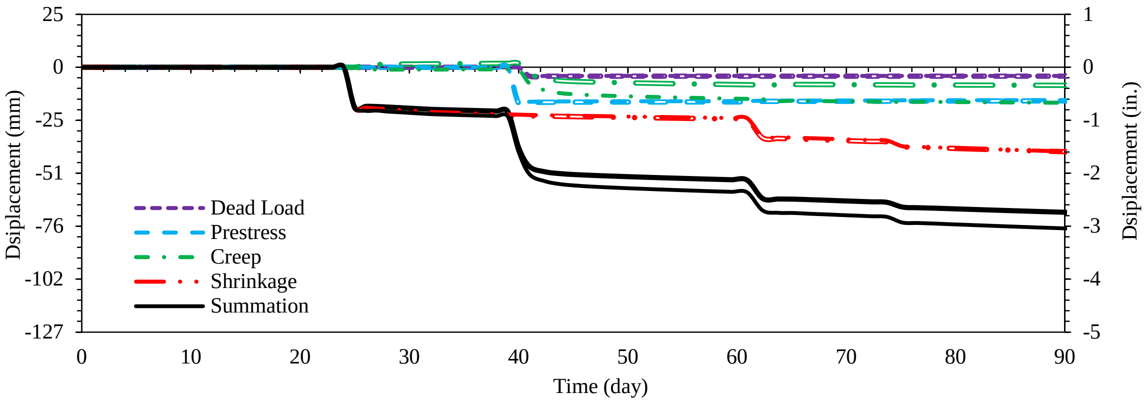

(e) B4-C26 – the first 90 days

Figure 5.7: Variation of column top lateral displacements calculated using the FEM with concrete relaxation (single line) and without concrete relaxation (double line) in columns

5.3.3 Column Base Shear Force

The contribution of the different components including dead load, prestress, creep, and shrinkage to the total base shear force was evaluated and is presented in Figure 5.8. In agreement with the displacements and strain rates, the shrinkage of the superstructure affected the base shear force more than the other components. After 2000 days, for B4-C26, the total base shear force is comprised of 125.5%, -82.6%, 44.0%, and 13.1% due to shrinkage, creep (in the superstructure), prestress, and dead load, respectively. As shown in Figure 5.8, the secondary effect of creep acted in the opposite direction to the dead load as well as the secondary effects of prestress and shrinkage. Moreover, the column creep (relaxation) significantly reduced the deformation-induced forces in the column, as seen in Figure 5.8. The reduction in the column base shear force in B4-C23 was 42.3% after 2000 days due to column relaxation. In general, the higher the column displacement was, the greater the induced shear force in the column. Thus, similar to the column displacement, the two exterior columns (i.e., B4-C23 and B4-C26) were subjected to significantly higher base shear forces than the two interior columns (i.e., B4-C24 and B4-C25). The maximum estimated column base shear force was -1819 kN (-409 kips) in B4-C23, while B4-C24 experienced the lowest shear force (i.e., -89 kN [-20 kips]).

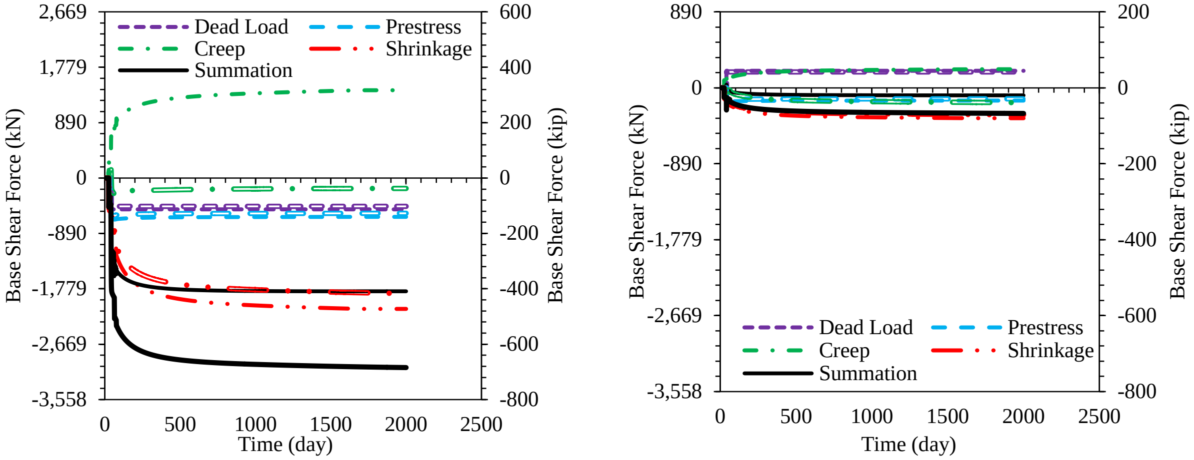

(a) B4-C23 (b) B4-C24

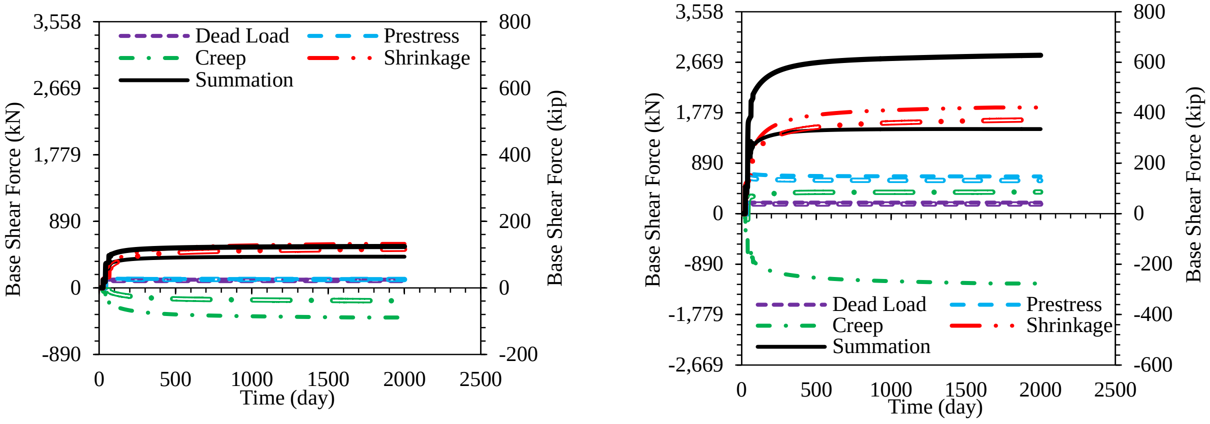

(c) B4-C25 (d) B4-C26

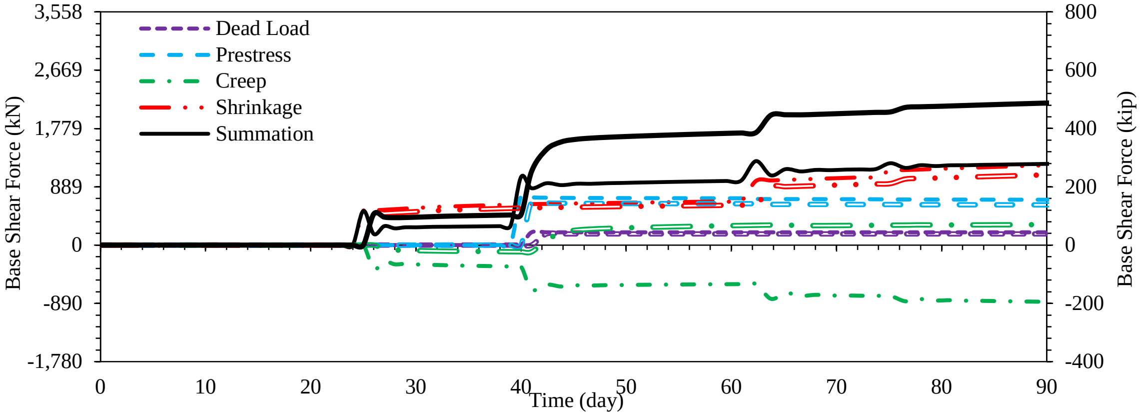

(e) B4-C26 - the first 90 days

Figure 5.8: Variation of column base shear force calculated using the FEM with concrete relaxation (single line) and without concrete relaxation (double line) in columns

Using the FEM results for the base shear force, the variation in the column moment with time was calculated and then compared to the results of the moment-curvature analysis, as shown in Figure 5.9. Based on the moment-curvature analysis, all of the columns were found to experience flexural cracking due to the time-dependent effects except B4-C24, which is located nearest to the PNM. Additionally, the calculated flexural moment demand by the FEM is less that the first yield moment for all columns, which was determined from the moment-curvature analysis results. This would not be true if the beneficial effects of concrete relaxation were not considered in the FEM analysis.

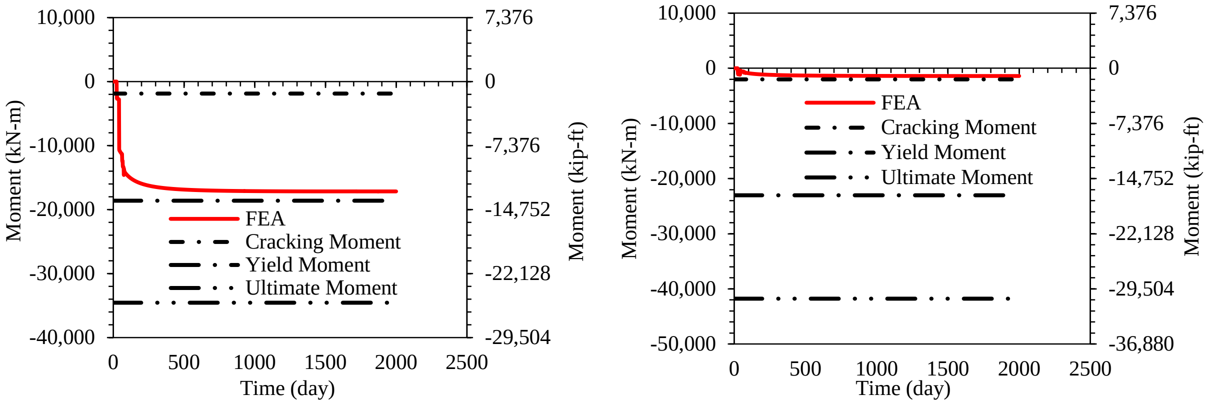

(a) B4-C23

(b) B4-C24

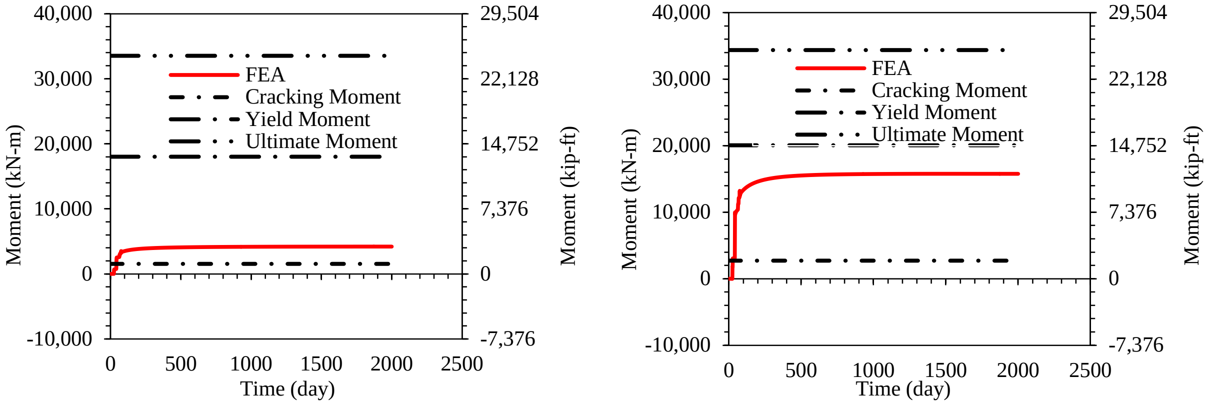

(c) B4-C25

(d) B4-C26

Figure 5.9: Comparison between the column moment calculated using the FEM and the critical column moments determined from the moment-curvature analyses

5.3.4 Effects of Loading Age on Displacement-Induced Forces

Due to the high dependency of the creep/relaxation function on the loading age, the effect of different loading ages on the AASHTO (2010) recommended creep coefficient, and consequently on the deformation-induced forces in the columns were examined. The following loading scenarios were included to cover a wide range of loading ages for columns:

- Loading age of three days: deformation-induced forces were assumed to develop in the columns when the columns were three days old. This is an extreme theoretical case, which is highly improbable from a practical standpoint.
- Loading age of 96 days: deformation-induced forces began to develop in the columns when the columns were 96 days old.
- Loading age of 190 days: deformation-induced forces began to develop in the columns when the columns were 190 days old, which is more typical of the current construction of CIP / PS Box.
- Loading age of 796 days: deformation-induced forces were assumed to develop in the columns when the columns were 796 days old. This scenario for the loading age might represent an extreme case of delays in the construction of CIP / PS Box.

The creep coefficients calculated for the different loading ages are shown in Figure 5.10. In line with the theory, the higher the loading age, the smaller the estimated value of the creep coefficient is. For the loading age of 796 days, the creep coefficient increases immediately after the application of the load and then reaches a plateau. These creep coefficients were employed in the FEMs to investigate the variability of base shear force associated with the variation in loading ages. The analyses reflected the effects of the column relaxation on base shear force by including and excluding creep in the columns.

The reduction in the base shear force with time due to the column relaxation is presented in Figure 5.11 by rerunning the FEM. Similar to the creep, the amount of reduction in the base shear force is highly dependent on the magnitude of the load. Hence, the reduction in the force was significantly larger for the exterior columns than for the interior columns, for which the force reduction was negligible. Furthermore, for the two exterior columns, using the creep coefficients associated with the loading ages of three and 790 days resulted in the largest and smallest reduction in the base shear force, respectively. The estimated reduction in the base shear forces was similar when the creep coefficients for loading ages of 96 and 196 days were used.

In addition, the reduction in the base shear force after 2000 days as a function of the column loading age is demonstrated in Figure 5.12 for each column of the CIP/ PS Box. Due to the larger base shear force for the exterior columns than the interior columns, the force reduction was again significantly larger in the exterior columns than the interior columns. The large portion of the reduction in the force occurred when the loading age of the column was less than 200 days.

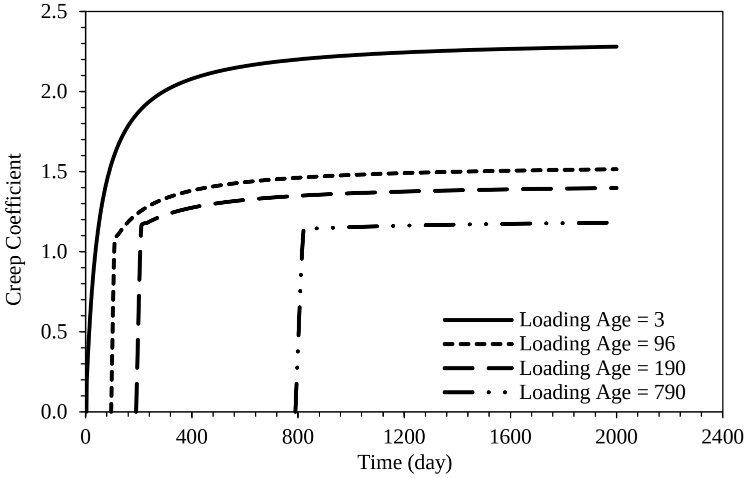

Figure 5.10: The AASHTO LRFD 2010 recommended creep coefficients for the different loading ages of concrete

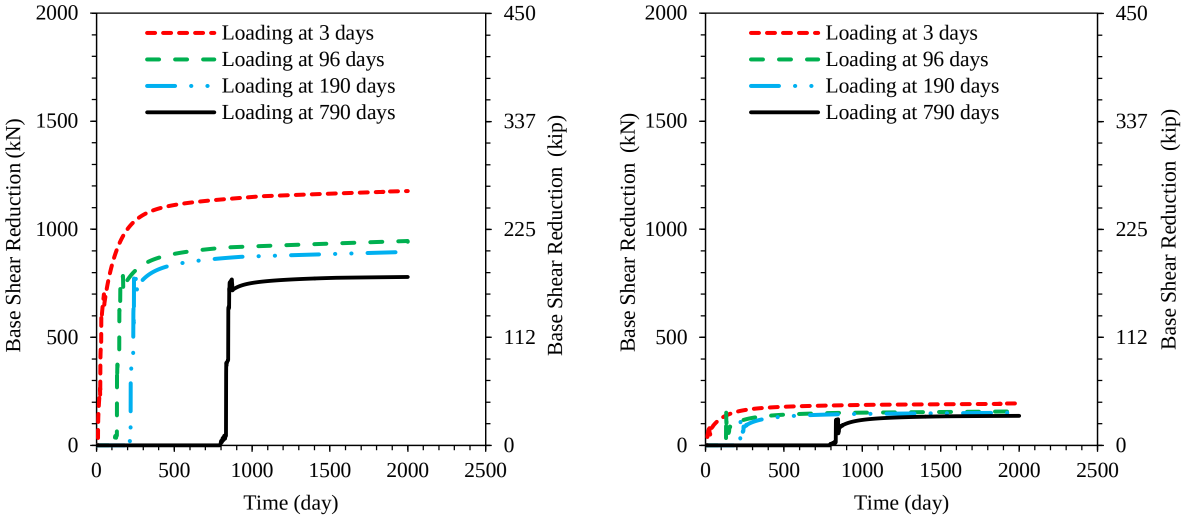

(a) B4-C23

(b) B4-C24

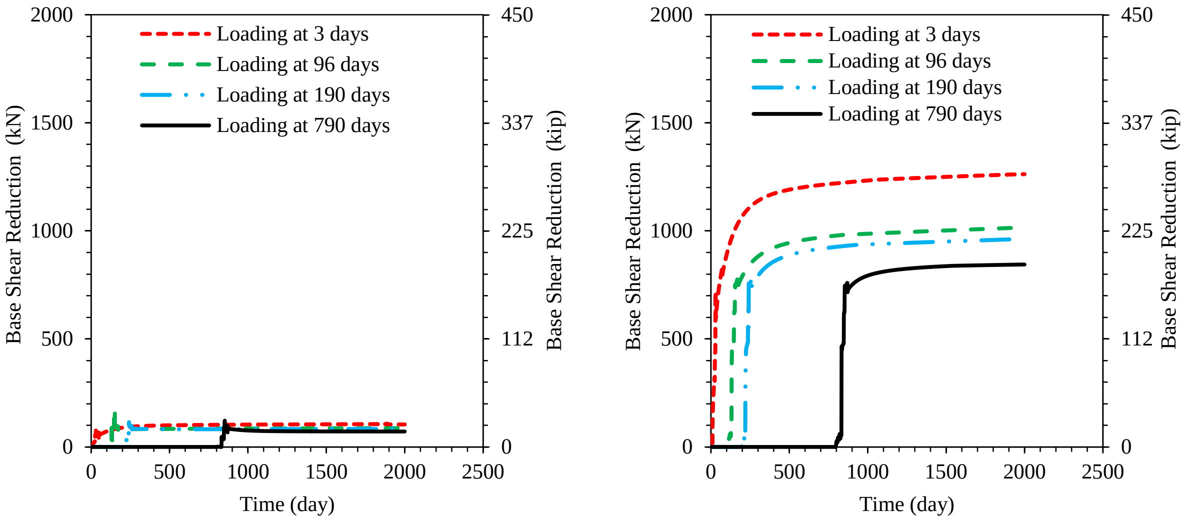

(c) B4-C25

(d) B4-C26

Figure 5.11: Variation of reduction in base shear force with time due to relaxation using different loading ages for columns

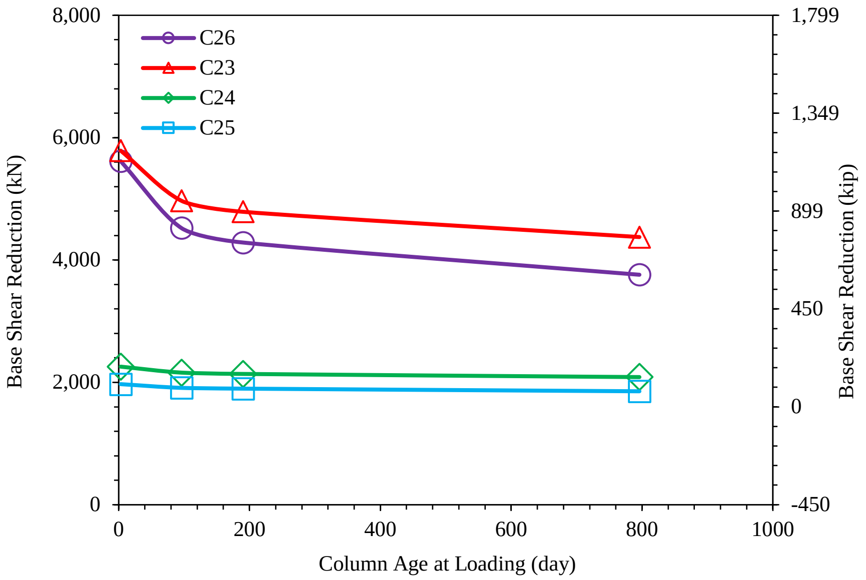

Figure 5.12: Reduction in base shear force after 2000 days due to relaxation as a function of column age

5.3.5 Effects of Creep and Shrinkage on Displacement-Induced Forces

The strain rate is mainly governed by the creep and shrinkage properties of concrete used in the box-girders. The accuracy of strain rate directly affects the magnitude of the column force and displacement demands. Hence, the selected creep and shrinkage models should be representative of the concrete used in the CIP/ PS Box to reduce the discrepancy between the actual and assumed values of creep and shrinkage.

To examine the effects of concrete creep and shrinkage variability on the time-dependent deformations and stresses, the recommendations provided by Lewis and Karbhari (2006) were given consideration for CIP/ PS Box frames. These authors concluded that the predicted values of creep and shrinkage of concrete by CEB-FIP (1992) specifications generally correlated better than other models, including ACI, AASHTO, NCHRP, and GL2000, with the values obtained through material testing of normal strength concrete. Thus, the curve-fitting analysis to find the best-fit to the measured data from Lewis and Karbhari (2006) was carried out using the CEB-FIP (1992) recommendations.

Therefore, the CEB-FIP predicted values and the curve-fit to the measured data by Lewis and Karbhari (2006) in addition to AASHTO predicted values were used to compute the time-dependent deformations and stresses in B4. The 2010 AASHTO LRFD creep and shrinkage models were included to determine the extent of variation in the predicted time-dependent stresses and deformations by the AASHTO compared to that of the CEB-FIP and best-fit curve. Due to preference of the bridge designers to use AASHTO, it was useful to compare the outcomes of results based on different creep and shrinkage models.

Additionally, the effects of column relaxation on the base shear force using different creep and shrinkage models were examined. As discussed in Section 2.3, the concrete relaxation and creep are the same viscoelastic phenomena, which can be mathematically related to each other by the creep and relaxation functions. Hence, the relaxation in the concrete columns was modeled by defining creep behavior for the columns. To comprehend the effect of the column relaxation on the base shear force, the column base shear force with and without including the creep in the columns was obtained. The analyses were performed for 365 days since most of the time dependent effects occurred within one year.

Figure 5.13 displays the predicted column base shear forces using the previously stated creep and shrinkage models with and without including the concrete relaxation in the columns. The inclusion of the column relaxation in base shear force estimation is represented by solid curves, while the dashed curves show the corresponding force when the relaxation was excluded. The sensitivity of the base shear force to the creep and shrinkage models is evident. Among different creep and shrinkage models, the best-fit curve proposed by Lewis and Karbhari (2006) produced the largest base shear forces, whereas CEB-FIP model resulted in the smallest base shear forces. The base shear force calculated by AASHTO LRFD 2010 was neither as large as the results calculated using Lewis and Karbhari (2006) model nor as small as CEB-FIP model.

By comparing the solid curves to the dashed curves, the effect of the column relaxation on mitigating the base shear force can be observed. For B4-C23, due to the column relaxation, the column base shear force was reduced by 50.0%, 44.1%, and 43.9% when the Lewis and Karbhari (2006), CEB-FIP, and AASHTO models were used, respectively.

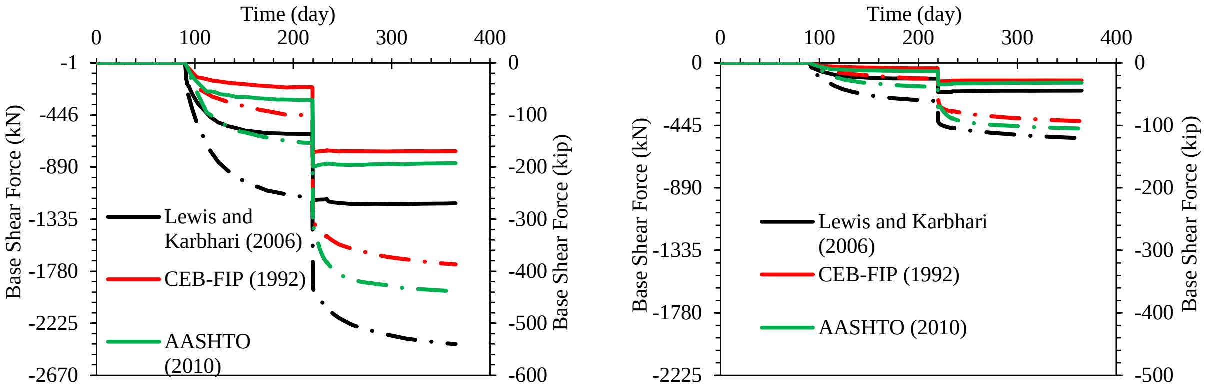

(a) B4-C23 (b) B4-C24

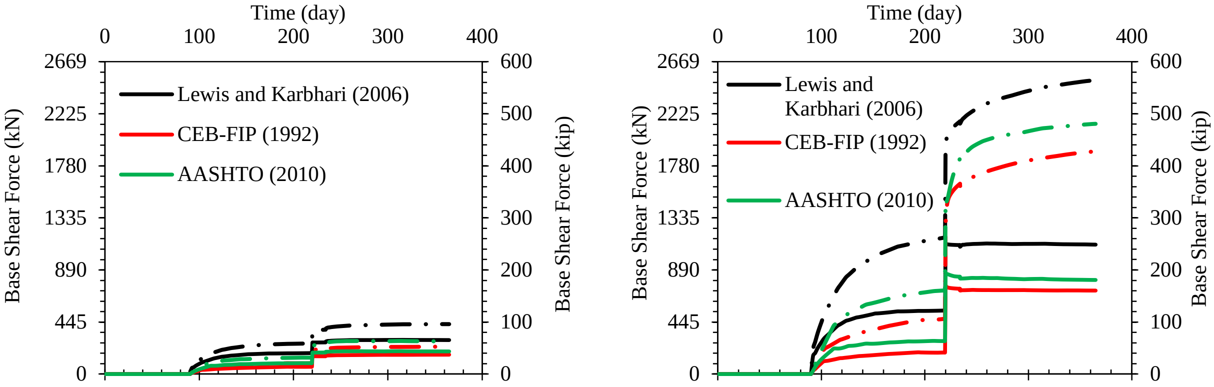

(c) B4-C25 (d) B4-C26

Figure 5.13: Determination of column base shear force using the different creep and shrinkage models in FEM of B4 (solid lines show the effcets of concrete relaxation in columns and dashed lines ignore the effects of concrete relaxation)

5.4 Summary and Conclusions

The methodology and the assumptions used to analyze the CIP / PS Box were demonstrated through detailed analyses of a bridge frame (i.e., B4) in this chapter. An FEM of the selected CIP / PS Box was developed using the midas Civil software (2013) to calculate the stresses and deformations over several hundred time-steps from the time of construction to the completion of the CIP / PS Box. The significant parameters affecting time-dependent behavior of CIP / PS BOX, including concrete creep/relaxation and shrinkage, prestress losses, support locations, column effective stiffness, and construction stages were taken into account in the FEM. The beneficial effects of concrete relaxation were demonstrated by comparing the results when the CIP / PS Box was analyzed by including and ignoring the relaxation functions for the columns. Based on the findings of the FEM analyses, the following conclusions have been drawn:

- The shrinkage of the CIP / PS Box superstructure had the largest contribution to the shortening strain rate of the superstructure, column top lateral displacement, and the column base shear force compared to the corresponding effects of dead load, prestress, and creep.
- In general, the further away the column was from the location of the PNM, the larger the column top lateral displacement and consequently the base shear force were. Thus, the exterior columns experienced higher lateral displacements and base shear forces than the interior columns.
- Based on the moment-curvature analysis, the exterior columns would crack due to displacement-induced forces, while the column adjacent to the PNM might not experience flexural cracking.
- The reduction in bending moment due to concrete relaxation prevented any columns

experiencing yielding, which would not be the case if the concrete relaxation was not included in the analyses.

- Due to the column relaxation, the ultimate base shear force was reduced by as much as 53% for the exterior column (i.e., B4-C26).
- The sensitivity analysis on the effects of the column loading age on the relaxation of displacement-induced forces indicated that a 51.8% reduction in creep coefficient between the loading ages of three and 790 days, which translated to a 32.8% increase in the column base shear force for C23 at 2000 days.
- The sensitivity analysis indicated that the variation in the predicted creep and shrinkage values resulting from different creep and shrinkage models resulted in significantly different column base shear forces. The AASHTO models were found to give results that are not too conservative or less conservative.
- The base shear force was not as sensitive as the AASHTO creep coefficient was to the column loading age. After 2000 days, a 51.8% reduction in creep coefficient between loading ages of three and 790 days was found, which translated to 32.8% increase in the column base shear force for B4-C23.

CHAPTER 6: ANALYSIS OF TIME-DEPENDENT EFFECTS OF EIGHT CIP / PS BOX FRAMES

6.1 Introduction

Following the procedure described in Chapter 5, a systematic investigation was undertaken in this Chapter to evaluate the time dependent effects on eight CIP / PS Box frames of various configurations and span lengths. An FEM for each frame was developed using the midas Civil software, in which construction stage analysis and the time step method were included. In the FEMs, the shortening strain rate of the superstructure, together with the variation of the column lateral top displacement and the corresponding column base shear force as a function of time, was quantified. Based on the results of the FEM, design recommendations are provided to more accurately compute the displacement-induced forces in the columns. By implementing these recommendations, cost-effective design solutions are expected to be achieved by optimizing the columns and foundations.

6.2 Creep and Shrinkage Models

Concrete creep and shrinkage properties for the superstructure and substructure of the CIP / PS Box were estimated using the models recommended by AASHTO LRFD Bridge Design Specifications 2010, as shown in Figure 6.1. For each CIP / PS Box frame, the creep coefficient and shrinkage strain were estimated separately for the box-girder and the columns. The loading ages of seven and 180 days were used in the estimation of the creep coefficients for the box-girder and the columns, respectively, based on the construction timeline (see Section 5.2.2).

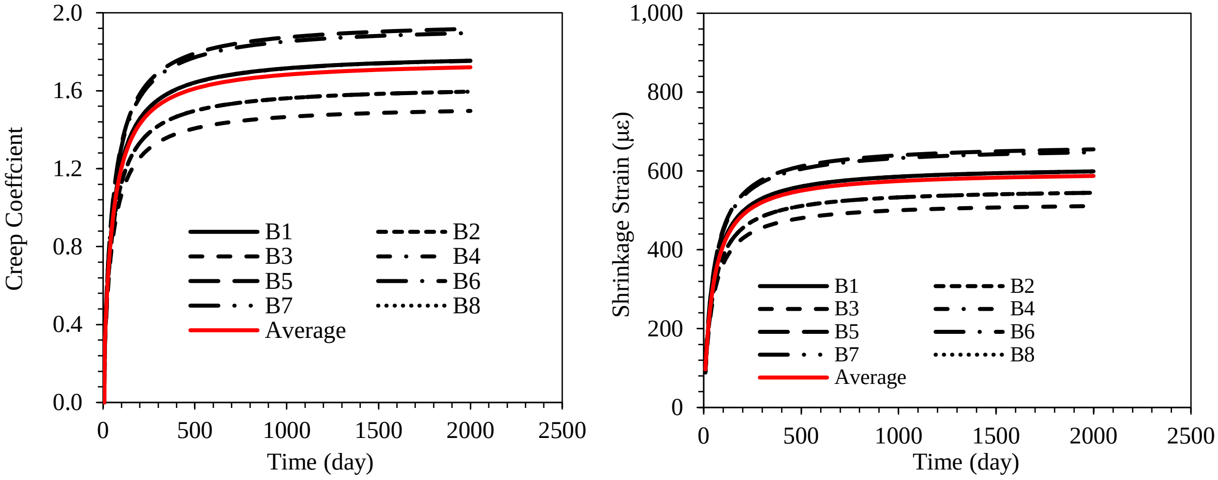

(a) Box-girder

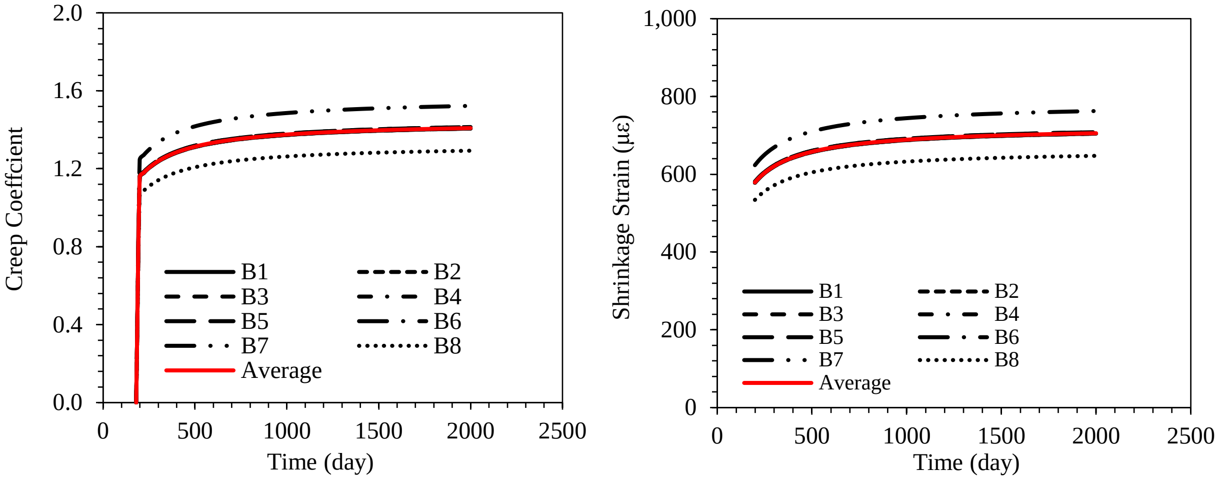

(b) Columns

Figure 6.1: Calculated creep coefficients and shrinkage strains for the eight CIP / PS Box using AASHTO recommendations (2010)

6.3 Finite-Element Models

The methodology and assumptions discussed in Chapter 5 were followed in developing the FEMs of the eight CIP / PS Box frames using midas Civil. Beam elements were used to model the superstructure and substructure with considerations given to the geometric details of the PPCB frame details presented in the bridge drawings. The prestressing steel was modeled along the length of the box-girder as beam elements with perfect bonding to the surrounding concrete elements. The variation in structural elements, loading, and boundary conditions throughout the construction of CIP / PS Box frames were accounted for by defining different construction stages in the FEMs.

Significant parameters affecting the time-dependent behavior of CIP / PS BOX frames, such as concrete creep/relaxation and shrinkage as well as prestress losses were included in the FEMs. Following estimation of short-term prestress losses in the FEM based on the AASHTOLRFD Bridge Design Specifications 2010 recommendations, long-term prestress losses were calculated using the creep and shrinkage properties of concrete defined by AASHTO LRFD Bridge Design Specifications 2010 (see Section 6.2). Long-term prestress losses were included by adopting the time-step method in the midas Civil software.

6.4 Finite Element Analysis Results

For the eight CIP / PS Box frames, the shortening strain rate of the superstructure and the variation of column top lateral displacement together with the corresponding base shear force were calculated using the FEMs. As a representative for the FEM results, Figure 6.2 demonstrates the longitudinal displacement of a short-, medium-, and long-span CIP / PS Box frames due to the time-dependent effects.

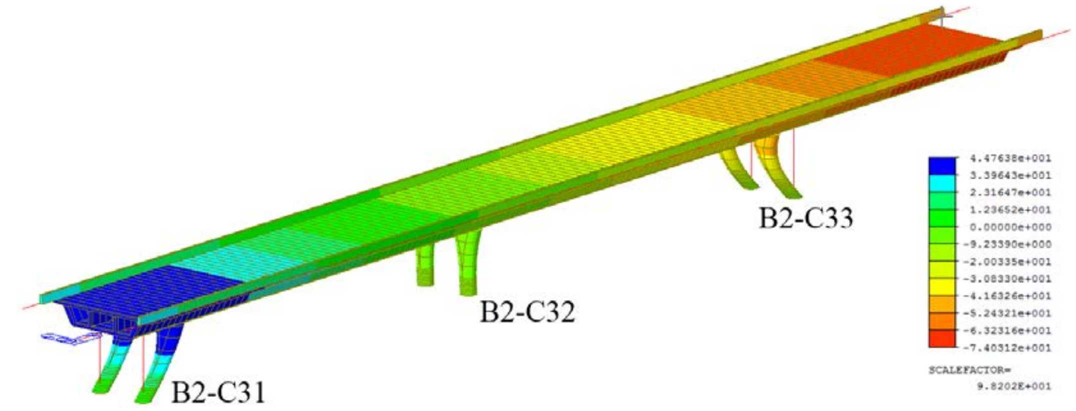

(a) B2

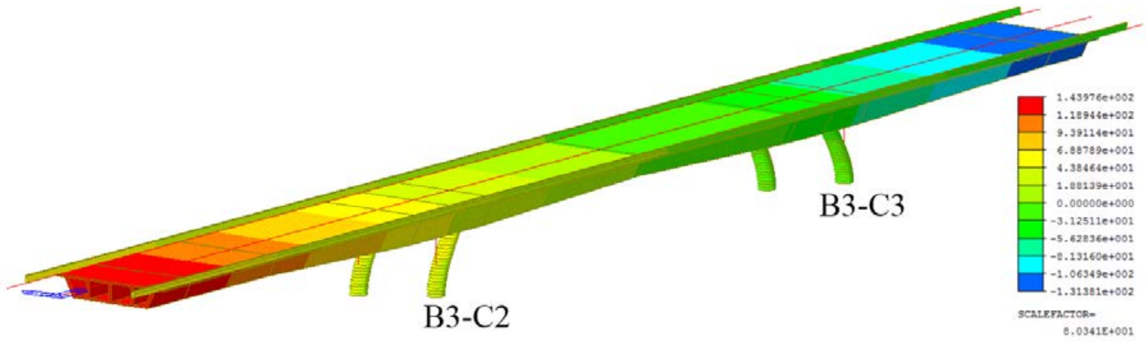

(b) B3

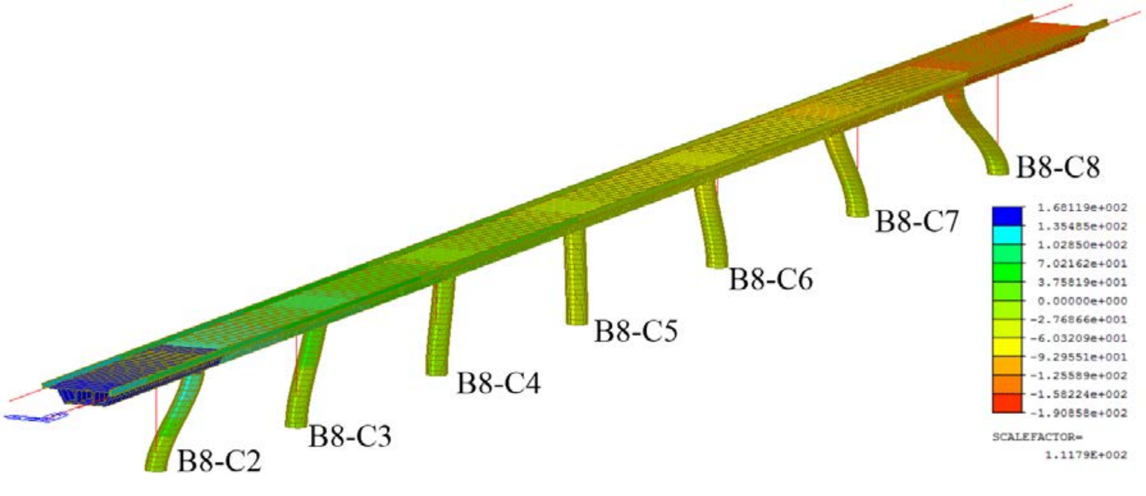

(c) B8

Figure 6.2: The FEM results (in meters) for the longitudinal displacement of CIP / PS Box frames due to time-dependent effects

6.4.1 Shortening Strain Rate of the Superstructure

Using the displacements at the ends of CIP / PS Box frames, the shortening strain rate of the superstructure caused by dead load, pretress, creep, and shrinkage components as well as the summation of these components were estimated, as shown in Figure 6.3. In addition, for the eight CIP / PS Box frames, the mean values for each component of shortening strain rate and their summation were determined in Figure 6.3.

As expected, it is observed that the dead load strain remained constant with time and contributed to a relatively small portion of the total strain. Due to the different initial stresses in conjunction with the different magnitudes of short-term and long-term prestress losses, a large variation in the pretress and creep strains were found among the eight CIP / PS Box frames. After 2000 days, the variation in the prestress and creep strains among the eight CIP / PS Box frames were 181 με and 262 με, respectively. The application of prestress corresponded to a sudden large increase in strain, followed by gradual reduction due to the prestress losses. Conceivably, B3 with the largest initial stress (see Section 4.4) was subjected to the largest prestress strain of all CIP / PS Box frames. The creep strain increased with time although the long-term losses stymied this increment. Similar to the prestress strain, the greatest creep strain was experienced by B3. The shrinkage strain, which had the greatest contribution to the total strain, increased with time and the shrinkage strain was found to be similar for the different CIP / PS Box frames. After 2000 days, the variation in shrinkage strains among the eight CIP / PS Box frames was found to be 143 με, which was less than the corresponding variation in the prestress and creep strains. In terms of the total strain, the largest and smallest strains were experienced by B3 and B8, respectively, with a difference of 481 με after 2000 days.

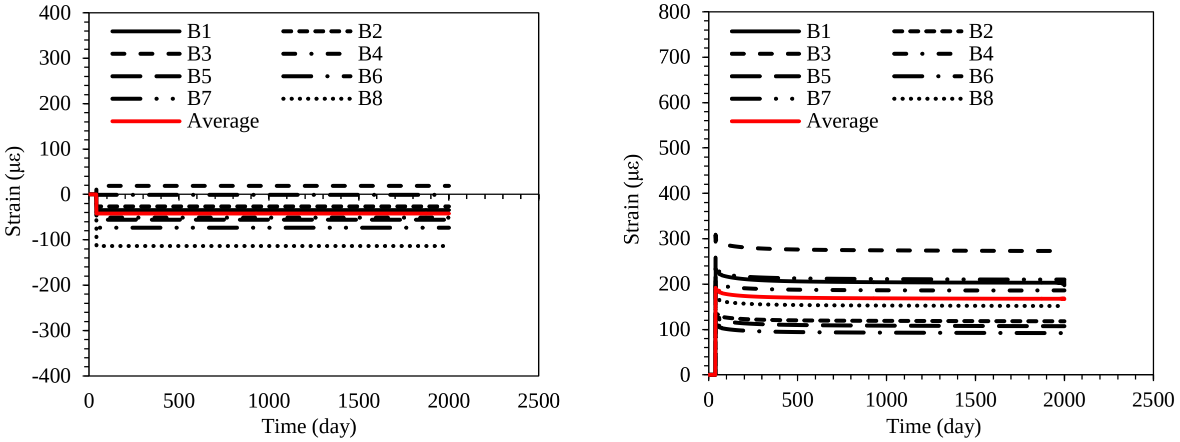

(a) Dead load

(b) Prestress

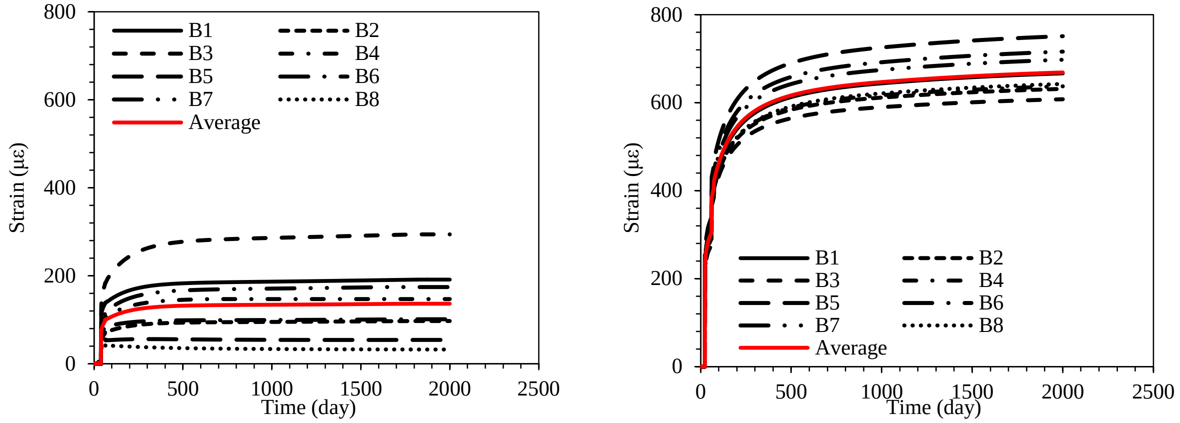

(c) Creep

(d) Shrinkage

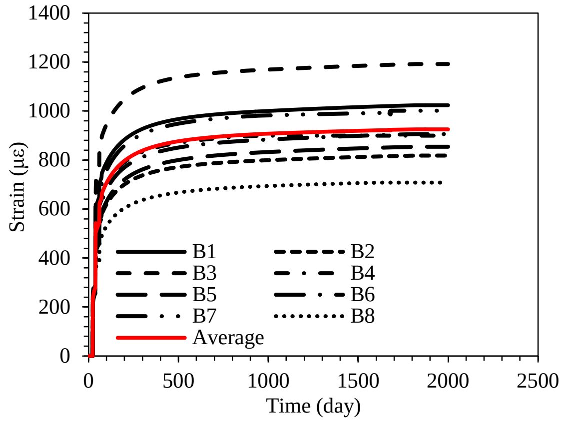

(e) Total

Figure 6.3: The FEM results for shortening strain rate of the superstructure

6.4.2 Column Top Lateral Displacement

The left sides of Figure 6.4 through Figure 6.6 exhibit the results for the total top lateral displacement of columns in short-, medium-, and long-span CIP / PS Box frames, sequentially. In each figure, the results for the two exterior columns are shown using a solid curve and a dotted curve. Simlarly for all CIP / PS Box frames, the extreior columns were subjected to the laregst displcaments due to their relative distance to the PNM, while the interior columns, which were the nearest to the PNM, had the smallest lateral displcements. Typically, the displcament of the extreior columns increased as the CIP / PS Box length increased, where B1-C2 and B7-C2 had the smallest and largest diplacments of 23 mm (0.9 in.) and 173 mm (6.8 in.), respectively.

6.4.3 Column Base Shear Force

The estimated total column base shear force caused by a combination of dead load, prestress, creep, and shrinkage for short-, medium-, and long-span CIP / PS Box frames are presented in the right sides of Figure 6.4 through Figure 6.6. In each figure, the two exterior columns are designated by a solid curve and a dotted curve. Similar to the displcaments, the largest base shear force was induced in the exterior columns, while the interior columns adjacent to the PNM experineced siginificantly smaller displacement-induced base shear forces. As a result, the exterior columns were found to experience cracking due to deformation-induced forces, while the columns adjacent to the PNM remained uncracked.

Since the estimated base shear force is predominatly affected by a combination of column displacment and the slenderness ratio, the columns in the long-span CIP / PS Box frames with higher column displacment do not necessarily have larger base shear forces compared to the columns in short-span CIP / PS Box frames. For instance, the column base shear forces in B5 are significantly less than the corresponding values in B1 even though the column displacements in

B5 weare significantly larger than those of B1. This can be attributed to the slender columns of B5, while the columns in B1 are reletively short and stiff. The smallest and largest base shear force among the exterior columns of the eight CIP / PS Box after 2000 days was found to be 297 kN (66.8 kips) and -11610 kN (2610 kips) for B5-C6 and B8-C2, respectively.

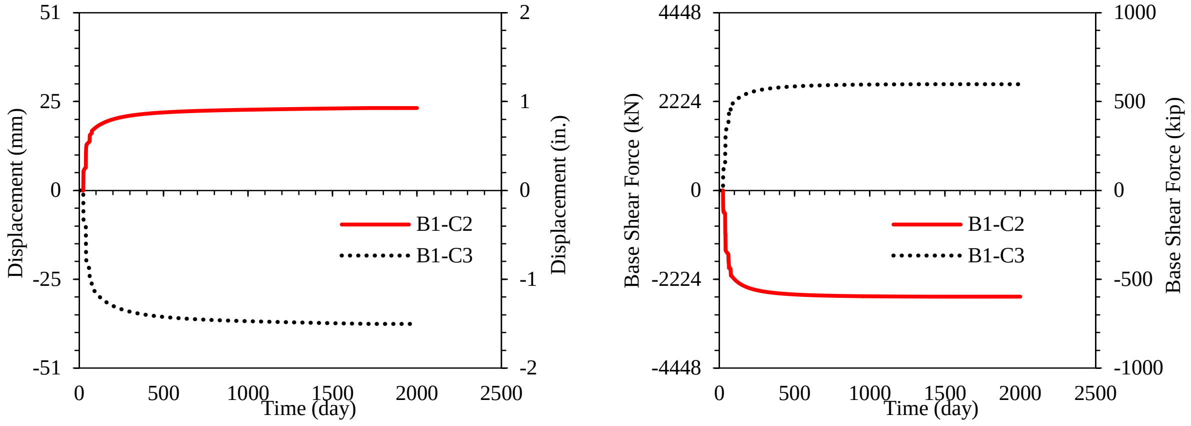

(a) B1

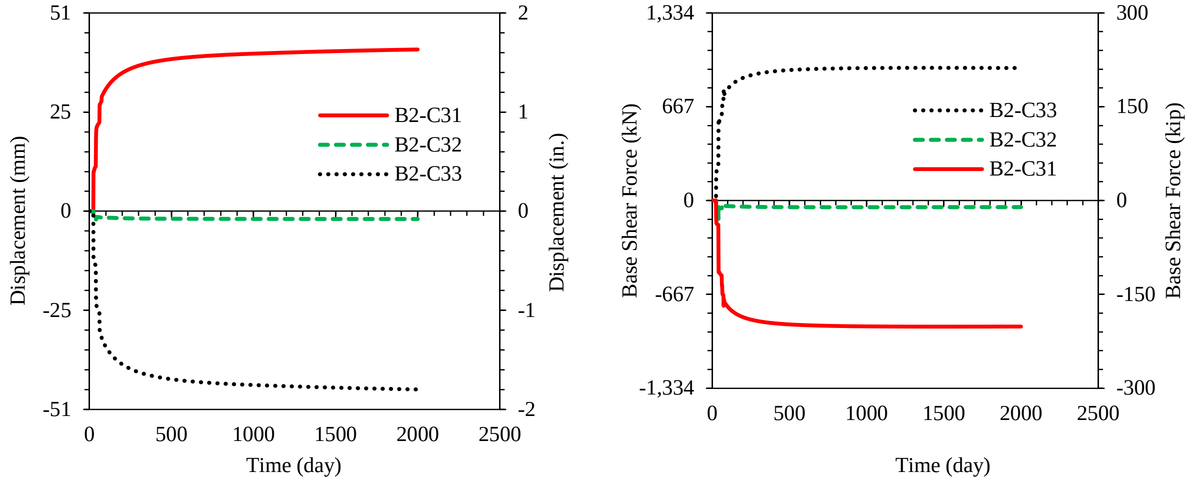

(b) B2

Figure 6.4: Variation of the FEM predicted column top lateral displacements and the corresponding base shear forces with time for the short-span CIP / PS Box frames

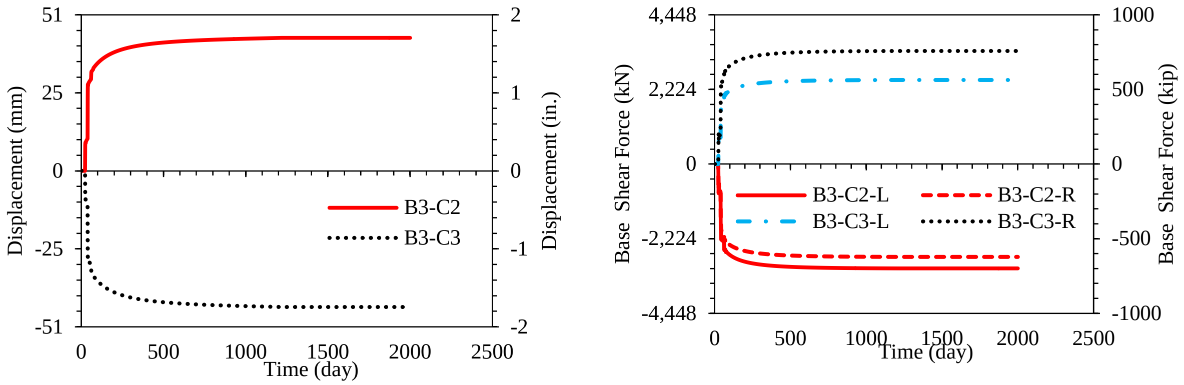

(a) B3

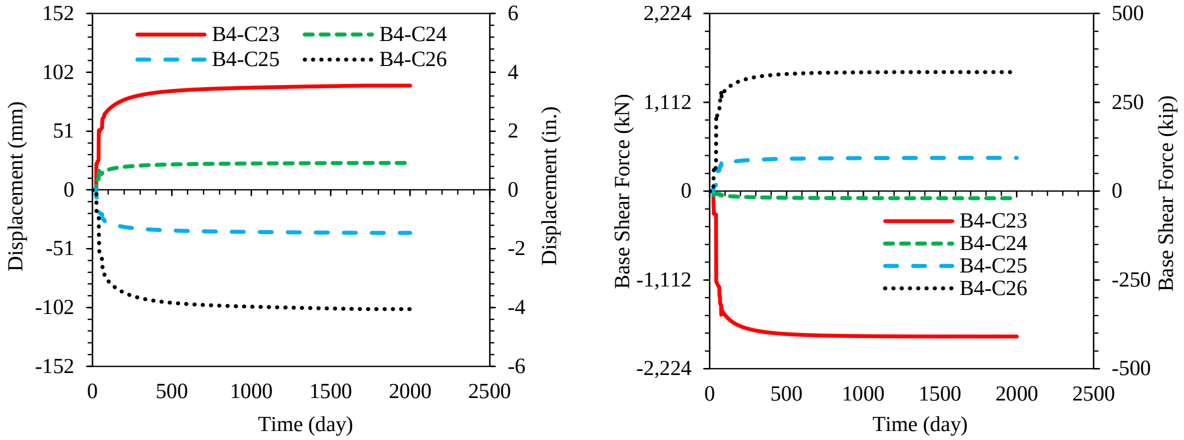

(b) B4

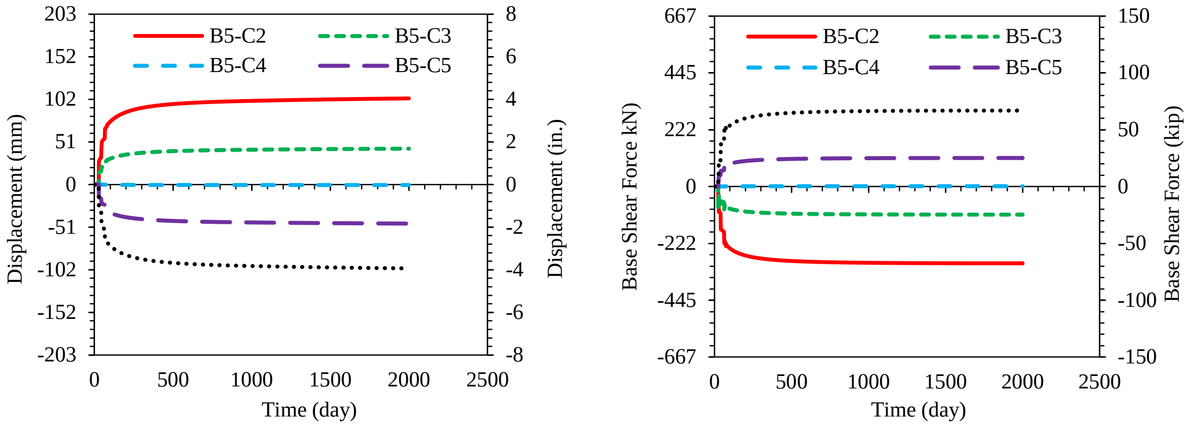

(c) B5

Figure 6.5: Variation of the FEM predicted column top lateral displacements and the corresponding base shear forces with time for the medium-span CIP / PS Box frames

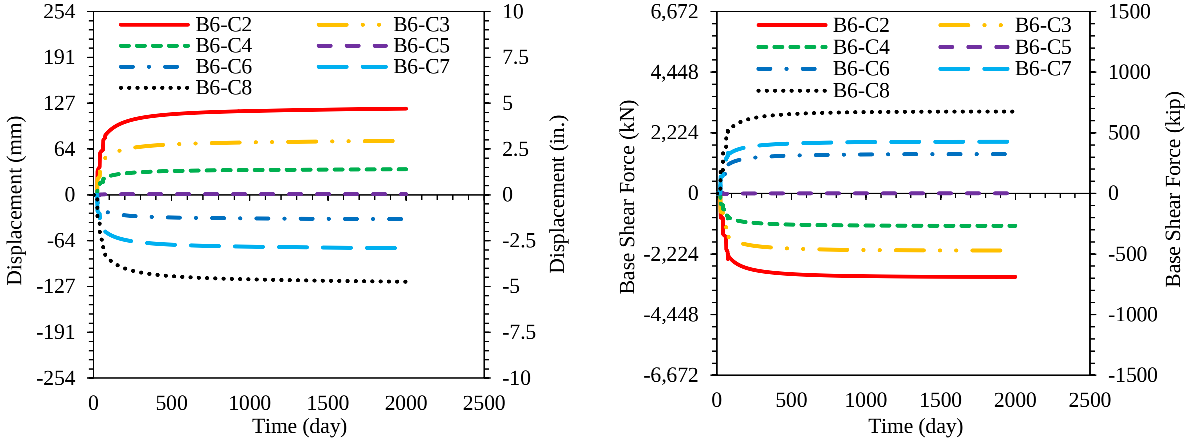

(a) B6

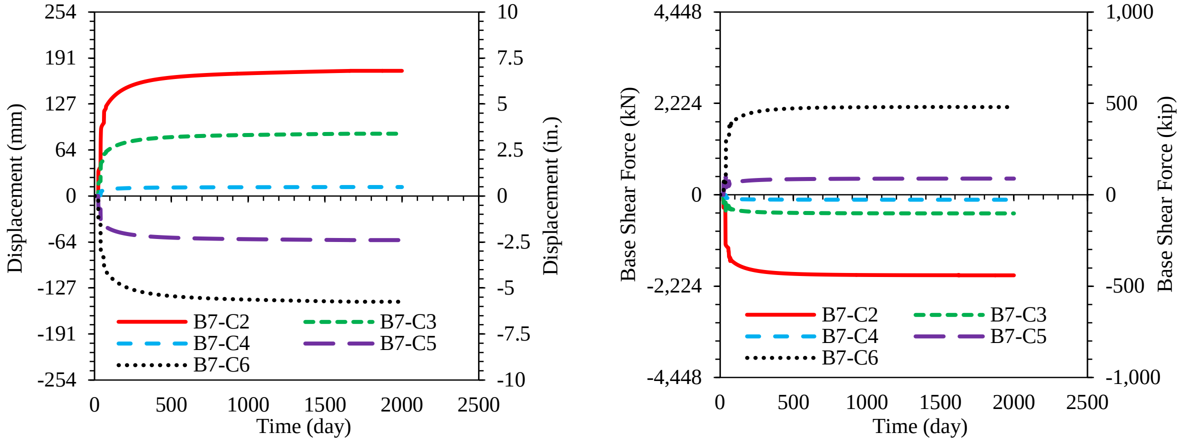

(b) B7

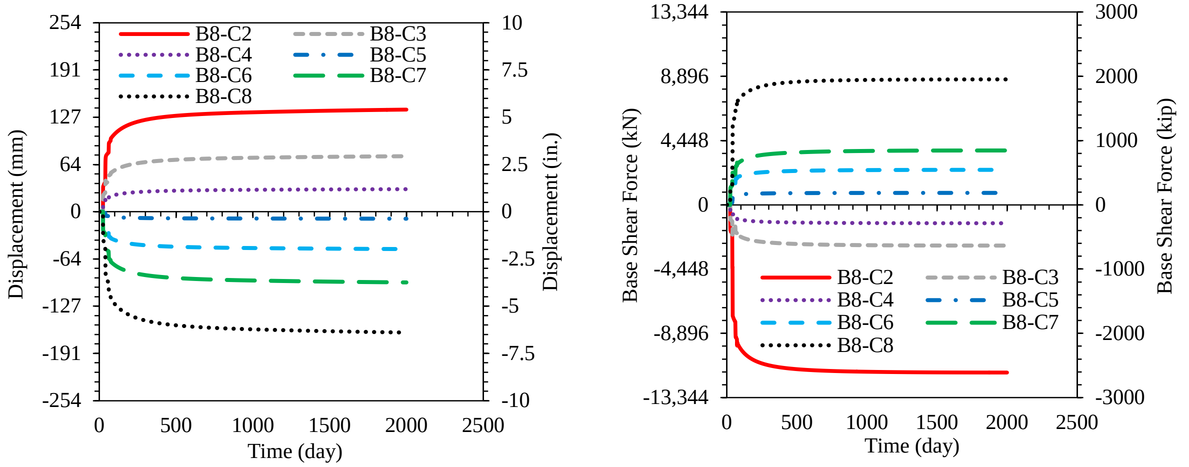

(c) B8

Figure 6.6: Variation of the FEM predicted column top lateral displacements and the corresponding base shear forces with time for the long-span CIP / PS Box frames

6.4.4 Maximum Displacements and Forces

In consideration of time-dependent effects on column design, the maximum values of column top lateral displacement due to the shortening of the superstructure and the corresponding base shear forces required for design were calculated, as shown in Figure 6.7 andFigure 6.8. It was assumed that the maximum values would have reached after 2000 days from the completion of pier construction, since the majority of concrete creep and shrinkage would have taken place after 2000 days. Therefore, the displacements and forces are not expected to vary with time due to the time-dependent effects beyond 2000 days.

The total estimated design values for column top displacements along with the percentage contribution of dead load, prestress, creep, and shrinkage to the total displacement are presented in Figure 6.7 for a total number of 37 columns analyzed in this study. Similarly, the total estimated base shear force and the contribution of different components to the total design base shear force for the 37 different columns are shown in Figure 6.8. As anticipated, shrinkage had the largest effects on the total displacements and base shear forces, while the dead load had the smallest effects. The largest displacement of 173 mm (6.8 in.) and the largest base shear force of 11605 kN (2609 kips) were experienced by B7-C2 and B8-C2, respectively. For the base shear force, the creep component in the box-girder and columns collectively acted in the opposite direction to the force resultant from dead load, prestress, and shrinkage.

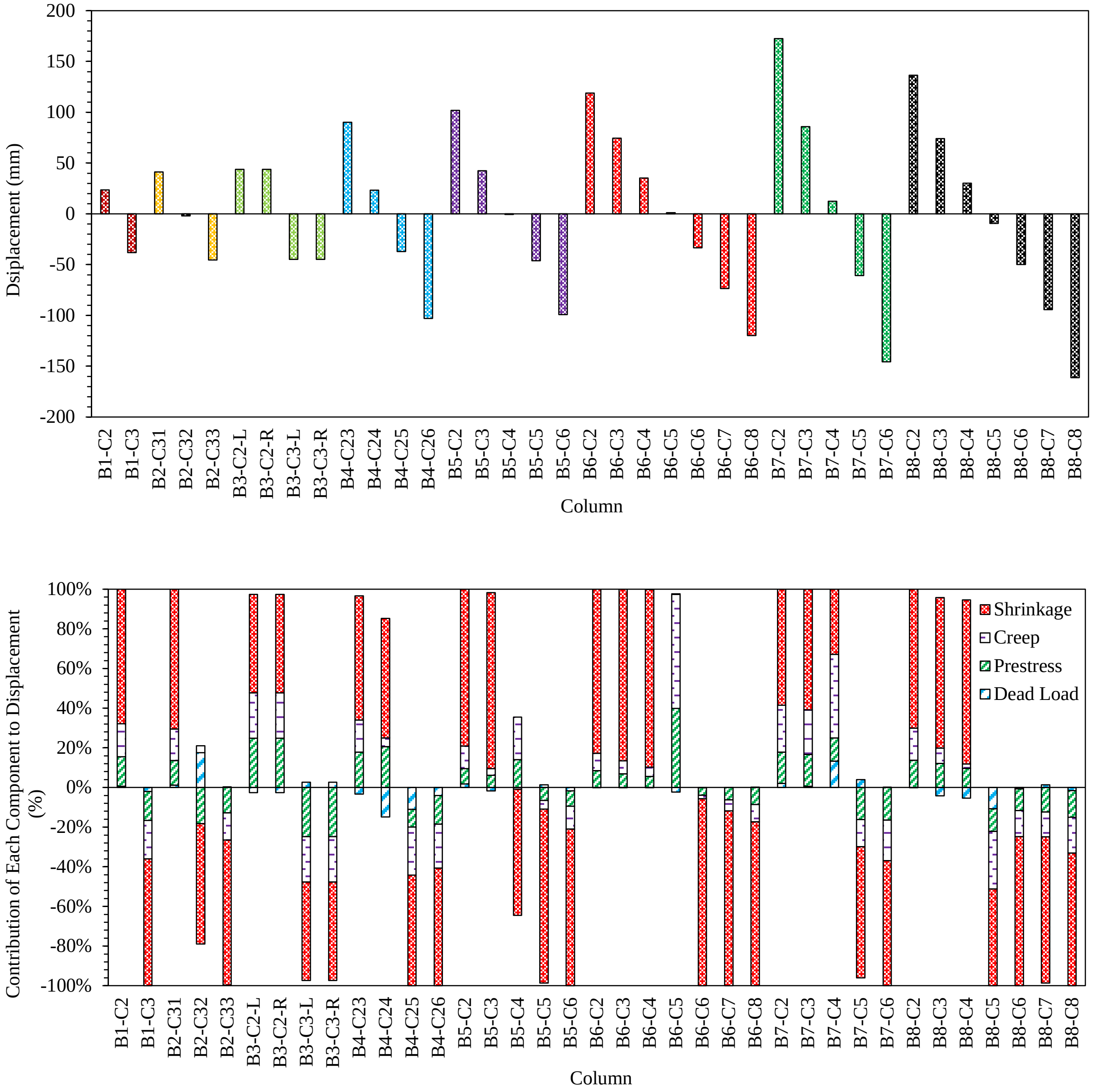

Figure 6.7: The FEM results for the maximum column top lateral displacements at the age of 2000 days

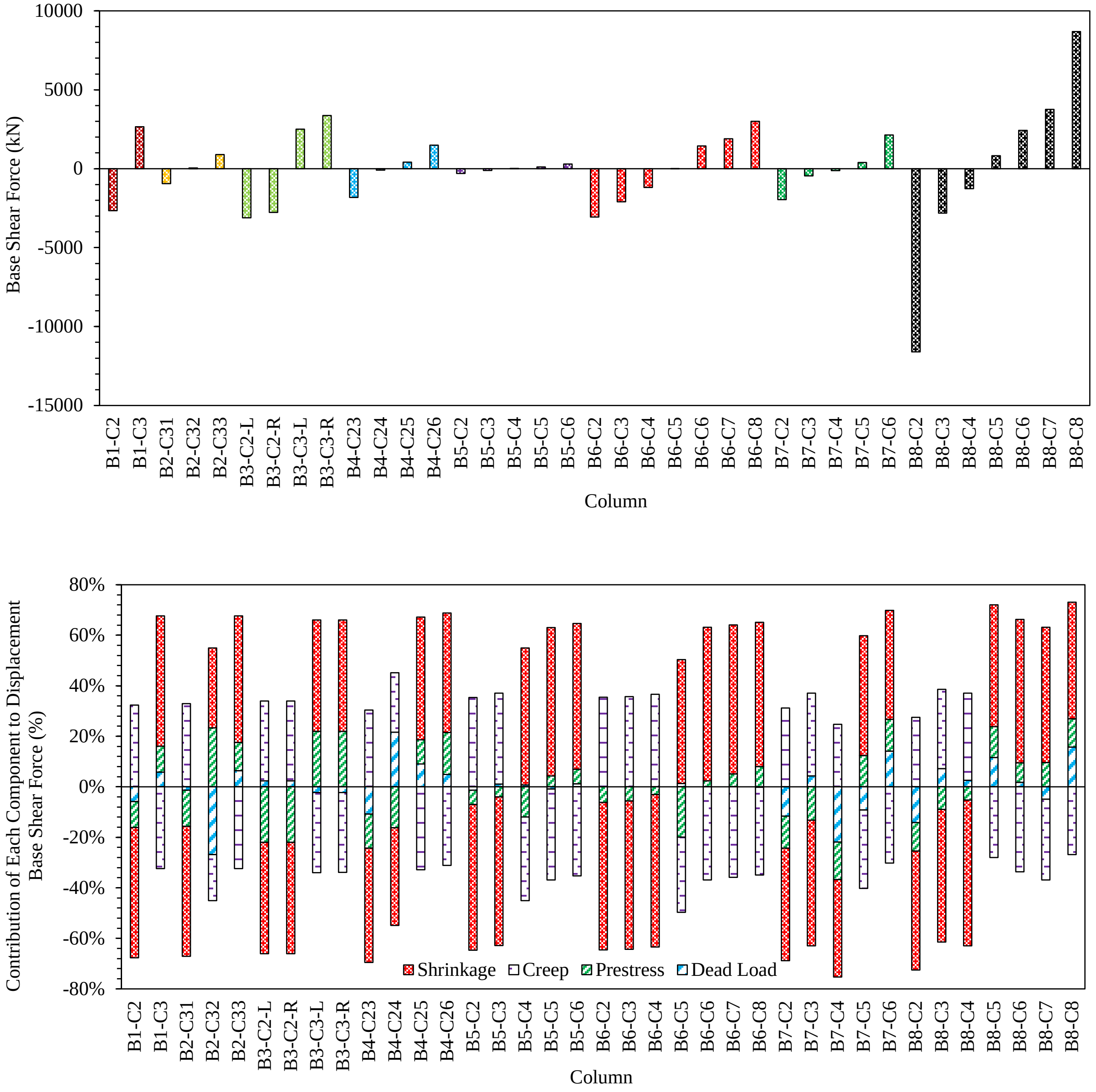

Figure 6.8: The FEM results for the maximum base shear forces at the age of 2000 days

6.5 Simplified Analysis

A simplified analysis based on the linear elastic analysis was developed to calculate the maximum displacement-induced forces for a given shortening strain of the superstructure. Unlike the current Caltrans SM (see Section 1.3), a more realistic prediction of the shortening strain rate was employed to compute the displacement-induced forces using the maximum strain rates calculated by the FEMs. In addition, the expected effects of concrete relaxation in the columns were integrated in this effort. The steps required to calculate the displacement-induced column forces using the simplified analysis is described in Section 6.5.1 to 6.5.3.

6.5.1 Prediction of Shortening Strain Rate of the Superstructure

The shortening strain rate of the superstructure is comprised of different components, including the effects of dead load, prestress, creep, and shrinkage. The FEM findings for the strain rate presented in Section 6.4.1 were used to establish the strain rate for the simplified analysis. Giving consideration to the current Caltrans SM (see Section 1.3), the strain caused by creep and shrinkage were investigated separately from the strain caused by a combination of dead load, prestress, creep and shrinkage. Using the FEM results, four different methods can be used to predict the strains, as follows:

1. Strains due to creep and shrinkage:
    1a. Use the average creep and shrinkage strain estimated by the FEM for each type of bridge
    1b. Use the average creep and shrinkage strain estimated by the FEM for all eight bridges
2. Total strains due to dead load, prestress, creep and shrinkage:
    2a. Use the average total strain estimated by the FEM for each type of bridge
    2b. Use the average total strain estimated by the FEM for all eight bridges

The strains predicted by the four different methods, derived from the FEM, were compared to that of the Caltrans SM, and are presented in Figure 6.9.

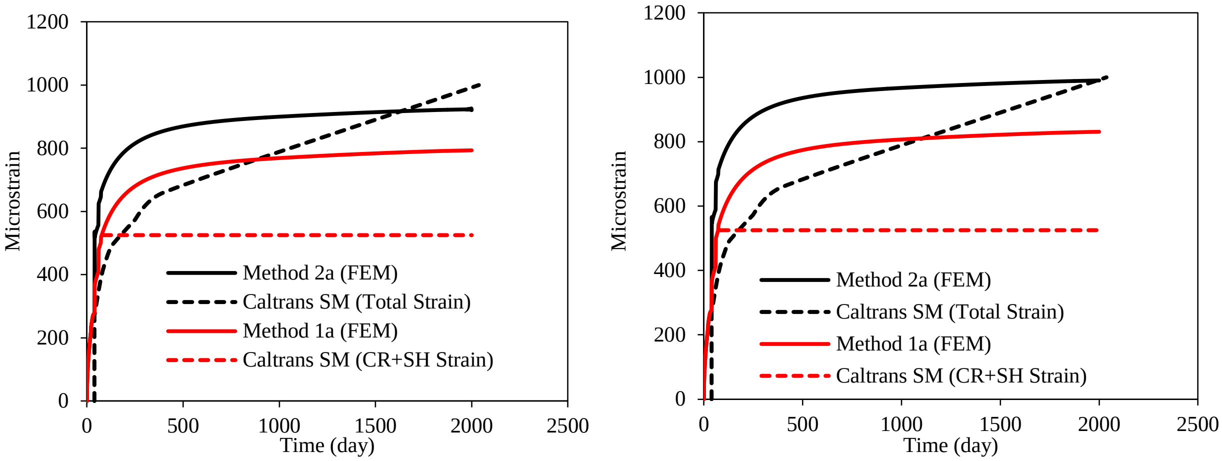

(a) Methods 1a and 2a vs. Caltrans SM for short-span CIP / PS Box frames

(b) Methods 1a and 2a vs. Caltrans SM for medium-span CIP / PS Box frames

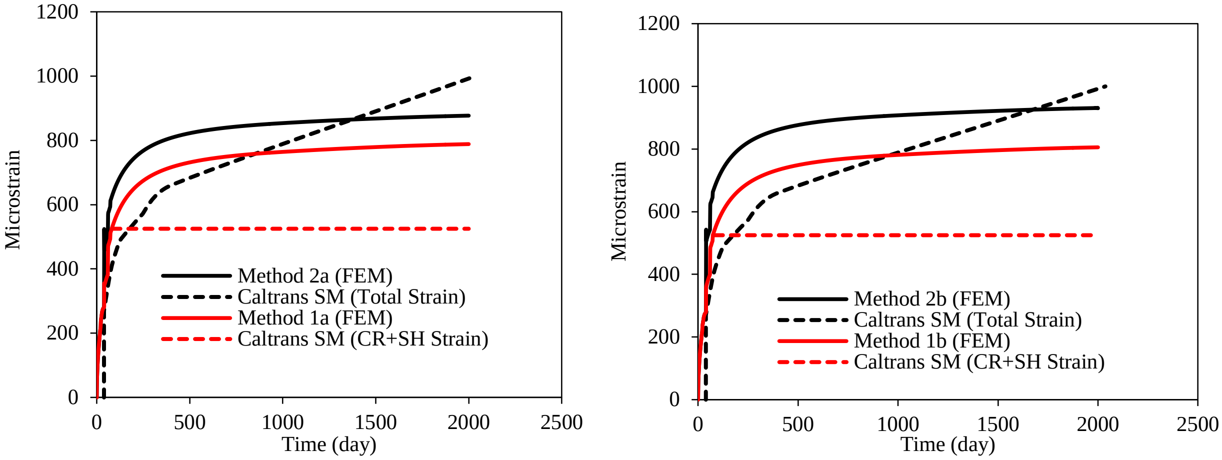

(c) Methods 1a and 2a vs. Caltrans SM for long-span CIP / PS Box frames

(d) Methods 1b and 2b vs. Caltrans SM for the eight CIP / PS Box frames

Figure 6.9: A comparison between the strains predicted by the four proposed methods and strains based on a deck expansion joint design memorandum (Caltrans 1994- Attachment 4)

As observed in Figure 6.9, the strains due to creep and shrinkage predicted by the Caltrans are consistently smaller than the strains predicted by the simplified analysis based on the four approaches to model the time dependent stains. This is attributed to the assumption in the Caltrans SM, which accounts for creep and shrinkage effects after 12 weeks, thereby disregarding the time-dependent shortening in the first 12 weeks (see Section 1.3). With respect to the total strain, the Caltrans and simplified approaches yield to comparable maximum strains at the age of about 1800 days, although the Caltrans resulted in smaller total strains compared to the recommended approaches in the early stages (i.e., less than 1500 days).

The maximum total strains due to the dead load, prestress, creep, and shrinkage in addition to maximum strains due to creep and shrinkage predicted by the different proposed methods and Caltrans are summarized in Table 6.1. It is observed that the current Caltrans SM results in noticeably smaller creep and shrinkage strains compared to the strains predicted by the four recommended approaches. By including the creep and shrinkage strain of the first 12 weeks in the Caltrans SM, the Caltrans results would be more comparable to the predicted values by the simplified approaches.

A better correlation was found between the maximum total strains incorporated into the simplified method and the maximum total strains estimated by the Caltrans SM. The largest difference of 323 με was found between the total strains predicted by the Caltrans and Approach 2a for long-span CIP / PS Box frames. The predicted total strains by the Caltrans had the best agreement with Approach 2a for medium-span bridges.

Table 6.1: The predicted maximum strains (με) based on the different simplified approaches at the age of 2000 days

PPCB Frames	Creep and shrinkage strain			Total strain		
	Caltrans SM	Approach 1a	Approach 1b	Caltrans SM	Approach 2a	Approach 2b
Short-span	525	794	806	1200	926	932
Medium-span	525	831	806	1200	990	932
Long-span	525	788	806	1200	877	932
All Eight	525	Not applicable	806	1200	Not applicable	932

6.5.2 Prediction of Column Top Lateral Displacement

Prior to estimating the design value of the column top lateral displacement using the simplified analysis, the PNM for the superstructure should be determined using the theory of elasticity. In determination of the PNM, the column stiffness should be adjusted based on the moment-curvature analysis to reflect the effective stiffness for those columns experiencing flexural cracking. Once the location of the PNM is found, Equation (6-2) can be used to calculate the column top displacement.

$$\Delta_{\mathrm{col}} = \mathrm{x}_{\mathrm{col}} \times \epsilon_{\mathrm{s}} \tag{6-2}$$

where x_{col} is the distance of the column to the PNM; and ϵ_s is the shortening strain rate of the superstructure and can be calculated using the recommendations presented in Section 6.5.1. In the estimation of the column top displacement using the simplified analysis, the different strains proposed by the different approaches, presented in Table 6.1, can be used. The calculated design displacements using the different approaches were compared to the displacements predicted by the FEM, as shown in Figure 6.10 through Figure 6.13.

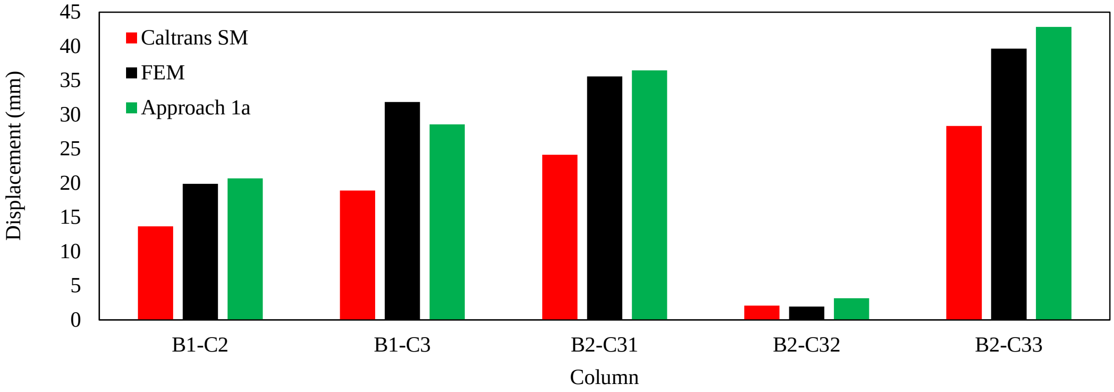

(a) Short-span CIP / PS Box frames

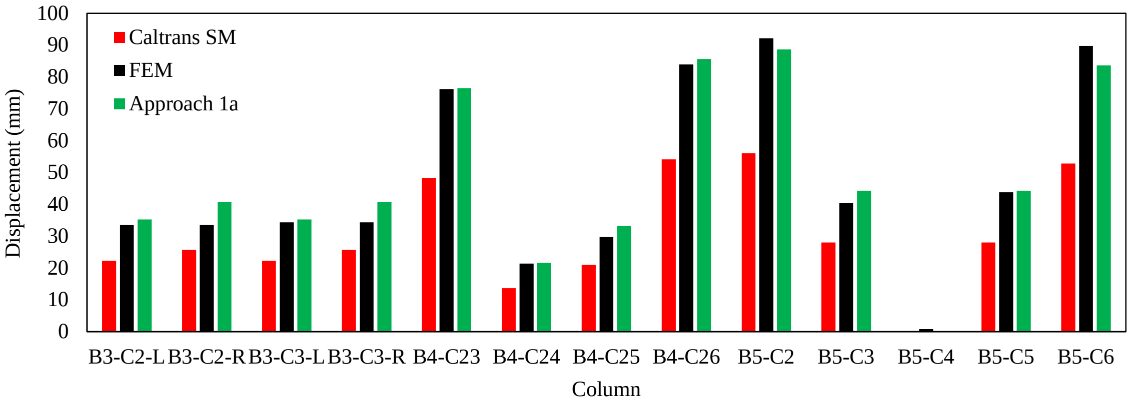

(b) Medium-span CIP / PS Box frames

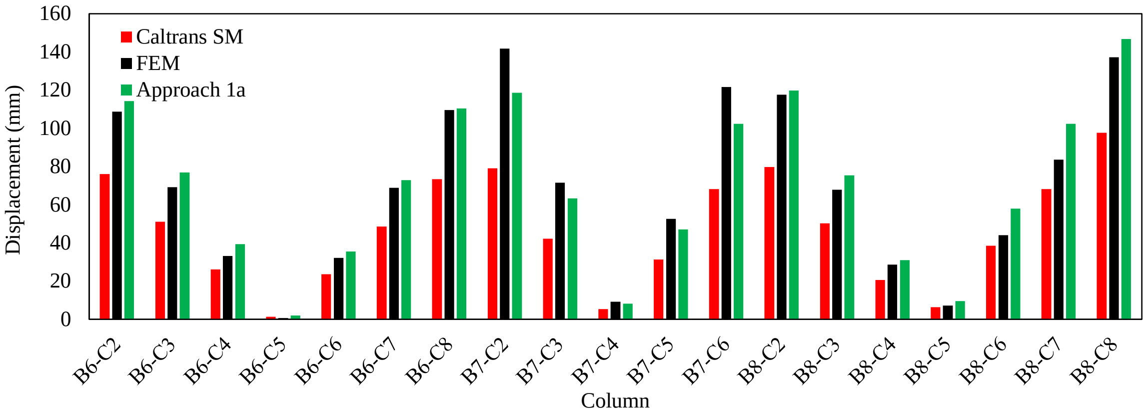

(c) Long-span CIP / PS Box frames

Figure 6.10: A comparison between the maximum displacements calculated by the FEM and those obtained by the Caltrans SM and the simplified analysis based on Approach 1a strains

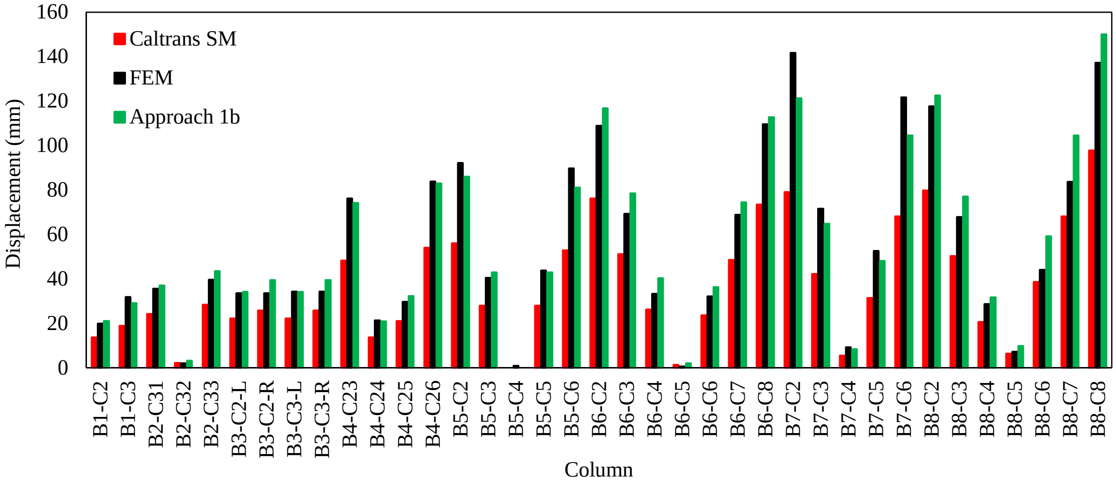

Figure 6.11: A comparison between the maximum displacements calculated by the FEMs and maximum displacements obtained using Approach 1b and the Caltrans SM

When creep and shrinkage strains were used to predict the column top lateral displacements, the Caltrans SM underestimated the displacement compared to the FEM results, while the displacement predicted by Approach 1 (both a and b) correlated well with the FEM results. The underestimation of displacements by the Caltrans is more pronounced for the long-span PPCB frames.

As shown in Figure 6.12 Figure 6.13, a better agreement between the FEMs and the simplified approaches, including the Caltrans was found when the total strains were used to calculate the displacements.

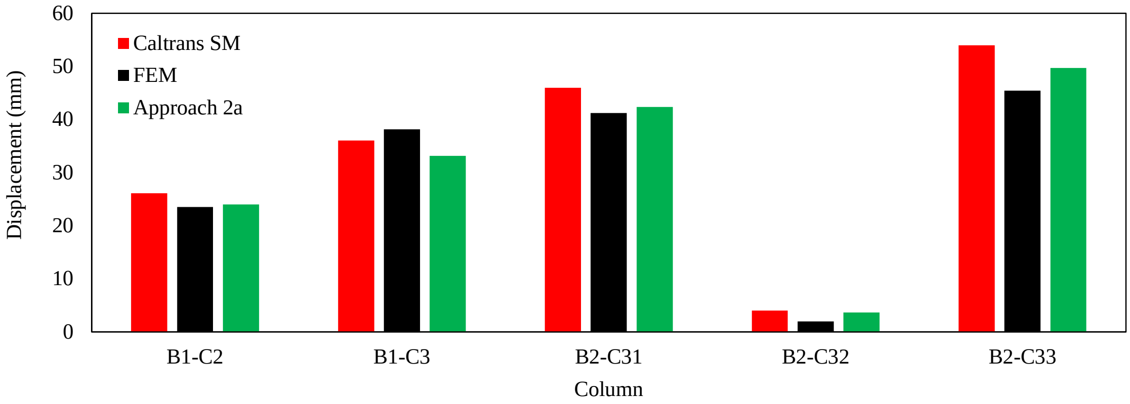

(a) Short-span CIP / PS Box frames

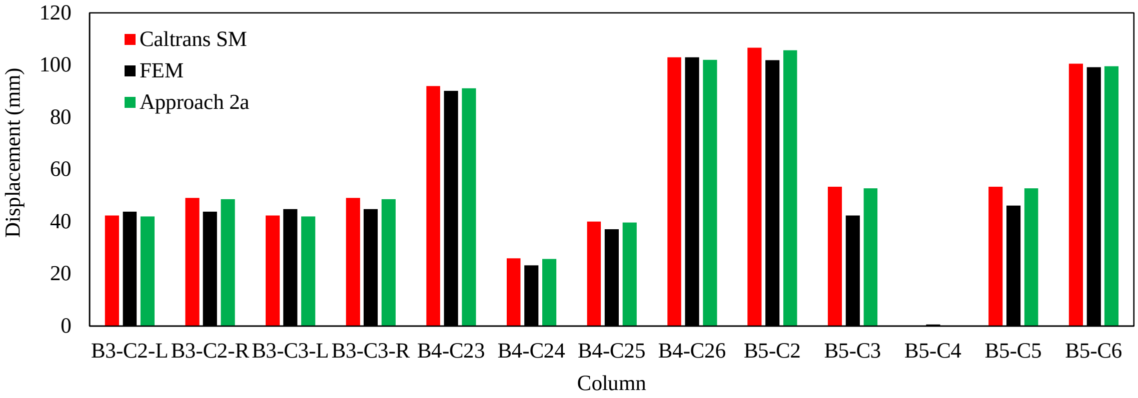

(b) Medium-span CIP / PS Box frames

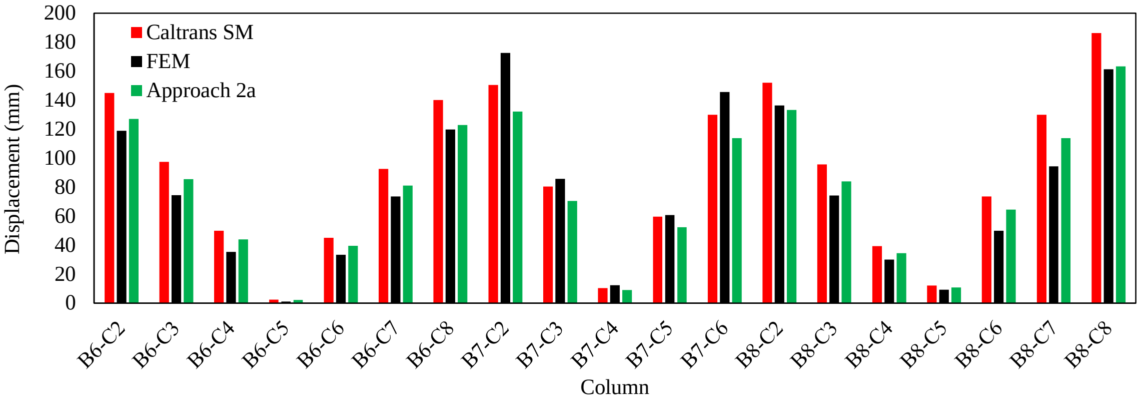

(c) Long-span CIP / PS Box frames

Figure 6.12: A comparison between the maximum displacements calculated by the FEM and those obtained by the Caltrans SM and the simplified analysis based on Approach 2a strains

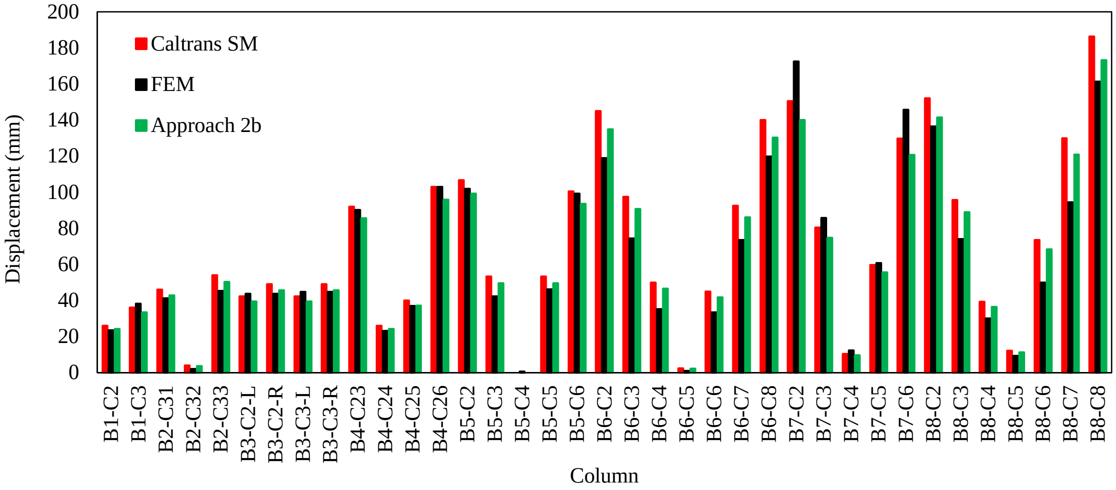

Figure 6.13: A comparison between the maximum displacements calculated by the FEMs and maximum displacements obtained using Approach 2b and the Caltrans SM

6.5.3 Estimation of Column Base Shear Force

After computing the column top lateral displacement, the corresponding design base shear force is calculated using Equation (6-4).

$$V_{\text{col}} = \Delta_{\text{col}} \times \text{k}_{\text{col}} \tag{6-4}$$

where Δ_{col} is the column lateral top displacement; and k_{col} is the column flexural stiffness.

If the concrete relaxation in columns is ignored in the Caltrans SM, the column base shear force will be overestimated. In addition, the column stiffness should be adjusted to reflect the effective stiffness in the case of flexural cracking of columns when the superstructure shortens due to the time-dependent effects. In the Caltrans SM, the effective column stiffness when the column cracks is typically estimated by $0.5k_g$, where k_g is the column gross flexural stiffness.

To include the beneficial effects of concrete relaxation, Equation (6-5) is recommended for estimating the column base shear forces:

$$v_{col} = \frac{\Delta_{col} \times k'_{col}}{(1+\emptyset_{2000,180})} \qquad \textbf{(6-5)}$$

where $\emptyset_{2000,180}$ is the creep coefficient at 2000 days when the columns are assumed to be loaded at the age of 180 days; and k'_{col} is the appropriate column stiffness (either based on uncracked section or cracked properties using a moment-curvature analysis).

The selected creep coefficient is consistent with the assumption considered for the loading age of column in the FEM. The estimated base shear force using the different displacements associated with the different strains were then compared to the shear force predicted by the FEM, as exhibited in Figure 6.15 to Figure 6.17.

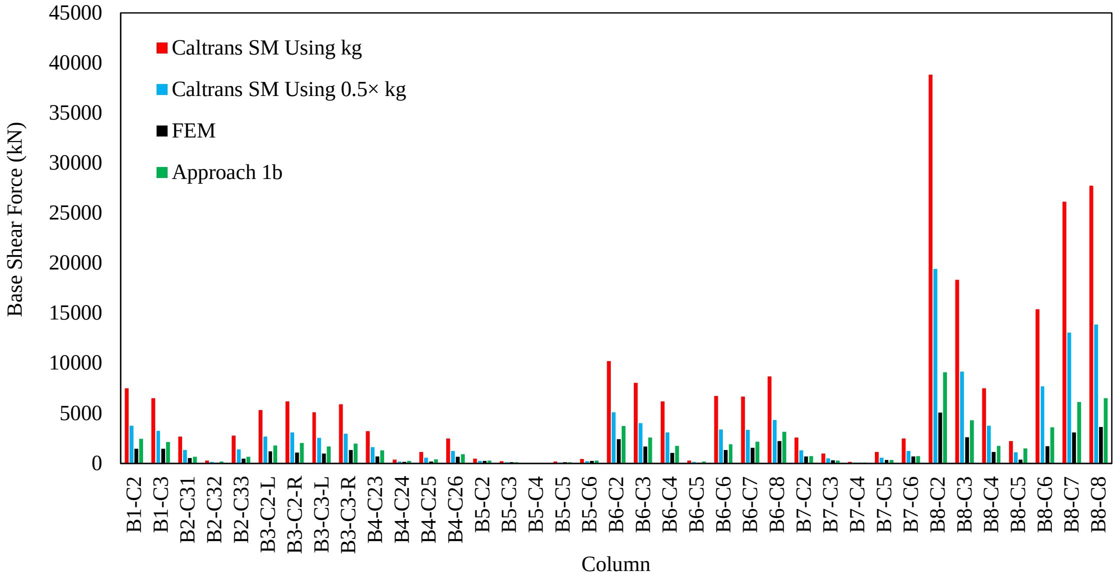

Figure 6.14: A comparison between the maximum base shear force calculated by the FEMs and maximum displacements obtained using Approach 1b and the Caltrans SM

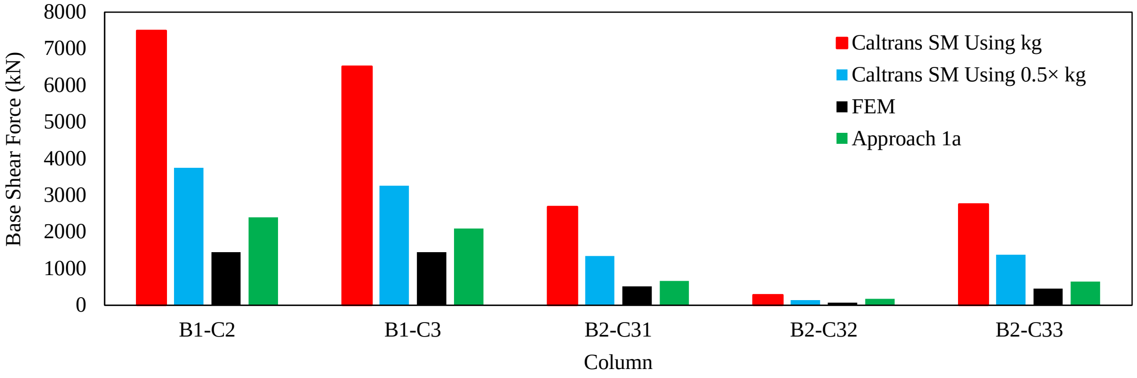

(a) Short-span CIP / PS Box frames

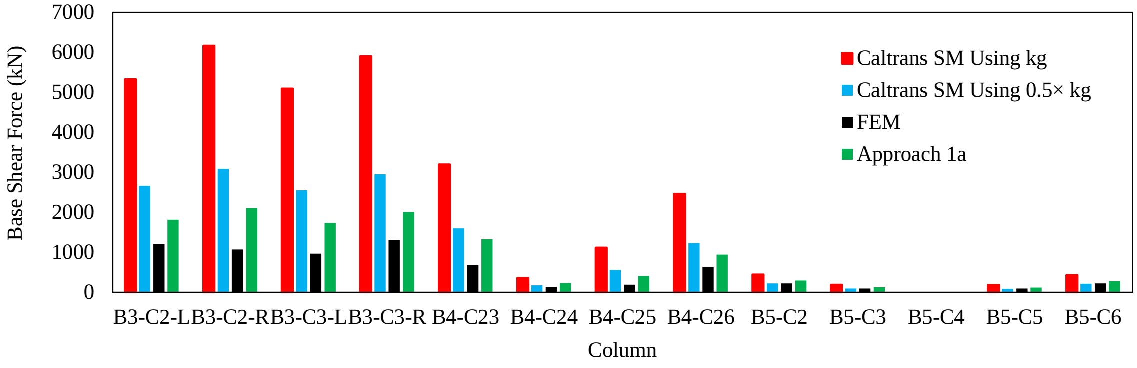

(b) Medium-span CIP / PS Box frames

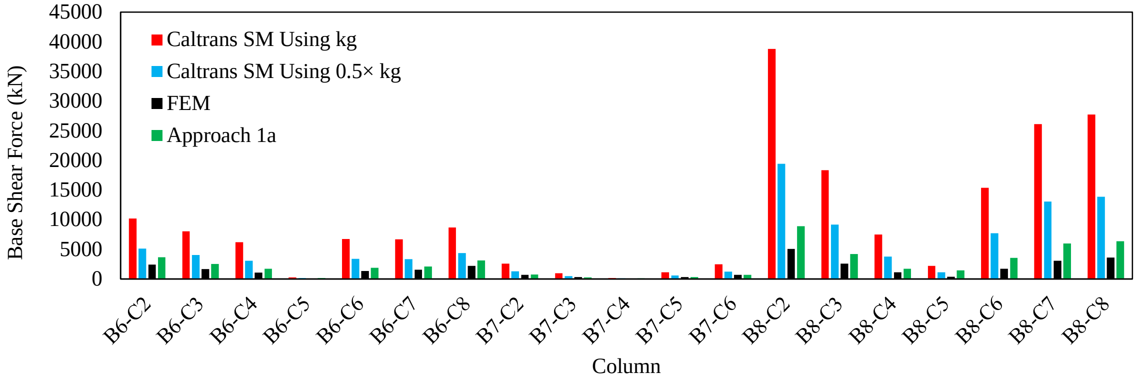

(c) Long-span CIP / PS Box frames

Figure 6.15: A comparison between the maximum base shear force calculated by the FEM and those obtained by the Caltrans SM and the simplified analysis based on Approach 1a strains

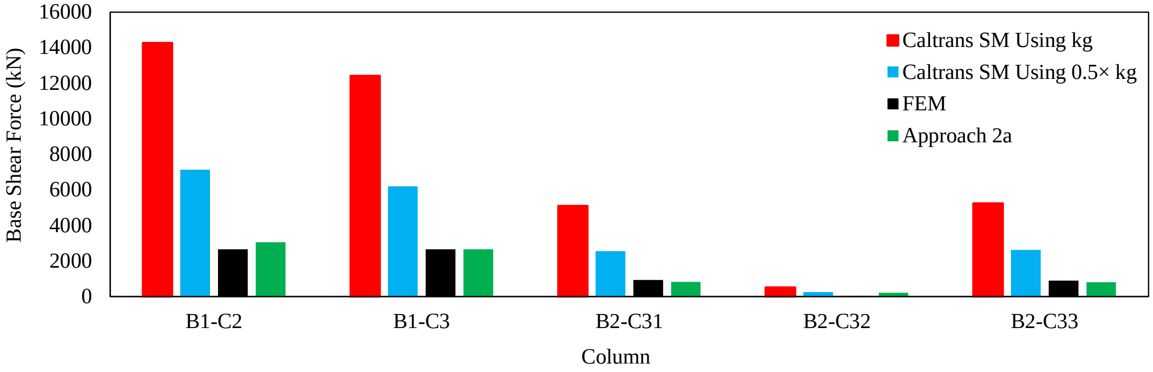

(a) Short-span CIP / PS Box frames

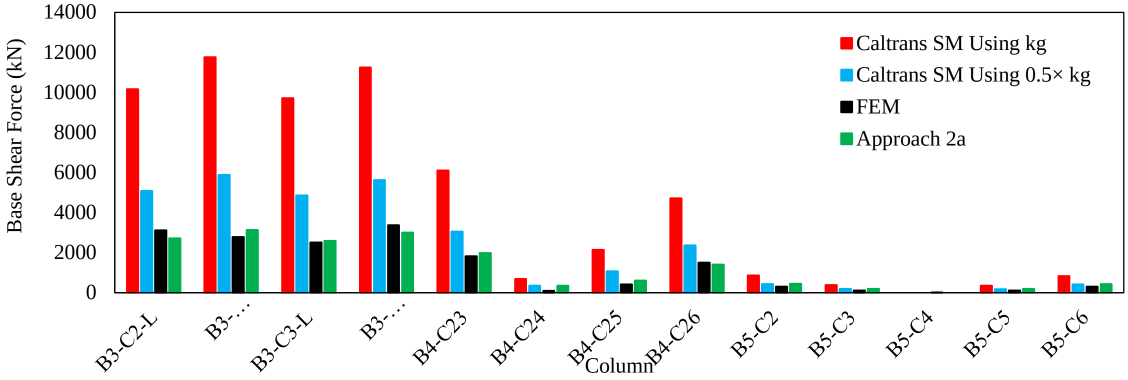

(b) Medium-span CIP / PS Box frames

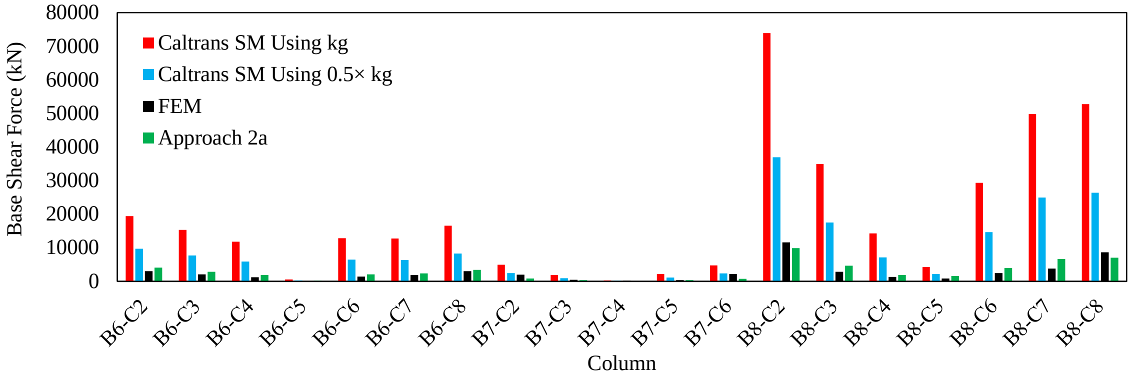

(c) Long-span CIP / PS Box frames

Figure 6.16: A comparison between the maximum base shear force calculated by the FEM and those obtained by the Caltrans SM and the simplified analysis based on Approach 2a strains

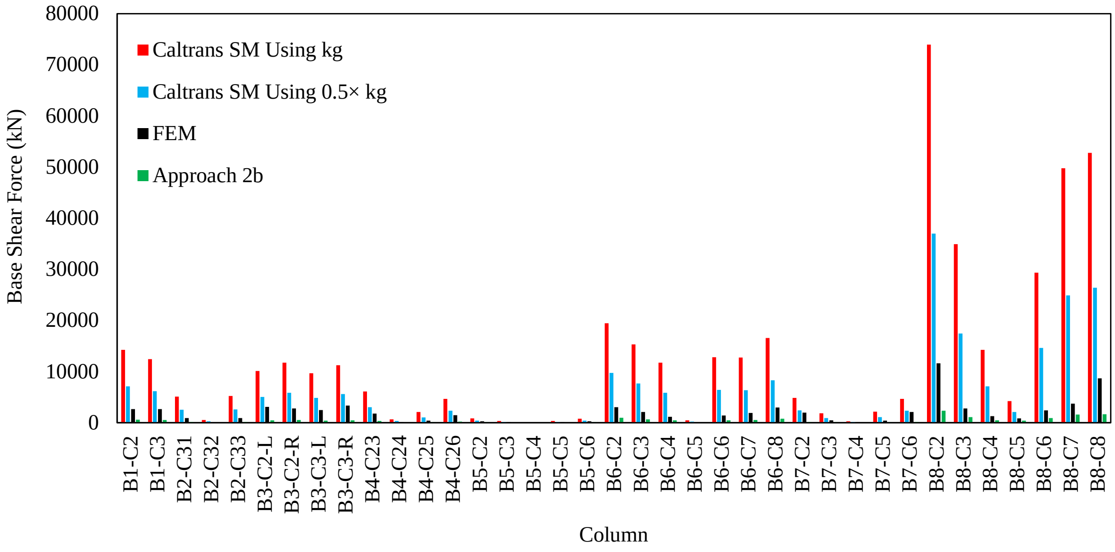

Figure 6.17: A comparison between the maximum base shear force calculated by the FEMs and maximum displacements obtained using Approach 2b and the Caltrans SM

As anticipated, using the Caltrans SM to predict the base shear force resulted in an overestimation of the base shear force due to ignoring the concrete relaxation when it was compared to the FEM results. The correlation between the predicted base shear force using the simplified analysis and the FEM was improved when the recommended approaches were used. The largest and smallest differences of 14350 kN (3226 kips) and 367 kN (82 kips) between the estimated and the FEM base shear forces were computed when the Caltrans methodology and Approach 2a were used, respectively.

6.5.4 Recommended Design Approach

In order to determine an appropriate design approach, a simplified approach was evaluated with four different options and they were evaluated against the FEM results to evaluate their accuracy. In addition to giving consideration to accuracy, input from Caltrans engineers was sought to ensure that the selected approach can be easily integrated within their design practice.

Figure 6.18 and Figure 6.19 show the ratio of column top lateral displacements and the corresponding forces estimated by the simplified approaches and the Caltrans method to those obtained from the FEMs. Additionally, the mean and standard deviation for these ratios were calculated and are presented in Table 6.2 and Table 6.3, respectively.

The Caltrans SM and the simplified approach resulted in accurate estimates of the column lateral displacements when compared to the FEM results for the displacements. However, the poorest agreement was found between the Caltrans and the FEM for the base shear forces. Approach 2b resulted in the best correlation for base shear forces with the FEM results and the corresponding mean and standard deviation were 1.09 and 0.40, respectively. Approach 1b produced better results compared to the Caltrans SM with the mean and standard deviation of 1.49 and 0.30, respectively. Although Approach 2b is the most appropriate simplified approach, Approach 1b has advantages in that it uses creep and shrinkage strains, similar to the Caltrans SM and account for the prestress strains as part of the structural analysis. Therefore, Approach 1b may be used for calculating the displacement-induced column forces. The resulting forces could be reduced by 1.2 (i.e., mean - standard deviation), which will still reduce the base shear forces by 50% the Caltrans bridge design procedures.

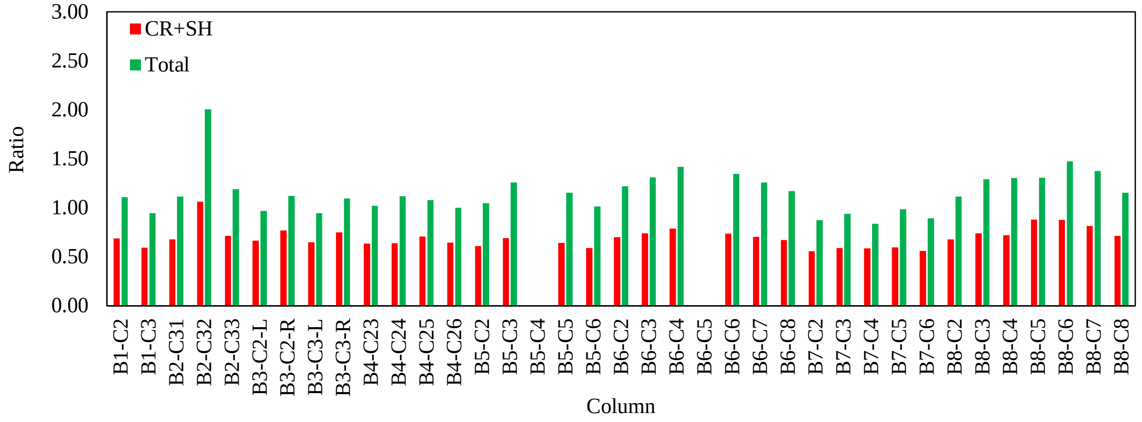

(a) Ratio of the Caltrans SM to the FEM

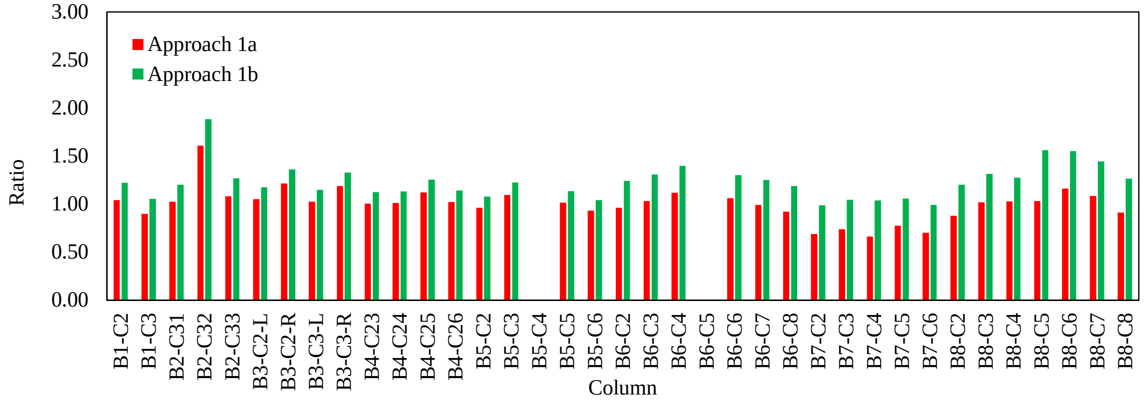

(b) Ratio of Approach 1 to the FEM

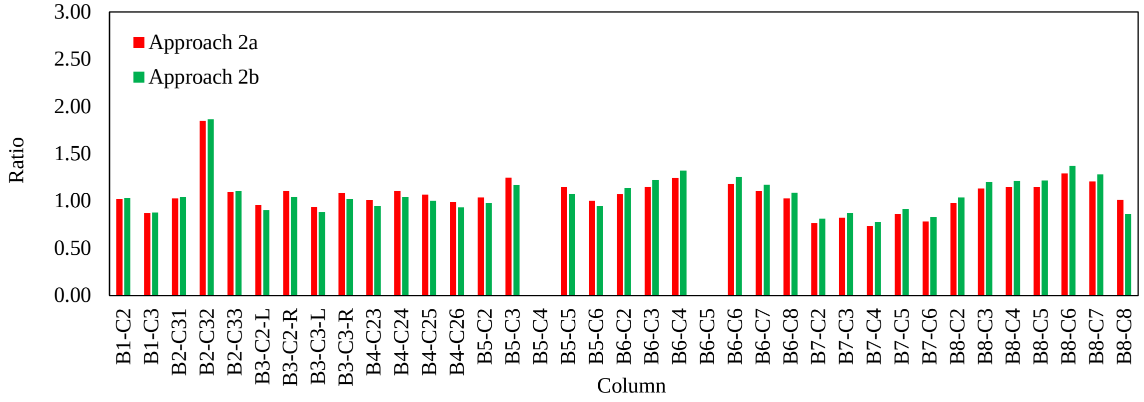

(c) Ratio of Approach 2 to the FEM

Figure 6.18: Ratio of column displacements predicted by the simplified approaches to the FEM

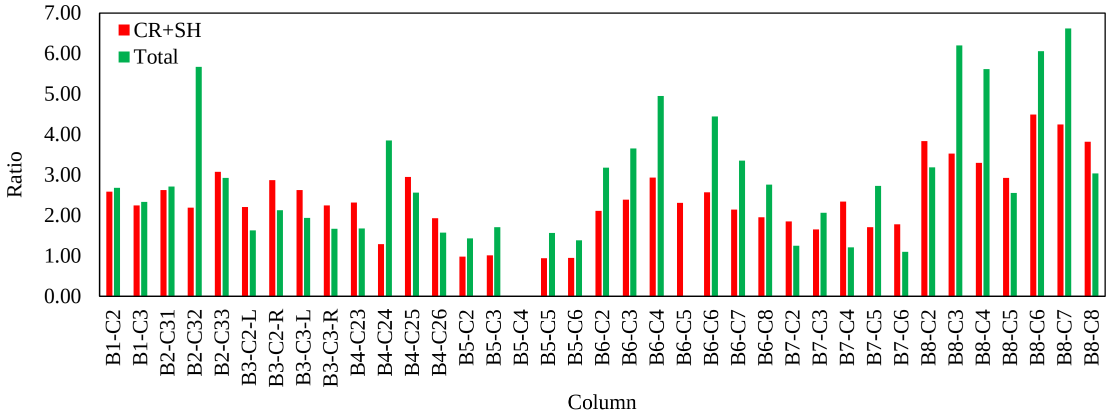

(a) Ratio of the Caltrans SM to the FEM

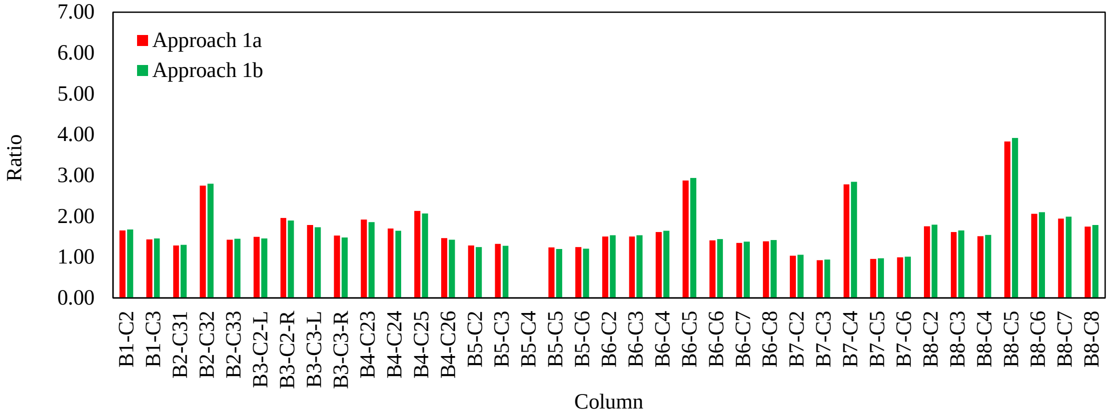

(b) Ratio of Approach 1 to the FEM

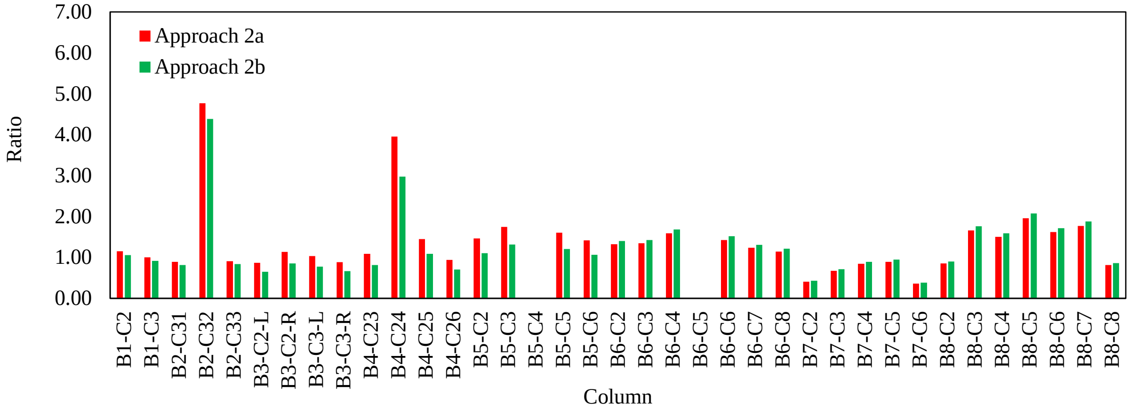

(c) Ratio of Approach 2 to the FEM

Figure 6.19: Ratio of base shear forces predicted by the simplified approaches to the FEM

Table 6.2: The mean and standard deviation of the ratio of the column top lateral displacement calculated by the simplified analyses to the FEM

Parameter	Creep and shrinkage strain			Total strain		
	Caltrans	Approach 1a	Approach 1b	Caltrans	Approach 2a	Approach 2b
Mean, μ	0.66	0.95	1.17	1.09	1.01	1.01
Standard Deviation, σ	0.19	0.28	0.33	0.34	0.31	0.32

Table 6.3: The mean and standard deviation of the ratio of the base shear force calculated by the simplified analyses to the FEM

Parameter	Creep and shrinkage strain			Total strain		
	Caltrans	Approach 1a	Approach 1b	Caltrans	Approach 2a	Approach 2b
Mean, μ	2.43	1.48	1.49	2.92	1.16	1.09
Standard Deviation, σ	0.94	0.30	0.30	1.58	0.38	0.40

6.6 Summary and Conclusions

In this chapter, a systematic investigation was undertaken to improve the treatment of displacement-induced column forces in CIP / PS Box frames. In doing so, time-dependent effects on eight CIP / PS Box frames of various lengths and configuration were examined using the FEM. The beneficial effects of concrete relaxation were incorporated into the FEM. For the eight frames, the shortening strain rate of superstructure together with the variation of column top lateral displacement and the corresponding were calculated as a function of time. Using the FEM results, a simplified analysis was developed to more accurately calculate displacement-induced column forces compared to the current Caltrans SM.

Based on the findings of the FEM, the following conclusions were drawn:

- For the eight analyzed CIP / PS Box frames, the shrinkage of the superstructure had a significantly larger contribution to the shortening strain rate of the superstructure, column top lateral displacement and the corresponding base shear force compared to the corresponding effects of dead load, prestress, and creep. The corresponding contribution of the dead load was the smallest compared to the prestress, creep, and shrinkage.

- The FEM predicted similar shrinkage strains for the eight CIP / PS Box, where the difference between the largest and smallest maximum shrinkage strain was estimated to be 143 με which was less than the corresponding differences for the prestress and creep.
- Typically, the longer the CIP / PS Box was, the larger the total displacement was imposed on the exterior columns.
- The column base shear force was affected by a combination of the column top displacement and the column stiffness. The large column displacement did not necessarily result in a large base shear force as it was observed for the slender columns in B5 due to low stiffness.
- For displacement calculation using simplified analysis, Approach 1a resulted in the best agreement with the FEM results. A better correlation was found between the Caltrans SM and the FEM results when the total strains were used rather than the creep and shrinkage stains.
- For shear calculation using simplified analysis, Approaches 2a and 2b resulted in the best agreement with the FEM results, while the Caltrans SM resulted in the poorest agreement with the FEM results.

CHAPTER 7: SUMMARY, CONCLUSIONS, AND FUTURE WORK

7.1 Summary

The superstructure of a CIP / PS Box frame experiences continuous movements due to shortening of the structure length resulting from shrinkage as well as prestressing and creep caused primarily by prestressing. As a result of these movements, columns within each continuous multi-span frame are subjected to lateral displacements and forces as a function of time following the construction of the superstructure. Accurately estimating displacement-induced column forces is critical for the design of the columns and their foundations. When these forces are underestimated, yielding of the columns can occur prematurely when they are subjected to external loads. This can cause the bridge to produce unexpected performance when it is subjected to event such as seismic excitation. When displacement-induced forces are overestimated, columns will become unnecessarily large, which in turn can attract more forces and amplify the problem.

In the absence of detailed computer modeling, the Caltrans SM calculates the displacement-induced column forces using the strain rates established for joints and bearing design. Two concerns are raised with this simplified method: (1) the selected shortening strain rate for the superstructure may not be appropriate; and (2) the beneficial effects of concrete relaxation on the displacement-induced column forces may not be accurately accounted for. Using a combination of an experimental program and analytical models, this report has investigated the displacement-induced column forces and presented recommendations to address the aforementioned concerns, thereby improving the calculation of column design forces.

Given the limited experimental data available on concrete relaxation, an experimental study was undertaken to characterize the concrete relaxation since it provides beneficial effects to displacement-induced column forces. Using three specimens and three loading protocols, seven relaxation tests were performed at different ages of loading. In all tests, the beneficial effects of concrete relaxation on the displacement-induced forces were observed. The induced forces in the test columns were reduced with time under the state of constant strains.

After demonstrating the beneficial effects of concrete relaxation on the displacement-induced forces through the experimental program, corresponding effects on eight CIP / PS Box frames of various lengths and configurations were evaluated using FEMs representing these frames. The shortening strain rate of superstructure together with the variation of column top lateral displacement and the corresponding force with time were calculated. Using the FEM results for strains rates, simplified approaches were formulated to take advantage of concrete relaxation and thus more accurately to calculate the displacement-induced column forces.

7.2 Conclusions

The detailed conclusions for the study presented in this report can be found at the end of Chapters 3, 5, and 6. In addition, the following general conclusions have been drawn:

- The beneficial effects of concrete relaxation on the displacement-induced forces were verified by the laboratory tests in addition to the FEA of a demonstrative CIP / PS Box frame. These effects cause reduction to the concrete forces/stresses with time under the state of a constant displacement/strain. The FEM of the CIP / PS Box frame showed that the displacement-induced column force (i.e., design base shear force) was reduced by as much as 53% for an exterior column due to the relaxation of the column concrete even though the column was 180 days old when it was first subjected to superstructure induced lateral displacement.
- For the eight CIP / PS Box analyzed with consideration to the effects of concrete relaxation

in the columns, the shrinkage of the superstructure had the largest contribution to the shortening strain rate of the superstructure, column top lateral displacement and the corresponding base shear force compared to the corresponding effects due to dead load, prestress, and creep.

- Among four simplified approaches and the Caltrans SM, column forces calculated by Approach 2b resulted in the best agreement with the corresponding FEM results. However, Approach 1b is recommended by this study since it has an advantage of using creep and shrinkage strains, like the Caltrans SM and account for the prestress strains separately as part of the structural analysis.

7.3 Future Work

The recent findings from analysis of bridge frames designed with concrete box-girders was that they undergo significant shortening due to creep and shrinkage effects, which imposed gradual lateral displacements to the columns following the construction phase. The expected shortening of long-span bridges can make the columns to experience displacements closer to their yield value. Impact of these columns under earthquake load is currently unknown.

A column that experiences gradual lateral displacement due to superstructure shortening does not build up any significant stresses as typically assumed in practice. This is because they experience stress relaxation, which has been confirmed in this project. This phenomenon is new in design calculations and opens up several questions. The answers to these questions are important to understand the true seismic behavior of bridges with columns experiencing displacement-induced forces. When columns undergo gradual lateral displacements, they may experience flexural cracking. This in turn will induce strains on the tension reinforcement. While the induced stresses are partly reduced in concrete, the strains in concrete and longitudinal reinforcement may remain the same. If the columns experience large strains, they could yield even under a small earthquake load. What needs to be understood is that as the concrete stresses are relaxed, if any changes in steel strains occur as steel can also experience relaxation. Once the long-term effects are matured, it is important to understand the true seismic performance of columns and their impact to the bridge response. This issue is not currently considered. A systematic experimental and analytical study needs to look at the column relaxation with and without flexural cracking with appropriate gravity load effects, and its impact on seismic behavior of individual columns and the entire bridge frame. Understanding the impact of long-term effects of superstructure on bridge columns and their expected seismic behavior, and a procedure to account for this phenomenon in routine design of long span bridges are considered to be the useful next steps.

REFERENCES

American Association of State Highway and Transportation Officials (AASHTO) (2010). *AASHTO LRFD Bridge Design Specifications, 5th edition*. Washington, DC.

Abdel Karim, A. and Tadros, M.K. (1993) "Computer analysis of spliced girder bridges," ACI Structural Journal, 90(1), 21-31.

ACI (1992). Building Code Requirements for Reinforced Concrete (ACI 318-89) and Commentary-ACI 318R-89. Detroit, MI.

ACI 209R (2008) "Guide for Modeling and Calculating Shrinkage and Creep in Hardened Concrete."

Atrushi, D. S., (2003). “Tensile and compressive creep of early age concrete: testing and modelling.” doctoral thesis, The Norwegian University of Science and Technology, Trondheim, Norway.

Bazant, Z.P., and Kim, S. (1979). “Approximate relaxation function for concrete.” Journal of the Structural Division, 105 (12), 2695-2705.

Bazant, Z. P. (2000) "Creep and shrinkage prediction model for analysis and design of concrete structures: Model B3." Adam Neville Symposium: Creep and Shrinkage - Structural Design Effects ACI SP-194, 1-83, Farmington, MI.

Bazant, Z.P., Yu, Q., and Li, H.G. (2012). “Excessive long-time deflections of prestressed box-girders. II: numerical analysis and lessons learned.” ASCE Journal of Structural Engineering, 138 (6), 687-696.

Bosnjak, D. (2001). "Self-induced cracking problems in hardening concrete structure." PhD dissertation, Department of Structural Engineering, NTNU, Trondheim, Norway.

California Department of Transportation. Caltrans. (2015). Bridge Design Practice. Concrete Columns.

California Department of Transportation. Caltrans. (1994). Memorandum to designers. Bridge deck joints and deck joint seals. Attachment 4.

CEB-FIP (1990). Evaluation of Time Dependent Behavior of Concrete, Comite Euro-International du Beton, Bulletin d'information, No. 199, Paris, France.

Choudhury, D., Mari, A.R., and Scordelis, A.C. (1988). "Design of reinforced concrete bridge columns subjected to imposed deformations." ACI, 85 (5): 521-529.

Collins, M. P., and Mitchell, D. (1997). “Prestressed concrete structures.” Response Publications, Ontario, Canada.

Digler, W., Ghali, A., and Kountouris, C (1970). "Time-dependent forces induced by settlement in continuous prestressed concrete structures." ACI, 80 (12), 507-515.

Ghali, A., Digler, W., and Neville, A.M. (1969). "Time-dependent forces induced by settlement of supports in continuous reinforced concrete beams." ACI, 66 (11): 907-915.

Ghali, A., Favre, R., and Elbadry, M., (2002) “Concrete structures- stresses and deformation.” Spon Press.

Gutsch, A. (2001). “Properties of early age concrete - experiments and modelling”. RILIM International Conference on ‘Early Age Cracking in Cementitious Systems’ (EAC'01), Haifa, pp. 11-18.

Hinkle, S. D. (2006). “Investigation of time-dependent deflection in long span, high strength, prestressed concrete bridge beams.” MS thesis, Virginia Polytechnic Institute and State Univ., Blacksburg, Va.

Honarvar, E., Sritharan, S., Rouse, J., and Aaleti, S. (2016). “Bridge decks with precast UHPC waffle panels: a field evaluation and design optimization,” ASCE Journal of Bridge Engineering, 21 (1): 1-13.

Huo, X. S., Al-Omaishi, N. and Tadros, M. K. (2001) "Creep, shrinkage, and modulus of elasticity of high-performance concrete." ACI Materials Journal, 98(6), 440-449.

Lark, J.R., Howells, W.R., and Barr, I.B. (2004). “Behavior of post-tensioned concrete box-girders.” Proceedings of the Institution of Civil Engineers, Issue BE2, Paper 13564, 71-81.

Lewis, M., and Karbhari, M.V. (2006). “Experimental verification of the influence of time-dependent material properties on long-term bridge characteristics.” FHWA/CA/ES-

2006/24, California Department of Transportation Division of Engineering Services, Sacramento, CA.

McHenry, D. (1943). “A new aspect of creep in concrete and its application to design”. Proc. ASTM., 43, 1069-84.

MIDAS Civil Software (2013). Analysis reference.

Mindess, S., Young, J. F., and Darwin, D. (2002). “Concrete.” Second Edition, Prentice Hall.

Morimoto H., Koyangi W. (1994). “Estimation of stress relaxation in concrete at early ages”, Proceeding of the RILEM International Symposium on ‘Thermal Cracking in Concrete at Early Ages’, edited by R. Springenschmid E & FN Spon, London, 95-120.

Naaman, A. E. (2004). “Prestressed concrete analysis and design: fundamentals.” Techno Press 3000, Ann Arbor, MI.

Nilson, A. H. (1987). “Design of prestressed concrete.” 2nd Ed., Wiley, NY.

Precast/Prestressed Concrete Institute (PCI) (1997). Bridge Design Manual, Chicago, IL.

Rostásy, F. S., Gutsch, A. and Laube, M. (1993). “Creep and relaxation of concrete at early ages: experiments and mathematical modelling”, in ‘Creep and shrinkage of concrete’, Z. Bazant and C. Carol, E&FN Spon, London, pp. 453-458.

Schutter, G.D. (2004). "Applicability of degree of hydration and maturity method for thermo-viso-elastic behavior of early age concrete." Cement & Concrete Composites, 26 (5): 437-443.

Tadros, M.K., Ghali, A. and Dilger, W.H. (1977) "Time- Dependent analysis of composite frames." ASCE Journal of Structural Engineering, 871-884.

Tadros, M. K., Ghali, A., and Meyer, A. W. (1985). “Prestress loss and deflection of precast concrete members.” PCI Journal, 301, 114–141.

Tadros, M. K. and Al-Omaishi, N. (2003). “Prestressed losses in pretensioned high-strength concrete bridge girders.” Washington D. C.: Transportation Research Board, 2003.

Vitek J. L. (1995). “Long-term deflections of large prestressed concrete bridges.” CEB Bulletin d’Information, No. 235 Serviceability Models, Paris, France.